UNIVERSITY OF CALIFORNIA, SAN DIEGO

The Role of ELOVL2 in Aging and Eye Disease

A dissertation submitted in partial satisfaction of the requirements for the degree Doctor of Philosophy

in

Biomedical Sciences

by

Daniel Chen

Committee in Charge:

Professor Kang Zhang, Chair
Professor Ju Chen
Professor George Sen
Professor Dong Wang
Professor Sheng Zhong

2018

The Dissertation of Daniel Chen as it is listed on UCSD Academic Records is approved, and it is acceptable in quality and form for publication on microfilm and electronically:

_____

_____

_____

_____

_____ Chair

University of California, San Diego 2018

TABLE OF CONTENTS

LIST OF FIGURES

Acknowledgements

I would like to acknowledge Professor Kang Zhang for his support as the chair of my committee and as my PhD advisor, and Professor Dorota Skowronska-Krawczyk for her guidance through countless drafts in preparing my publication.

I would also like to acknowledge Zhang lab and my BMS friends for their support in my years of research, and for making this time in my life enjoyable.

Part of this dissertation is currently being prepared for submission for publication of the material. Maryam Jafari, Viet Anh Nguyen Huu, Xin Li, Mary Jabari, Lorena Rocha, Sherrina Patel, Jonathan Sun, Anthony Ao, Dorota Skowronska-Krawczyk, Kang Zhang will be co-authors. The dissertation author was the primary author of this material.

VITA

2007-2011	Bachelor of Science, University of California, Berkeley
2011-2013	Research Assistant, University of Colorado, Denver
2013-2018	Doctor of Philosophy, University of California, San Diego

PUBLICATIONS

1. **Chen D**, Gibson ES, Kennedy MJ. A light-triggered protein secretion system. J. Cell Biol. 2013 May 13;201(4):631-40. doi: 10.1083/jcb.201210119. PMID: 23671313

2. Taslimi A., Vrana J.D., **Chen D**., Borinskaya S., Mayer B., Kennedy MJ, and Tucker CL An optimized optogenetic clustering tool for probing protein interaction and function. (2014) Nature Commun. 5: 4925. doi 10.1038/ncomms5925. PMID: 25233328

3. Li G, Xu F, Zhu J, Krawczyk M, Zhang Y, Yuan J, Patel S, Wang Yujuan, Lin Y, Zhang M, Cai H, **Chen, D**, Zhang M, Cao G, Yeh E, Lin D, Su Q, Li W, Sen G, Afshari N, Chen S, Maas R, Fu X, Zhang K, Liu Y, and Ouyang H. Transcription factor Paired Box 6 controls limbal stem cell lineage in development and disease. J Biol Chem. 2015 Aug 14;290(33):20448-54. doi: 10.1074/jbc.M115.662940. Epub 2015 Jun 4. PMID: 26045558

4. Zhao L, Chen X, Zhu J, Yang X, Hu L, Ouyang H, Patel S, Jin X, Lin D, Wu F, Flagg K, Cai H, Li G, Cao G, Lin Y, **Chen D**, Wen C, Chung C, Wang Y, Qiu A, Yeh E, Wang W, Hu X, Grob S, Abagyan R, Su Z, Tjondro HC, Zhao X, Luo H, Hou R, Jefferson J, Perry P, Gao W, Kozak I, Granet D, Li Y, Sun X, Wang J, Zhang L, Liu Y, Yan Y, Zhang K. Lanosterol reverses protein aggregation in cataracts. Nature. 2015 Jul 30;523(7562):607-11. doi: 10.1038/nature14650. Epub 2015 Jul 22. PMID: 26200341

5. Skowronska-Krawczyk D, Zhao L, Zhu J, Weinreb RN, Cao G, Luo J, Flagg K, Patel S, Wen C, Krupa M, Luo H, Ouyang H, Lin D, Wang W, Li G, Xu Y, Li O, Chung C, Yeh E, Jafari M, Ai M, Zhong Z, Shi W, Zheng L, Krawczyk M, **Chen D**, Shi C, Zin C, Zhu J, Mellon PL, Gao W, Abagyan R, Zhang L, Sun X, Zhong S, Zhuo Y, Rosenfeld MG, Liu Y, Zhang K. P16INK4a Upregulation Mediated by SIX6 Defines Retinal Ganglion Cell Pathogenesis in Glaucoma. Mol Cell. 2015 Sep 17;59(6):931-40. doi: 10.1016/j.molcel.2015.07.027. Epub 2015 Sep 10. PMID: 26365380

6. Fritsche LG, et al. A large genome-wide association study of age-related macular degeneration highlights contributions of rare and common variants. Nat Genet. 2015 Dec 21. doi: 10.1038/ng.3448. [Epub ahead of print]. PMID: 26691988

7. Lin H, Ouyang H, Zhu J, Huang S, Liu Z, Chen S, Cao G, Li G, Signer RA, Xu Y, Chung C, Zhang Y, Lin D, Patel S, Wu F, Cai H, Hou J, Wen C, Jafari 2, Liu X, Luo L, Zhu J, Qiu A, Hou R, Chen B, Chen J, Granet D, Heichel C, Shang F, Li X, Krawczyk M,

Skowronska-Krawczyk D, Wang Y, Shi W, **Chen D**, Zhong Z, Zhong S, Zhang L, Chen S, Morrison SJ, Maas RL, Zhang K, Liu Y. Lens regeneration using endogenous stem cells with gain of visual function. Nature. 2016 March 17: 531, 323-328. Doi:10.1038/nature17181. PMID: 26958831.

8. Gross AM, Jaeger PA, Kreisberg JF, Licon K, Jepsen KL, Khosroheidari M, Morsey BM, Swindells S, Shen H, Ng CT, Flagg K, **Chen D**, Zhang K, Fox HS, Ideker T. Methylome-wide Analysis of Chronic HIV Infection Reveals Five-Year Increase in Biological Age and Epigenetic Targeting of HLA. Mol Cell. 2016 April 21. doi: 10.1016/j.molcel.2016.03.019. PMID: 27105112

9. **Chen D**, Jafari M, Huu V, Li X, Jabari M, Rocha L, Patel S, Sun J, Ao A, Skowronska-Krawczyk D, Zhang K. Role of ELOVL2 in the Aging Retina. *In Preparation*.

ABSTRACT OF THE DISSERTATION

The Role of ELOVL2 in Aging and Eye Disease

By

Daniel Chen

Doctor of Philosophy in Biomedical Sciences

University of California, San Diego, 2018

Professor Kang Zhang, Chair

Our group recently developed a quantitative model for human aging based on genome-wide DNA methylation patterns using measurements at 470,000 CpG markers from whole blood[1]. It is highly accurate at predicting age, and can also discriminate relevant factors in aging, including gender and genetic variants. With this model, there is evidence that metabolic traits such as body mass index and diabetes impact biological

aging. In addition, these methylation patterns are strongly correlated with cellular senescence and aging. The top age-predictive CpG marker in our model, and 3 out of the top 12 markers, reside on *ELOVL2*, a gene involved in elongation of fatty acids. Because of the links between lipid metabolism and aging[2–4], we focused our study on the relationship between this gene and aging. We found that in WI-38 and IMR-90 human fibroblasts, two common model cell lines of aging, *ELOVL2* methylation increases and expression decreases substantially with passage number, and that knocking down *ELOVL2* negatively influences cellular aging phenotypes. In mice, we found that mutant ELOVL2 results in an eye aging phenotype which may relate to age-related macular degeneration (AMD). In addition, we identified Aza-2-deoxycytidine (5-Aza) and L-ascorbic acid 2-phosphate (VcP) as modulators of aging phenotypes. We observed amelioration of aging phenotypes, and increased expression and decreased methylation of *ELOVL2* upon administration of VcP and 5-Aza in aging cell lines. Furthermore, we observed a reduction of AMD phenotypes in mice upon intraocular injection with 5-Aza. We hypothesize that VcP and 5-Aza can modulate aging phenotypes by influencing DNA methylation, and that *ELOVL2* plays a role in aging.

INTRODUCTION

As humans age, global DNA methylation decreases on average. Presumably, this is due to inefficiency of methylation maintenance upon DNA replication. However, some loci progressively methylate with age. *ELOVL2*, in particular, very reliably shows increased methylation as humans age, as revealed by our aging model[1]. This model draws from a dataset including 470,000 CpG markers from the whole blood of a large cohort human individuals spanning a wide age range, and can accurately predict the chronological age of humans based on the methylation state of 71 CpG markers. With this model, there is evidence for differential aging within the population that can be partially attributed to biometric and clinical states. Key findings show that metabolic traits such as body mass index and diabetes impact biological aging. Our model has also been validated in other tissues, indicating that these methylation trends may be common throughout many tissues of the human body. *ELOVL2*, the top age-predictive gene in our model, is involved in lipid metabolism. DNA methylation is impacted by cellular metabolism[5], which in turn is tied into the function of *ELOVL2*. Given the links between aging, methylation of *ELOVL2*, and metabolic activity, we were interested in further investigating the relationship between this gene and aging phenotypes. Furthermore, we identified Aza-2-deoxycytidine (5-Aza) and L-ascorbic acid 2-phosphate, or vitamin C phosphate (VcP) as modulators of DNA methylation and aging phenotypes. We plan to explore the relationship between aging, *ELOVL2*, and VcP.

In the first chapter, we analyze the effects of manipulating *ELOVL2* expression on aging phenotypes. First, using mortal human fibroblasts as a model, we will assess the proliferative capacity and amount of senescence, as well as alterations of the ‘methylomic

age' as determined by the analysis of CpG methylation and our predictive aging model. We have already established a negative influence on these phenotypes upon knockdown of *ELOVL2*. The next step is to overexpress *ELOVL2* in these cells. We will also assay the effects of *ELOVL2* mutations in mouse models. Because *ELOVL2* knockout mice are infertile, we generated C217W mutants, which we expect to delete the function of *ELOVL2* to elongate fatty acids. We will analyze behavioral traits associated with aging in these mice in addition to lifespan.

Based on the increasing methylation of CpG sites with age in humans, *ELOVL2* is the top gene in our aging model. We postulate that, along with other genes that are progressively methylated with age, increasing *ELOVL2* promoter methylation will decrease its expression, and negatively influence aging phenotypes. Using 5-Aza in aging model cell lines and in mouse eyes, we checked for DNA demethylation and increased expression of *ELOVL2*. We functionally analyzed the effects of perturbing DNA methylation by gene expression and cellular aging phenotypes.

In a screen of aging-related drugs, we identified and VcP as modulators of aging phenotypes in mortal human fibroblast cell lines, WI-38 and IMR-90. VcP increased proliferation, decreased senescence, and increased *ELOVL2* expression in these cell lines. This is in contrast to regular ascorbic acid, which had similar beneficial effects at low concentrations, but detrimental effects at higher dosages. Because of the ability of vitamin C to induce Tet-dependent DNA demethylation[6], we propose that it could be demethylating CpG sites in *ELOVL2*, thus increasing expression and eventually influencing aging phenotypes. In addition, we are currently treating aged *ELOVL2* mutant

mice as well as wild-type mice with high-dosage VcP, and plan to observe aging phenotypes and lifespan differences.

Our *ELOVL2* mutant mouse could serve as a new murine model of AMD, and 5-Aza can potentially ameliorate some AMD phenotypes.

BACKGROUND & SIGNIFICANCE

Aging.

From a population perspective, chronological age is arguably the most important clinical trait in predicting disease risk, mental and physical performance, mortality, and other important health concerns. The use of chronological age is limited, however, in explaining the large biological variation among individuals of a similar age. Biological age is a concept that attempts to quantify different aging states influenced by lifestyle, genetics, disease, and environment. Environmental and lifestyle choices such as smoking and diet also have clear implications with respect to age-associated diseases[7]. While epidemiological studies have succeeded in providing quantitative assessments of their impact on human longevity, advances in molecular biology now offer the ability to look beyond population questions of mortality, and to hone in on the specific effects of disease and other factors on aging within single organisms.

Active DNA methylation and demethylation.

DNA methylation at the 5-position of cytosine (5-methylcytosine, 5mC) is catalyzed and maintained by a family of DNA methyltransferases (DNMTs) in eukaryotes[8], and constitutes ~2-6% of the total cytosines in human genomic DNA[9]. Alterations of 5mC patterns within CpG dinucleotides are associated with numerous cellular conditions, both physiological and pathological. Changes in DNA methylation are most dynamic in germline lineages and in pre-implantation embryos, where genome-wide erasure and re-establishment of CpGme patterns are precisely controlled by time and lineage-specific developmental mechanisms controlling activities of DNMT1, DNMT3A, and DNMT3B, as well as the TET and BER families of enzymes[10]. DNMT1 is known as the primary

maintenance methyltransferase, while DNMT3A and DNMT3B have higher *de* novo methylating activity[11]. The TET and BER enzymes act in active demethylation. Deregulation of these mechanisms results in aberrant CpGme patterns causing infertility, embryonic lethality and developmental defects[12,13]. However, most changes in CpGme are gradual and accumulate progressively over the individual lifespan. Studies in monozygotic twins revealed the existence of 'epigenetic drift' where individual differences in CpG patterns increased as a function of age[14]. The degree of discordance between individual CpGme patterns was greatest between twins separated early in life, indicating that alterations were acquired independently over life and were at least partially dependent on environmental factors. Genome-wide hypomethylation with age has been observed, accompanied by localized hypermethylation of both at functionally neutral sites and at regulatory regions (promoters and enhancers) whose methylation affected mRNA expression of linked gene loci[15]. A number of recent studies have shown that CpGme patterns progressively change during aging in a variety of tissues and cells such as blood, muscle, brain, lung and colon[16]. The rates of CpGme changes at subsets of affected sites were calculated and used to determine the cellular 'epigenetic' age which generally well correlates with chronological age and therefore can be used as a measure to assess biological aging in a quantitative manner[17].

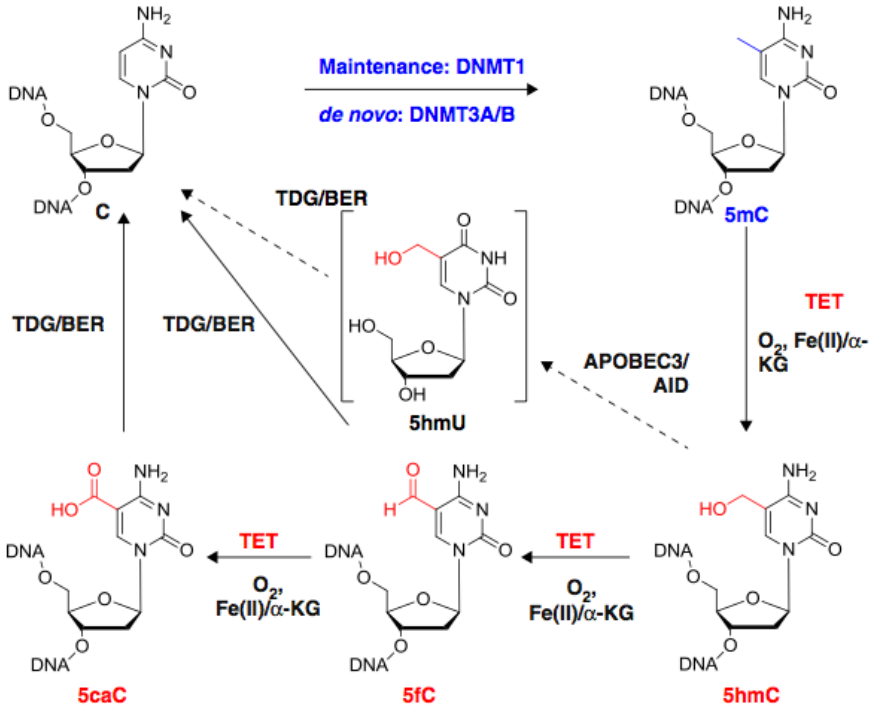

Figure 1. Dynamic regulation of cytosine methylation in DNA. DNMT3A and DNMT3B are responsible for de novo methylation to establish new methylation patterns, while 5mC is maintained during replication by DNMT1-catalyzed methylation of the newly synthesized DNA strand. TET enzymes can catalyze the oxidation of 5mC to 5hmC, 5fC, and 5caC in Fe(II) and α-ketoglutarate(α-KG)-dependent manner. 5fC and 5caC are recognized by DNA glycosylase TDG and converted to cytosine through base excision repair (BER) in an active demethylation reaction. 5hmC may be deaminated by APOBC3 or AID to form 5hmU, which can undergo base excision by TDG and BER to restore the unmodified cytosine. *adapted from Fu et al.

Epigenetic aging of tissues and organs has profound impact on human health. Aging-related global hypomethylation accompanied by CpG island hypermethylation closely resembles known patterns of aberrant CpGme in a variety of human cancers[18]. Outside of cancer, CpGme leading to de-regulated gene expression has been observed in other age-related diseases such as diabetes and four major neurodegenerative diseases (Alzheimer's, AD; Parkinson's, PD; Huntington's, HD and amyotropic lateral sclerosis (ALS)[19,20]. In addition, premature aging disorders Hutchinson-Gilford Progeria

and Werner Syndrome are characterized by extensive changes in genome-wide methylation landscapes affecting expression of many genes and pathways that can be linked to the premature aging phenotype[21].

The maintenance methyltransferase DNMT1 has been shown to decline steadily in activity with cellular senescence and immortalization. DNMT3B, which has significant *de novo* methylating activity, was found to increase markedly in activity in aging and immortalized cells. These studies indicate that reduced genome-wide methylation in aging cells may be attributed to attenuated DNMT1 activity, whereas gene-localized hypermethylation may be linked to increased *de novo* methylation by DNMT3A and/or DNMT3B[11].

In addition to passive demethylation from absence of DNMT1 activity, DNA methylation can be reversed through active demethylation mediated by the newly discovered iron(II)/αKG-dependent dioxygenases, TET family proteins [TET1, 2 and 3][22] (**Fig. 1**). TET proteins catalyze the conversion of 5mC to primarily 5-hydroxymethylcytosine (5hmC), and further to 5-formylcytosine (5fC) and 5-carboxylcytosine (5caC). While 5hmC is found in most mammalian cells and tissues with levels ranging from <0.1% to 0.4% of cytosines[22–24], 5fC and 5caC exist at much lower abundances. Both 5fC and 5caC can be recognized and excised by human thymine DNA glycosylase (TDG), followed by base excision repair (BER) to replace the modified cytosine with a normal cytosine in an active demethylation process[22]. Thus, 5hmC, 5fC, and 5caC are intermediates of active demethylation. While the 5hmC base represents a mark for active demethylation in mammalian genome, it also appears to play a role in gene regulation as an epigenetic mark. 5fC and 5caC are considered to be “committed”

to demethylation[25–29].

Vitamin C and DNA methylation.

L-ascorbic acid, or vitamin C, functions as an enzymatic cofactor for Tet1, since it has been found to increase levels of 5hmC in mouse embryonic fibroblasts and human cancer cell lines. Knockdown of Tet1 attenuated this increase[30]. It is involved in synthesis of collagen, a protein important for extracellular synthesis[31]. Furthermore, vitamin C acts as an antioxidant, and thus may help to protect the genome from damage[32]. The accumulation of free radicals, known as oxidative stress, can contribute to the senescence increase and cellular redox unbalance[33]. In various studies, vitamin C has been linked to diverse activities in different biological systems[34–36]. Linus Pauling, one of the most influential scientists of the 20th century, claimed in his later years that high-dosage intravenous vitamin C has antitumor effects[37]. His idea caused many scientists to turn toward researching the potentially beneficial effects of vitamin C. Research done by Takamizawa and colleagues showed that vitamin C can cause proliferation and differentiation increase in human osteoblast-like cells through the upregulation of collagen expression in a concentration dependent manner[38]. Furthermore, vitamin C has been demonstrated to selectively kill KRAS and BRAF mutant colorectal cancer cell through generating a derivative that targets GAPDH[39].

In this study, we use three derivatives of vitamin C: L-ascorbic acid, L-ascorbic acid 2-phosphate, and L-dehydroascorbic acid (**Fig. 2**). L-ascorbic acid 2-phosphate is a long-acting derivative of vitamin C. It must undergo hydrolysis to L-ascorbic acid in the presence of phosphatase from living tissues in order to become effective[40,41]. L-dehydroascorbic acid is an oxidized form of vitamin C.

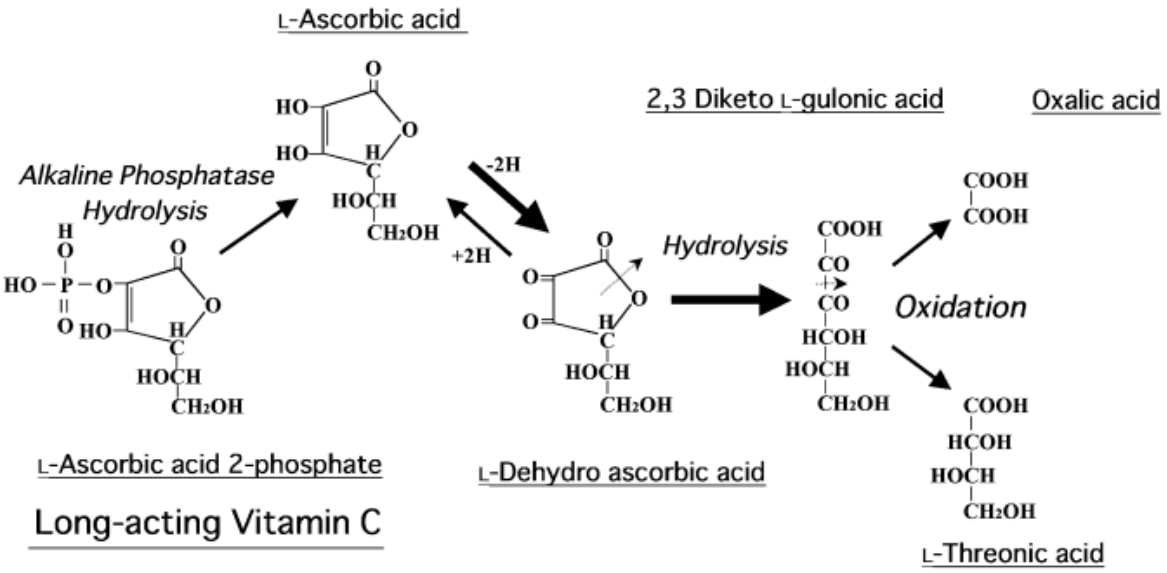

Figure 2. Vitamin C derivatives. *Adapted from Takamizawa et al.

ELOVL2.

ELOVL2 (Elongation Of Very Long Chain Fatty Acids-Like 2) encodes for a transmembrane protein involved in the synthesis of long (C22 and C24) ω3 and ω6 polyunsaturated fatty acids (PUFA)[42]. Specifically, ELOVL2 is capable of converting docosapentaenoic acid (DPA) (22:5n-3) to 24:5n-3, which is the precursor of 22:6n-3, docosahexaenoic acid (DHA)[43]. Given that PUFAs are involved in crucial biological functions including energy production, modulation of inflammation, and maintenance of cell membrane integrity, it is possible that *ELOVL2* methylation plays a role in the aging process through the regulation of different biological pathways.

An epigenetic clock in aging.

Our lab recently built a predictive model of aging on a large cohort of patients using a penalized multivariate regression method known as Elastic Net[44], combined with bootstrap approaches[1] (**Fig. 3, Fig. 5A**). Whole blood was taken from patients of age 19 to 101, and methylation was read by Illumina's Infinium HumanMethylation BeadChip assay[45]. The model included both methylomic and clinical parameters such as type 1 and type 2 diabetes, gender and body mass index (BMI). The optimal model selected a set of 71 methylation markers that were highly predictive of age. The accuracy of the model was high, with a correlation between age and predicted age of 96% and an error of 3.9 years (**Fig. 5B**). Nearly all top markers in the model lay within or near genes with known functions in metabolism and diabetes, and oxidative stress. Since our results have been published, the epigenetic clock has been verified across 51 different human tissues and cell types[17].

ELOVL2 is the top gene in our model, meaning its methylation fraction was the most highly correlated with age. Three of the top twelve CpG markers in our model reside in the CpG island in this gene (**Fig. 4**).

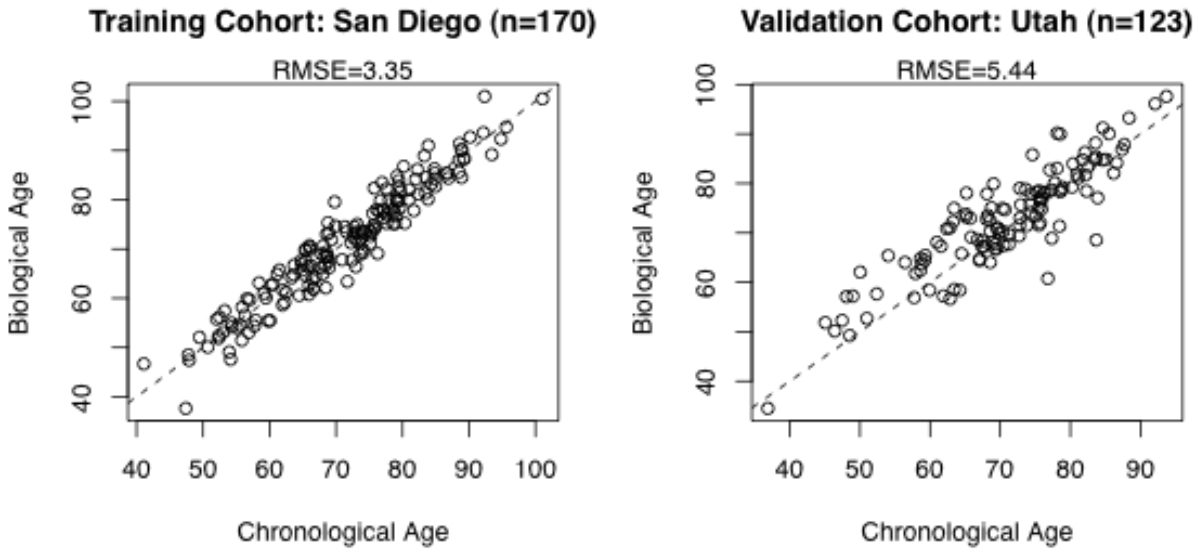

Figure 3. Aging model. Independent training (n=170) and validation (n=123) Caucasian cohorts were used. Methylation marks were assessed using the 450k Illumina methylation array.

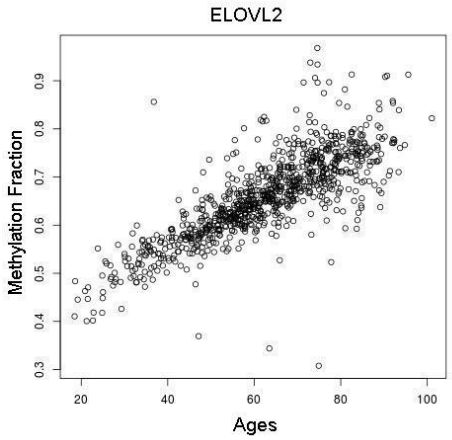

	cgmarker	*Adjusted p value*	*UCSC RefGene Name*
1	*cg16867657*	*1.80E-175*	*ELOVL2*
2	*cg10501210*	*6.62E-122*	
3	*cg22454769*	*6.67E-111*	*FHL2*
4	*cg07553761*	*4.60E-92*	*TRIM*
5	*cg06639320*	*1.61E-87*	*FHL2*
6	*cg24724428*	*6.13E-87*	*ELOVL2*
7	*cg04875128*	*1.54E-86*	*OTUD7A*
8	*cg08097417*	*2.07E-82*	*KLF14*
9	*cg14361627*	*3.32E-81*	*KLF14*
10	*cg19283806*	*2.12E-80*	*CCDC102B*
11	*cg24079702*	*8.15E-79*	*FHL2*
12	*cg21572722*	*5.51E-72*	*ELOVL2*

Figure 4. *ELOVL2* methylation versus age. Methylation fraction versus age for the top methylation marker on *ELOVL2*. Table shows the top 12 markers and their adjusted p-values in the aging model, with *ELOVL2* markers highlighted.

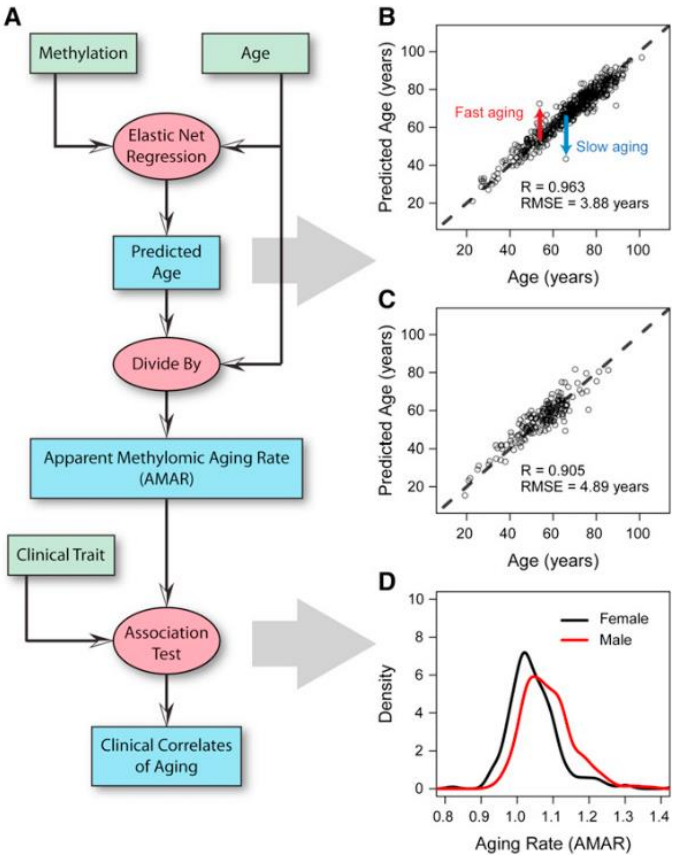

Figure 5. Aging model prediction and clinical variables. A. A flow chart of the data (green boxes) and analyses (red ovals) used to generate aging predictions (blue boxes). B. A comparision of predicted and actual ages for all individuals based on the aging model. C. Out-of-sample predictions for individuals in the validation cohort. D. Apparent methylomic aging rate (AMAR) for each individual, based on the aging model without clinical variables. The distribution of aging rates shows faster aging for men than women. Methylation fraction versus age for *ELOVL2*. *Adapted from Hannum, et. al.

CHAPTER 1: INVESTIGATION OF ELOVL2 IN AGING CELLS.

ELOVL2 baseline expression in WI-38 cells

WI-38 and IMR90 cell lines have been previously established as models of cellular aging. It has been shown that both cell lines show significant changes in phenotype over time and population doubling (PD) number[46,47]. Their growth rate, as shown by confluency measured by imaging software, markedly decreases from lower PD to higher PD. The percentage of senescence-positive cells, as measured by senescence associated-beta-galactosidase staining (SA-β-Gal) increases as PD grows, and their morphology changes from a more elongated shape to a broader, flatter shape (**Fig. 6**).

The most significant age-correlated methylation marks for *ELOVL2* are located within its promoter region. Because methylation marks in promoter regions typically are associated with gene repression[48], we would expect that expression of *ELOVL2* decreases with age, as its promoter methylation increases. To investigate the changes in level of *ELOVL2* promoter methylation in aging WI38 and IMR90 cells, we used Methylated DNA Immunoprecipitation (MeDIP). We designed primers encompassing the specific CpGs described in our previous work. Using this approach, we found that promoter methylation increases with increasing cell population doubling (**Fig. 7**). As it has been previously shown that methylation of the promoter region is inhibitory for transcription[49], we investigated whether the expression level of *ELOVL2* inversely correlates with ELOVL2 promoter methylation. Using qRT-PCR, we found that the expression level falls as cells age (**Fig. 7**). We concluded that ELOVL2 expression is downregulated in aging cells, which is accompanied by an increased level of ELOVL2 promoter methylation and increased number of senescent cells in culture.

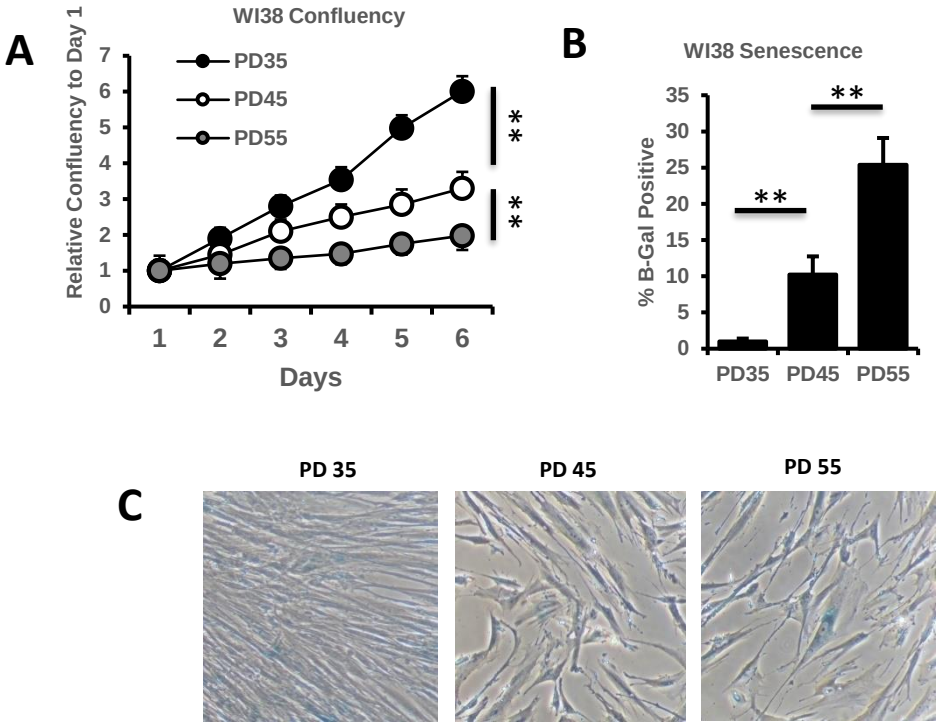

Figure 6. Aging characteristics of WI38 cells. A. Proliferation of WI38 cells as measured by surface area covered at population doublings (PD) 35, 45, 55. B. Percent senescence by beta-galactosidase staining in WI38 cells. C. Representative images of cell morphology and beta-galactosidase staining of WI38 cells. (**p<0.005, t-test)

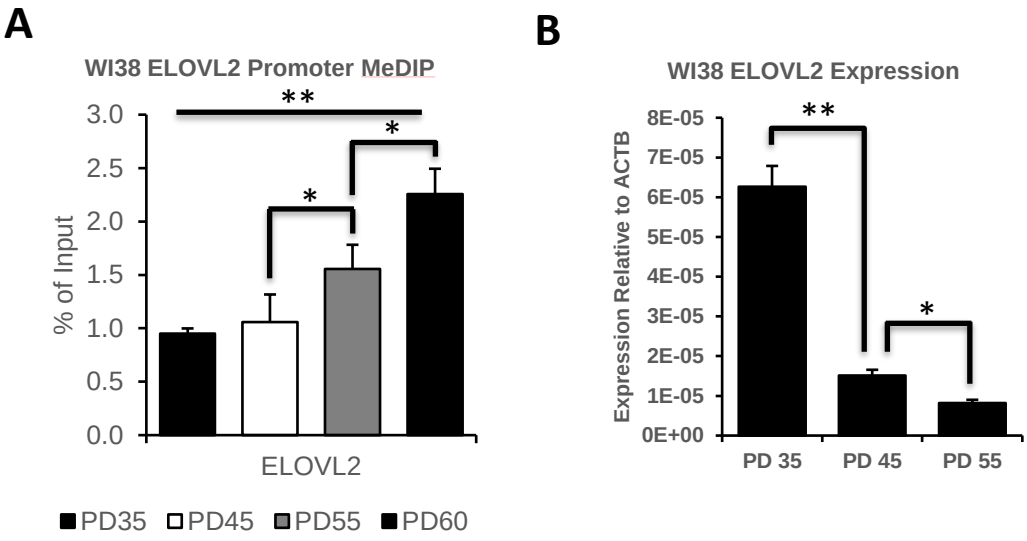

Figure 7. ELOVL2 expression and methylation in WI38 cells. A. ELOVL2 expression by qPCR in WI38 cells at PD35, 45, 55. (**p<0.005 ANOVA, *p<0.05, t-test) B. Methylation level in ELOVL2 promoter region in WI38 cells by methylated DNA immunoprecipitation followed by qPCR. Primers amplify region containing CpG markers cg16867657, cg24724428, and cg21572722.

WI-38 cell methylation age and aging phenotypes.

To study aging in the context of our methylation model in cell lines, we validated that methylation age correlates with population doubling (PD) number according to our Elastic Net regression model, shown below. Methylation data was obtained by Illumina Infinium BeadChip assay.

Cell line		PD number	Methylation Age
WI38	Young	PD33.77	-13
	Middle	PD 42.76	2.78
	Old	PD 63.7	4.33

Figure 8. Methylation age of WI-38 cells calculated by our aging model.

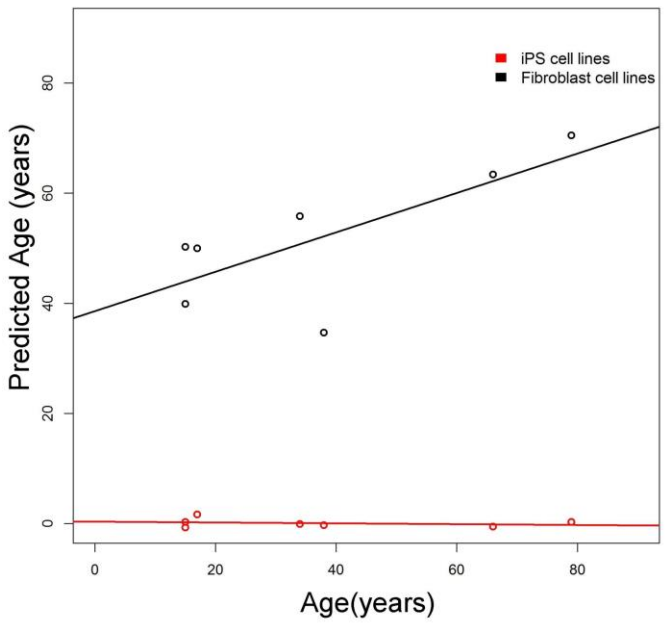

Figure 9. Cell line methylation aging. Predicted age versus actual age using our aging model of iPS and fibroblast cell lines derived from patients.

Furthermore, we found that fibroblast cell line predicted ages are correlated with actual ages of patients they were derived from, while iPS cell lines generated from patients all had a predicted age around 0 using our model (**Fig. 9**). We have also observed that as passage number increases in WI-38 and IMR-90 cells, proliferation rate decreases, and senescence increases. Around PD 60, proliferation stops completely, and all cells are senescent.

***ELOVL2* knockdown in fibroblasts.**

We then asked whether we could influence cellular aging by modulating the expression of ELOVL2. First, using lentiviral shRNA, we knocked down *ELOVL2* expression in WI-38 and IMR-90 cells (**Fig. 11,12**) and observed a significant decrease in proliferation rate, an increased number of senescent cells in culture as detected by SA-β-Gal staining, and a change in morphology to that similar to the morphology of older cells. All the observations together indicated an increase in apparent fibroblast age. Of two candidate shRNAs, shE1 and shE4, shE4 was a more efficient knockdown, and displayed larger changes in aging phenotypes (**Fig. 10, 13, 14, 15**).

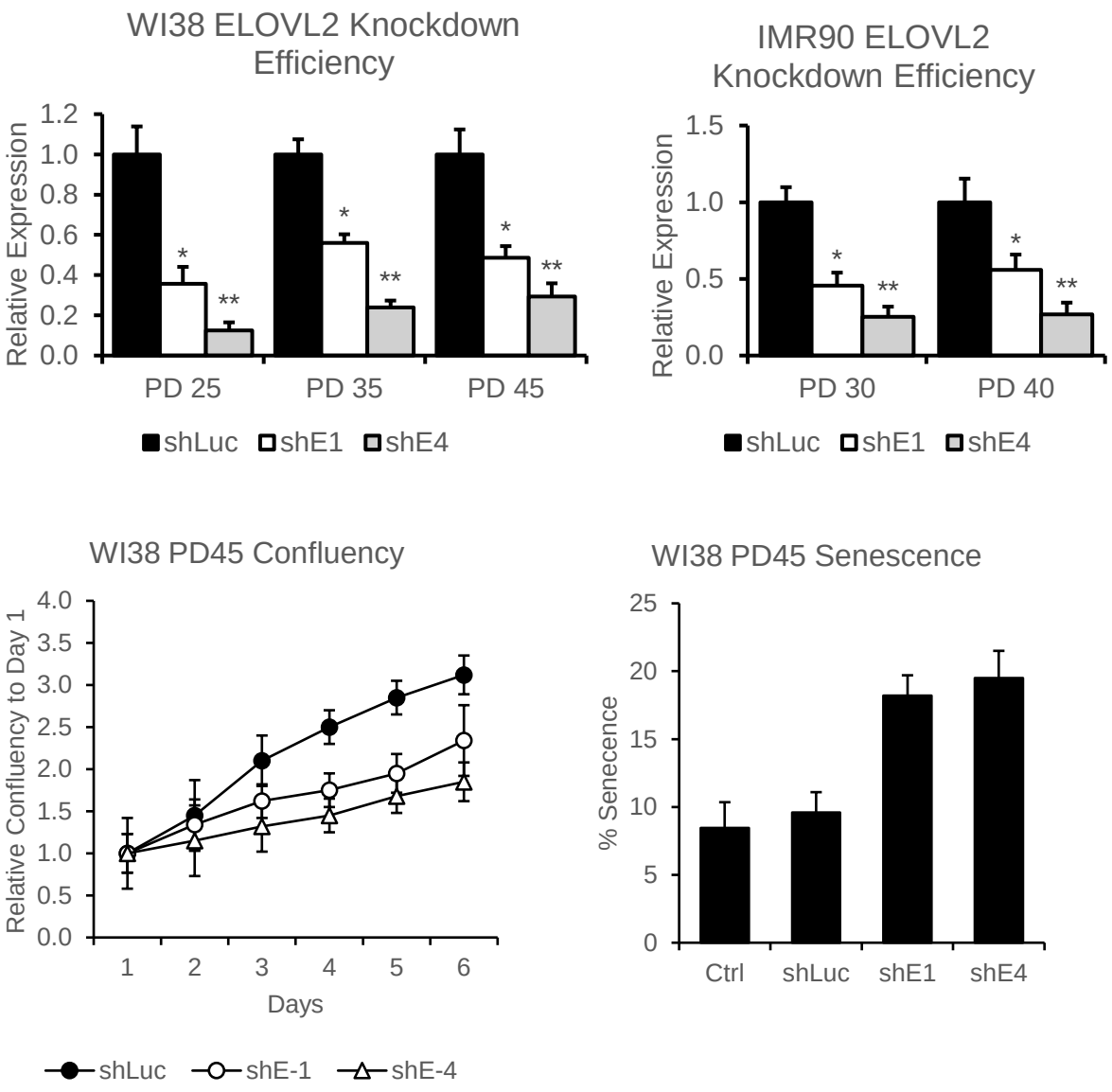

Figure 10. ELOVL2 knockdown candidates. shE1 and shE4 WI-38 cell lines were generated. shE4 was the most effective knockdown, and thus was chosen for subsequent experiments.

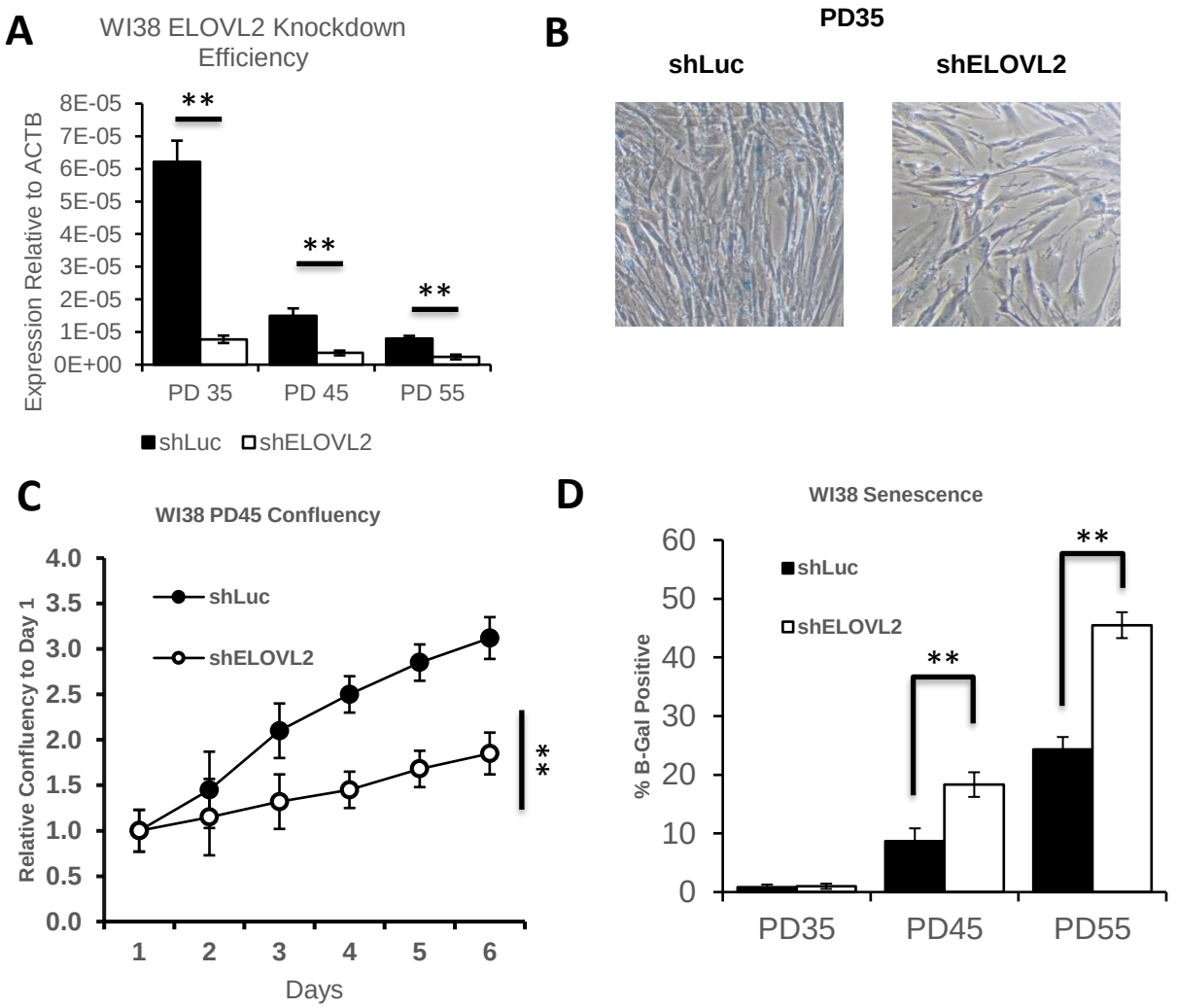

Figure 11. Knockdown efficiency and aging characteristics of ELOVL2 knockdown WI-38 cells, including morphology, proliferation rate, and senescence. A. ELOVL2 knockdown efficiency in WI38 cells by qPCR. B. Representative images of cell morphology and beta-galactosidase staining of ELOVL2 knockdown WI38 cells, compared to luciferase knockdown controls. C. Proliferation of WI38 knockdown cells and Luciferase knockdown controls as measured by surface area covered over time. D. Percent senescence by beta-galactosidase staining in WI38 knockdown cells. (*p<0.05, **p<0.005, t-test).

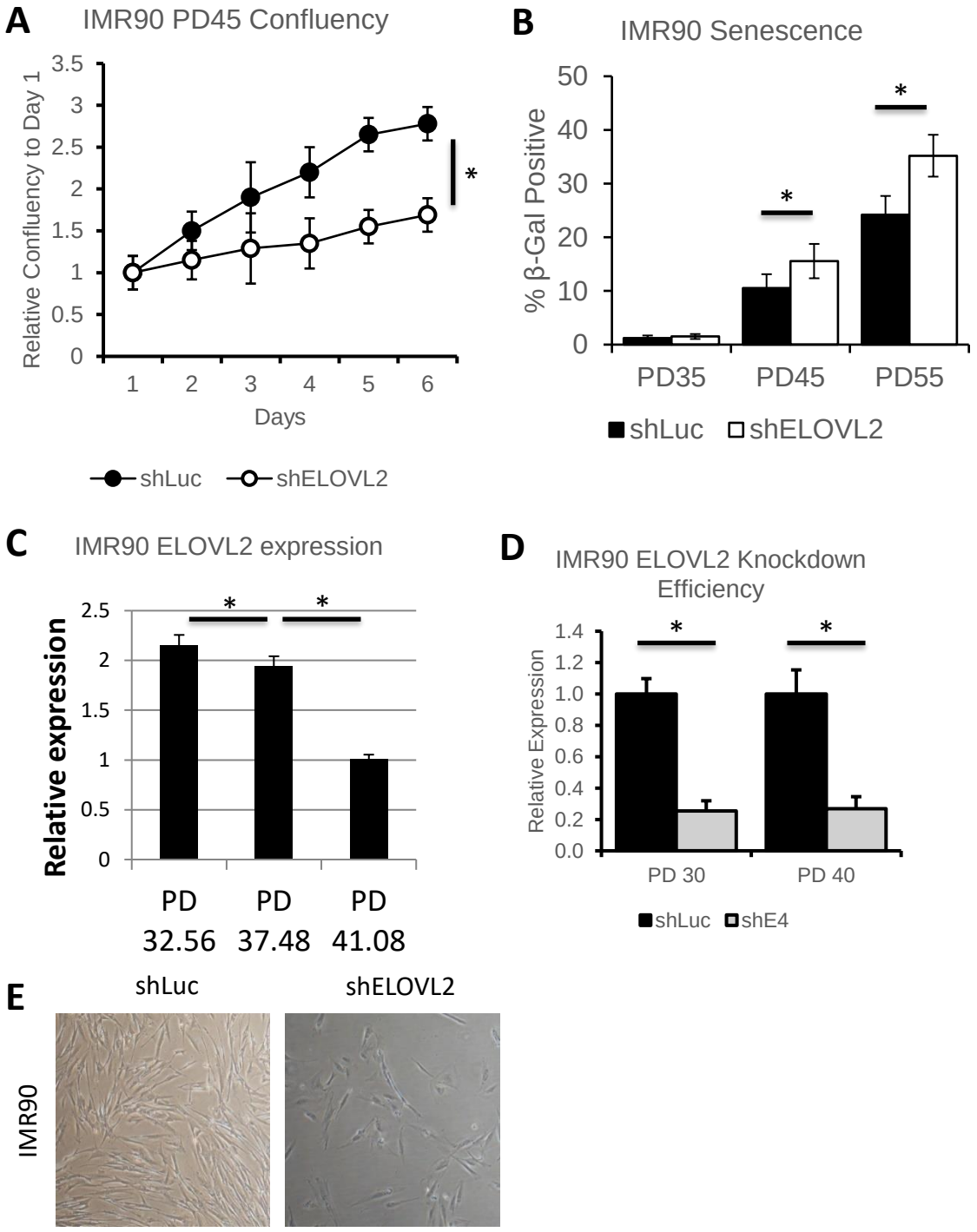

Figure 12. Knockdown efficiency and aging characteristics of ELOVL2 knockdown IMR-90 cells. A. Proliferation of IMR90 cells as measured by surface area covered at population doublings (PD) 35, 45, 55. B. Percent senescence by beta-galactosidase staining in IMR90 cells. C. ELOVL2 expression by qPCR in IMR90 cells. D. ELOVL2 knockdown efficiency in IMR90 cells by qPCR. E. Representative images of ELOVL2 knockdown morphology with luciferase knockdown control in IMR90 cells. (*p<0.05, **p<0.005, t-test)

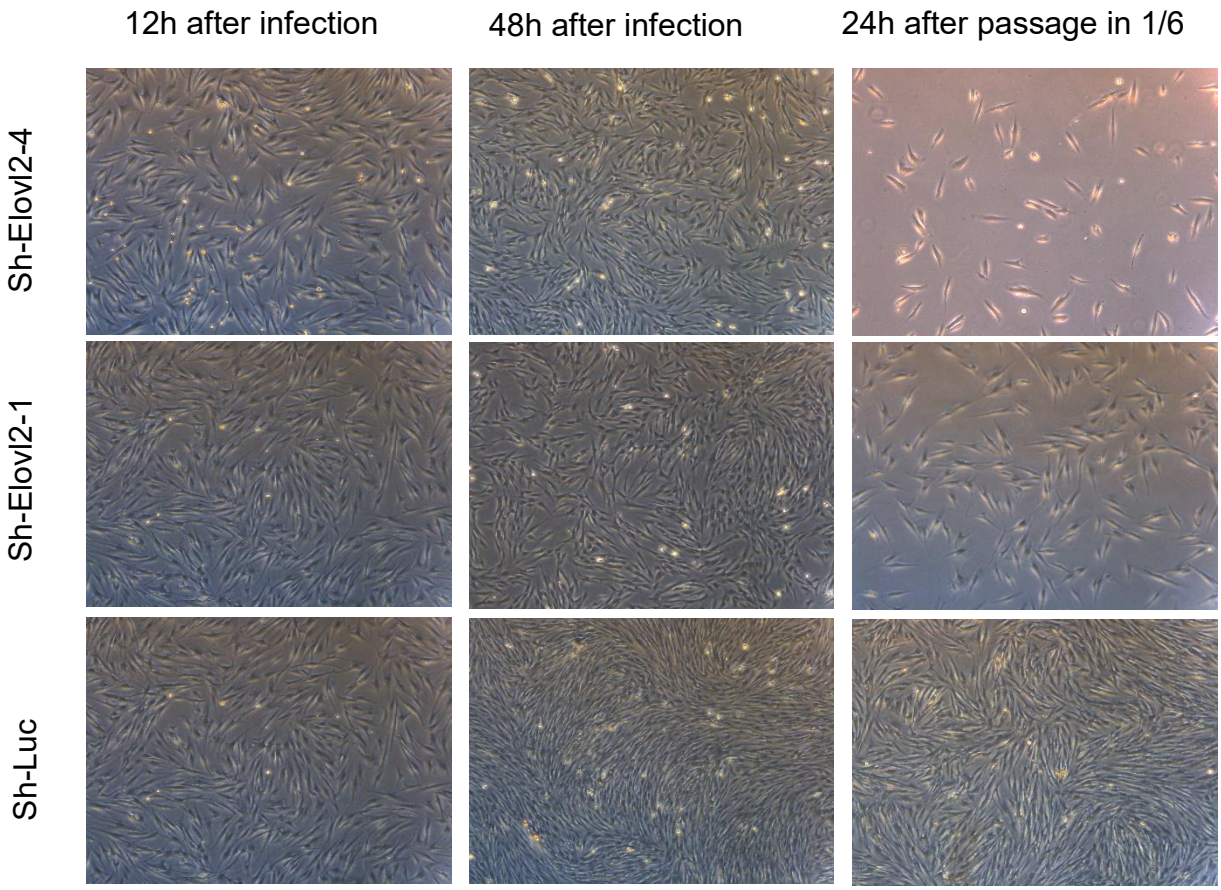

Figure 13. ELOVL2 knockdown morphology.

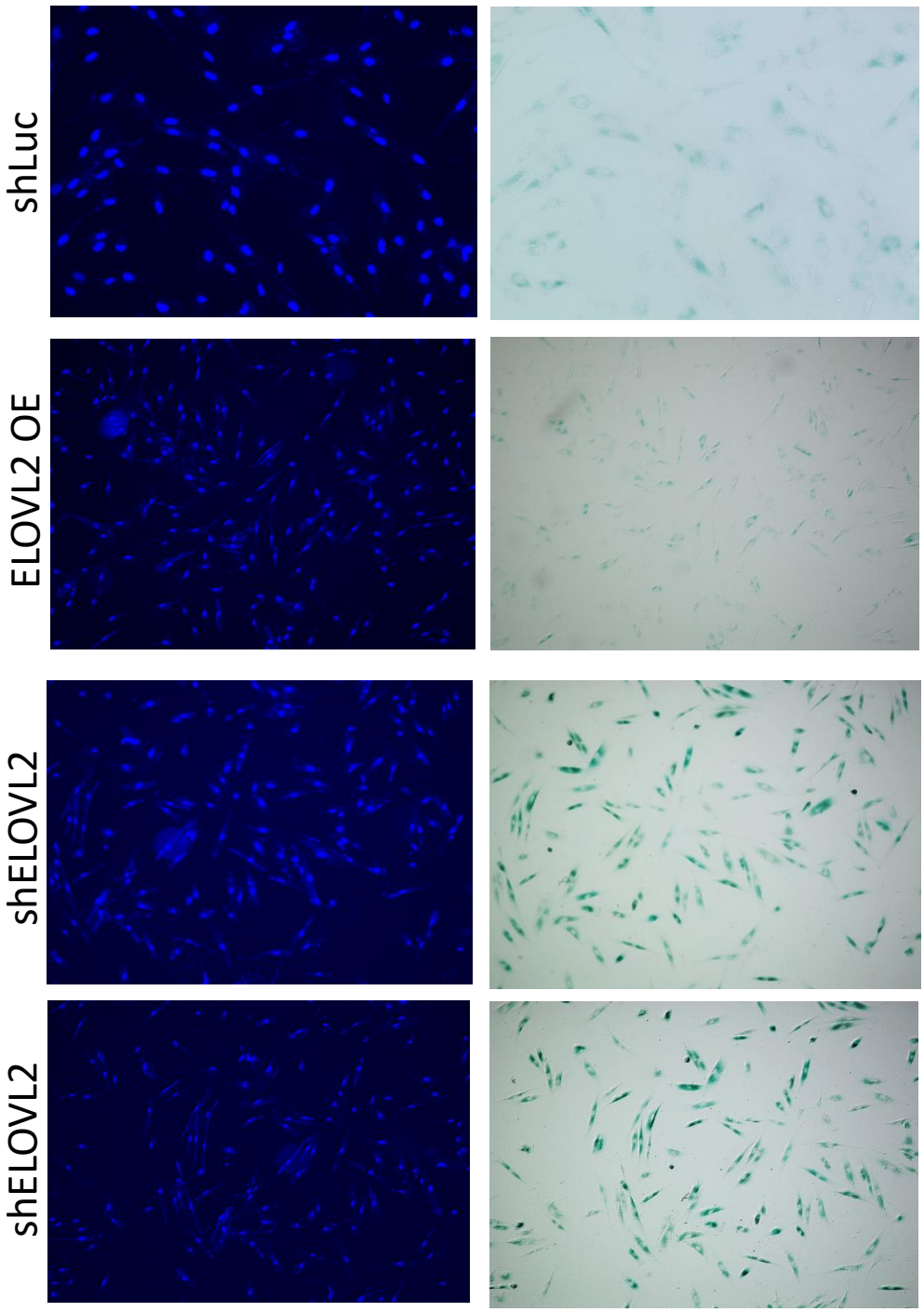

Figure 14. ELOVL2 knockdown and overexpression cell senescence. Staining of PD35 WI-38 ELOVL2 knockdown and overexpressing cells. DAPI staining is shown on the left, and beta-galactosidase staining is shown on the right.

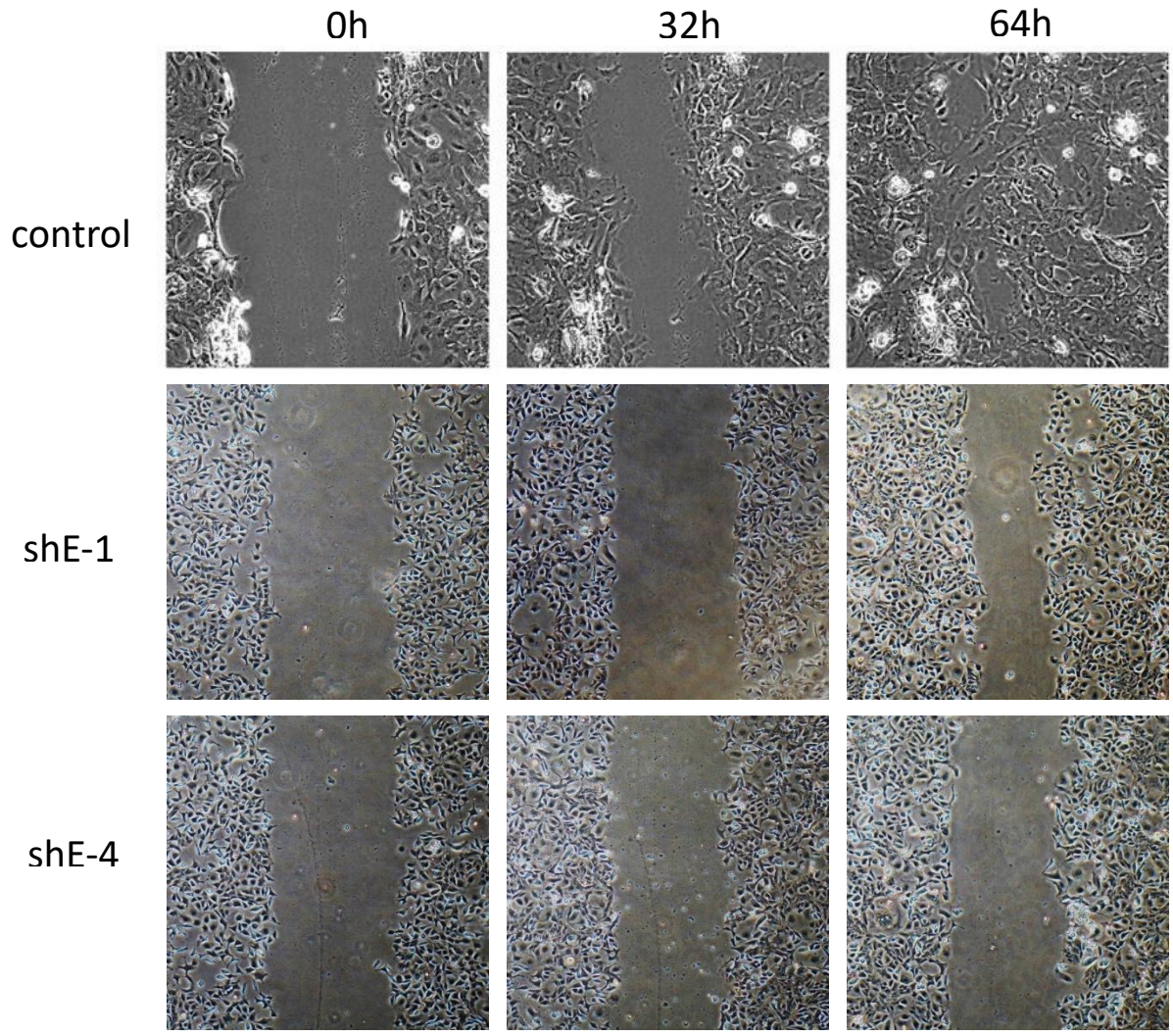

Figure 15. Scratch wound experiment in knockdown cells. Cells were subjected to scratch wounds, then allowed to recover for 64 hours.

***ELOVL2* overexpression in fibroblasts.**

Next, we asked whether we could rescue aging phenotypes in cells by overexpressing *ELOVL2*. Using a cumate-inducible DNA construct, we transduced WI-38 and IMR-90 cells and treated them with cumate for the duration of the experiment. We found no differences in proliferation or senescence characteristics (**Fig. 16**), but there was an increase in survival after cells reach the age of proliferation arrest, at 56 population doublings (**Fig. 17**).

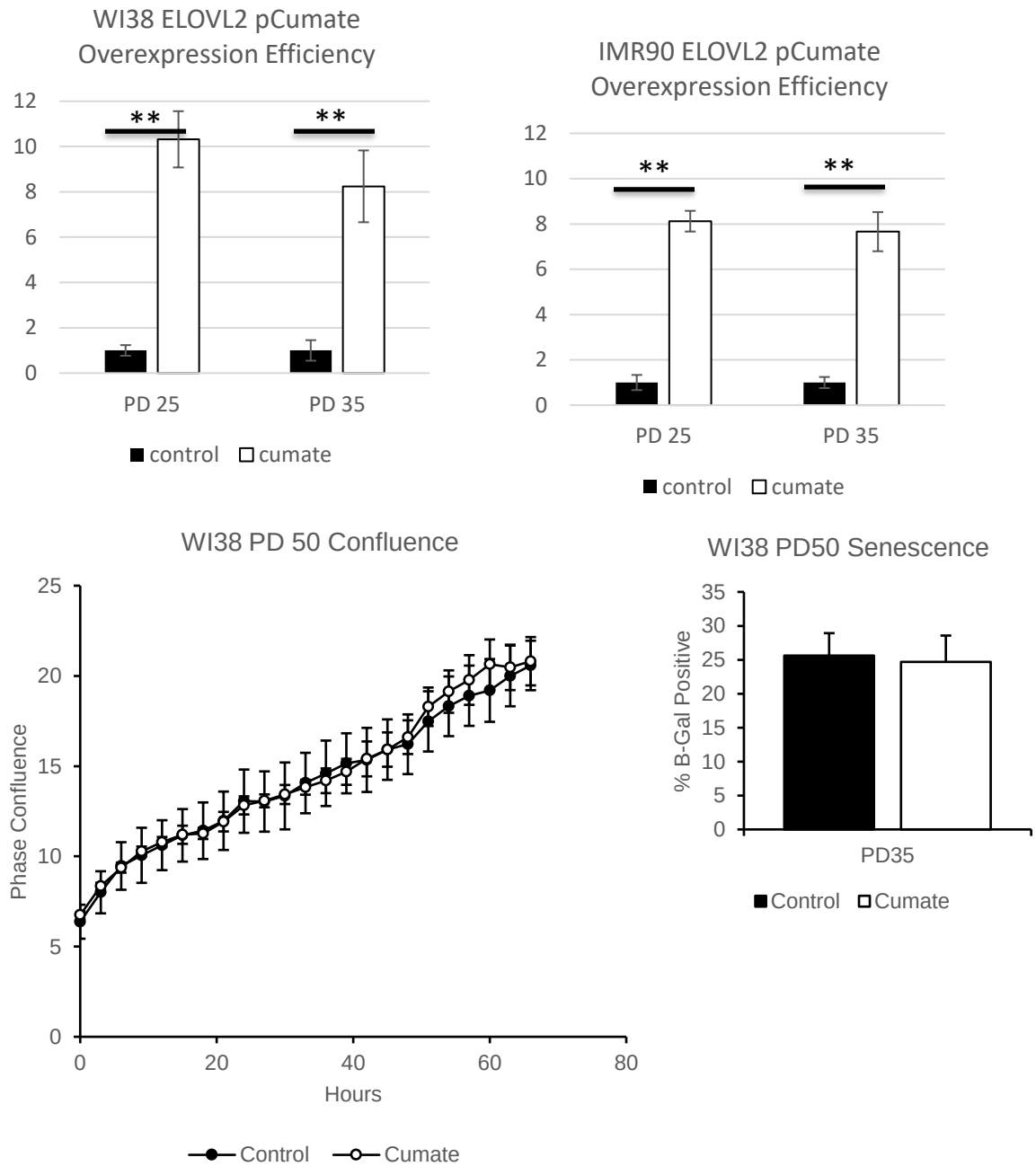

Figure 16. ELOVL2 overexpression efficiency and aging characteristics of ELOVL2-overexpressing WI-38 cells, shown by proliferation rate and senescence.

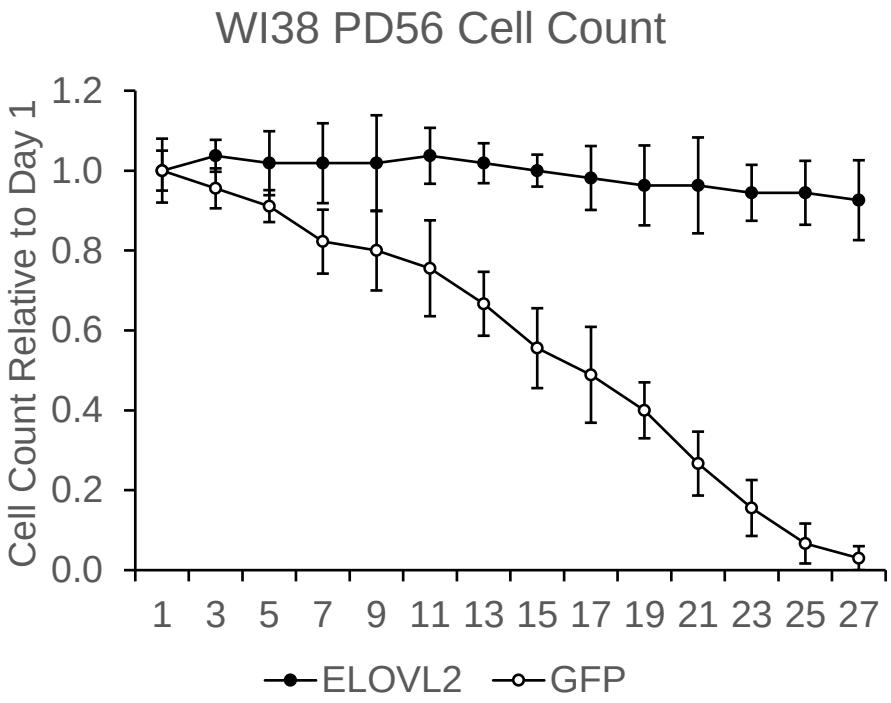

Figure 17. Increased survival of ELOVL2 overexpressing cells.

Screen of aging-related drugs.

Having identified *ELOVL2* as a gene that correlates with cellular age, we next asked whether we could pharmacologically influence *ELOVL2* along with cellular age. We screened docosahexaenoic acid (DHA), mitochondrial open reading frame of the 12S rRNA-c (MOTS-c), growth differentiation factors 9 and 11 (GDF9, GDF11), and fibroblast growth factors 1 and 2 (FGF1, FGF2), metformin (Met), and L-ascorbic acid (Vc) for effect on *ELOVL2* expression by qRT-PCR. DHA is the product of the fatty acid elongation pathway of which *ELOVL2* is the limiting enzyme (**Fig. 44**). MOTS-c is a peptide encoded in the mitochondrial genome which protects against age- and diet-dependent insulin resistance and obesity[50]. Metformin is a commonly used anti-diabetic drug that activates AMPK, which can potentially extend lifespan[51].

We found that of these chemicals, only ascorbic acid significantly influenced cellular aging phenotypes and *ELOVL2* expression (**Fig. 18**).

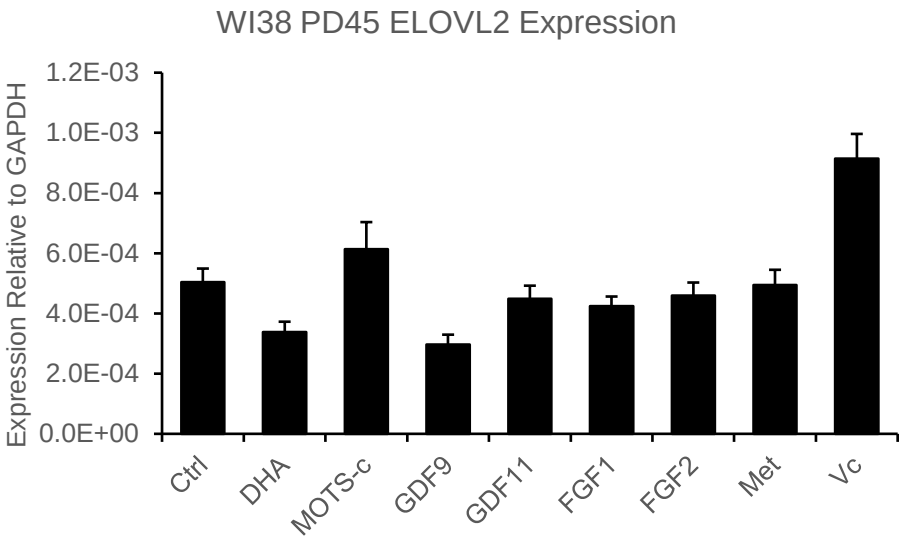

Figure 18. Chemical screen of aging-related drugs by qPCR of *ELOVL2* and *KLF14*.

Vitamin C treatment in fibroblasts.

To further examine the influence of ascorbic acid on cellular aging, we treated WI-38 and IMR-90 fibroblasts with L-ascorbic acid (Vc) and two derivatives of Vc, dehydroascorbic acid (DHAA) and L-ascorbic acid 2-phosphate (VcP). At low concentration (0.3 mM), Vc and VcP both increased proliferation and decreased senescence, while DHAA did not significantly alter either phenotype. At high concentration (1.2 mM), Vc and DHAA were detrimental to aging phenotypes, decreasing proliferation and increasing proliferation. VcP, however, remained beneficial, increasing proliferation and decreasing senescence. In addition, *ELOVL2* expression correlated with these phenotypes, increasing with increasing proliferation and decreasing senescence (**Fig. 19**).

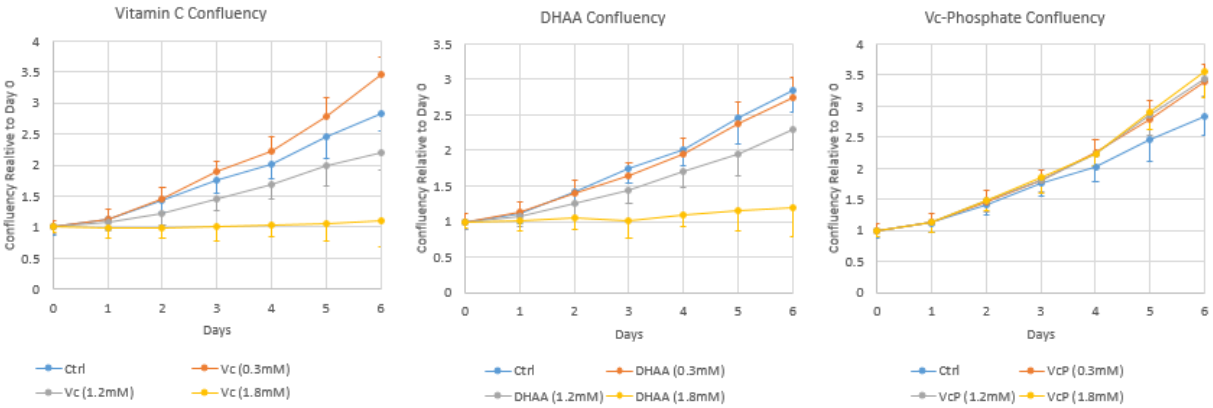

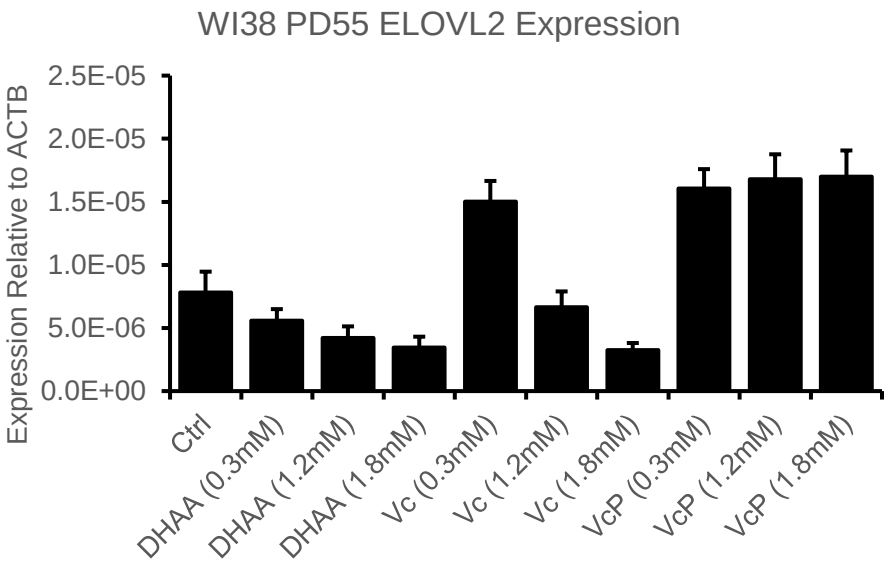

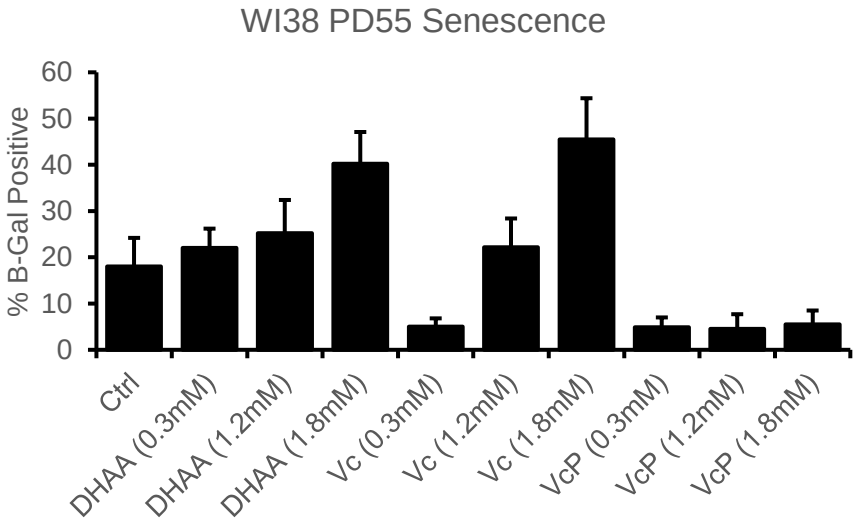

Figure 19. Effects of DHAA, Vc, and VcP on WI-38 fibroblast proliferation, senescence, and *ELOVL2* expression.

In addition, we assayed the antioxidant properties of Vc, VcP, and DHAA. We found that while Vc and VcP reduced ROS in cell culture, DHAA did not (**Fig. 20**). Interestingly, Vc decreased ROS at both low and high concentrations, a contrast from its detrimental effects on senescence and proliferation at high concentration (**Fig. 19**). This suggests that Vc could be acting through a mechanism other than as an antioxidant to influence cellular aging.

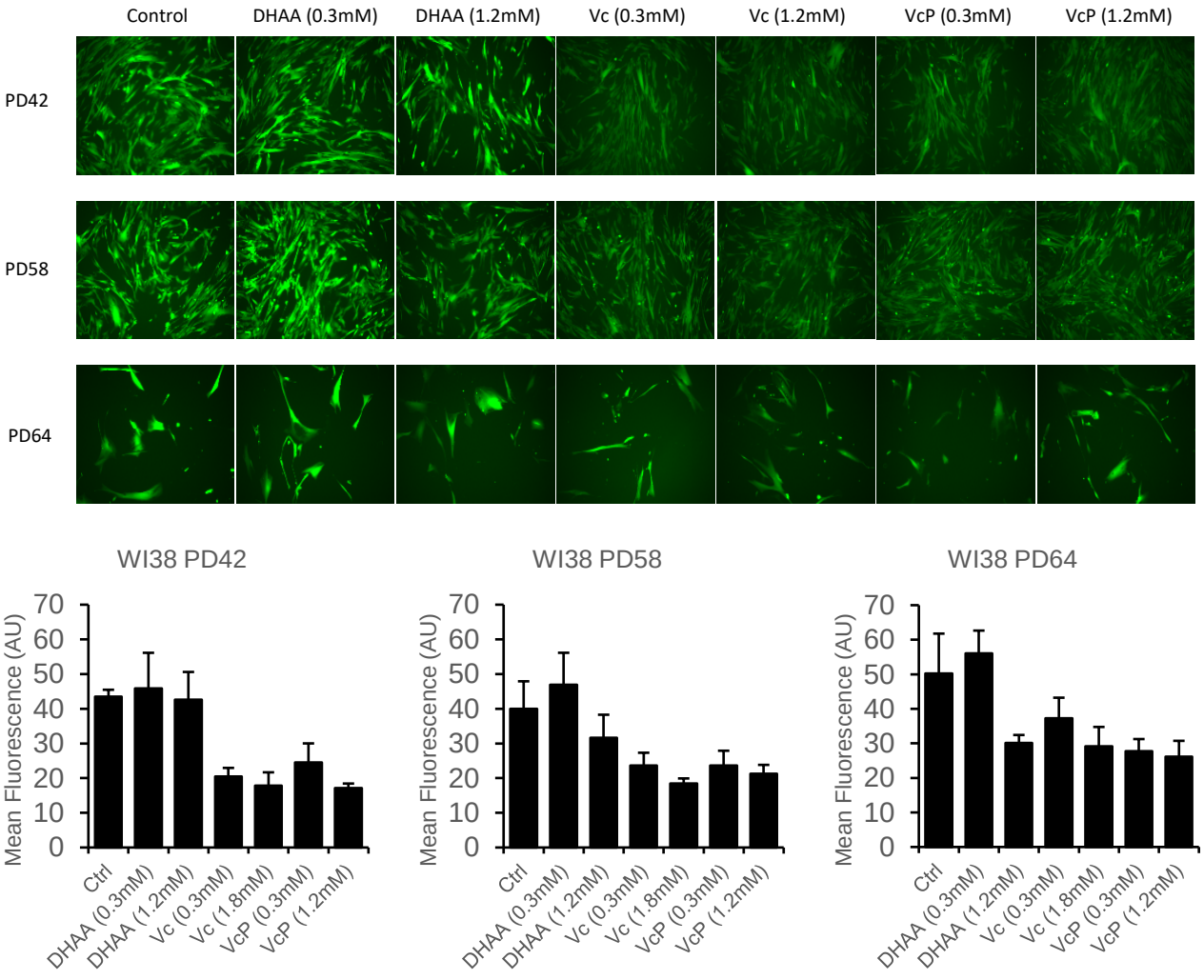

Figure 20. Reactive oxygen species assay on vitamin C-treated WI-38 cells.

5-deoxy-2-azacytidine treatment in fibroblasts.

Next, we decided to affect the methylation level of *ELOVL2* promoter in an attempt to influence the expression of the ELOVL2. To do that, we treated WI-38 fibroblasts with 5-Aza-2-deoxycytidine (5-Aza), a well-known cytidine analog that inhibits DNA methyltransferase[52]. We treated the cells for 2 days with 2μM 5-Aza and we continued the culture for next 5 days without the compound. At the end of experiment, we assessed the expression of ELOVL2 by qRT-PCR. Interestingly, we found that upon treatment with 5-Aza, *ELOVL2* promoter methylation is reduced, while *ELOVL2* expression is upregulated. Moreover, upon 5-Aza treatment a lower number of senescent cells is observed in culture (**Fig. 21**). These data suggest that decreasing *ELOVL2* promoter methylation positively influences *ELOVL2* expression, and apparent age of fibroblasts.

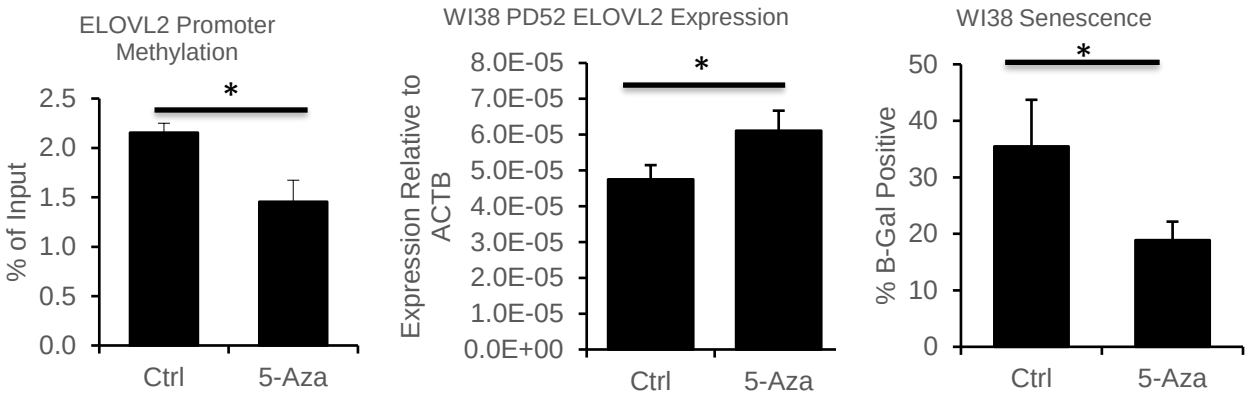

Figure 21. Effects of 5-Aza on *ELOVL2* methylation, expression, and senescence in WI-38 cells.

CHAPTER 2: INVESTIGATION OF ELOVL2 IN AGING MICE.

Vision is among the top predictors of aging. Visual contrast sensitivity score was among the top 5 individual predictors relative to 377 variables evaluated[53]. ELOVL proteins are highly expressed in eye, and several of them have been implicated in eye diseases[54,55]. However, in our methylation model only *ELOVL2* contains methylation marks that are highly correlated with age[1]. Therefore, we investigated whether the expression level of *Elovl2* in wild-type C57BL/6 mouse retinas is changing with mice age. We found by qRT-PCR and Western blot that, similarly to data obtained in aging human fibroblasts, expression level of ELOVL2 inversely correlates with age of the animal. Additionally, our MeDIP analysis indicated that ELOVL2 promoter methylation in the retina increases with age of the animal (**Fig. 22**).

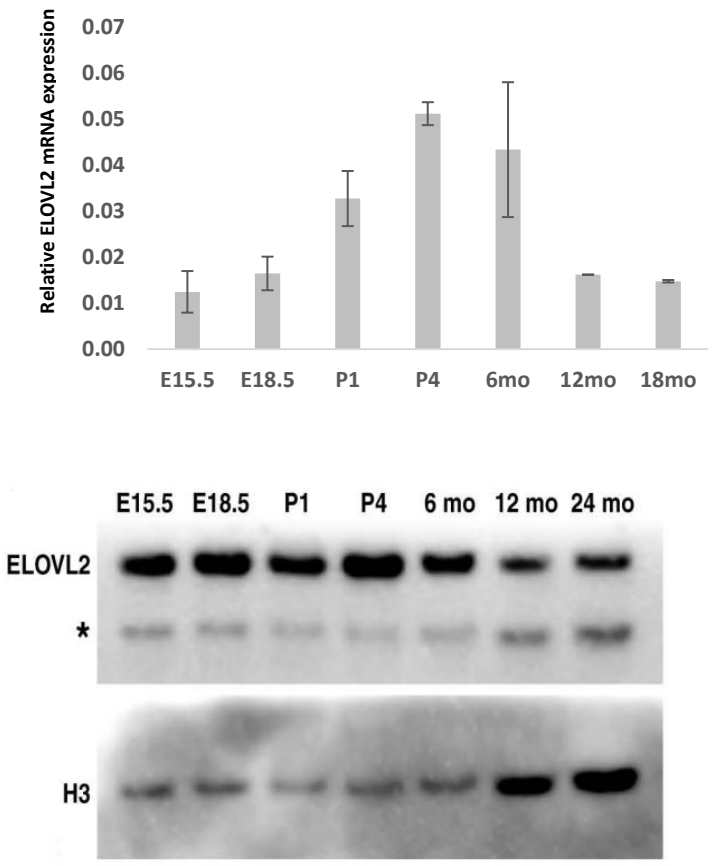

Figure 22. *ELOVL2* RNA and protein expression in mice of varying age.

Next, we evaluated whether the visual performance and eye structure are changing during the studied age span of animal. First, we evaluated structural changes using fundus autofluorescence imaging of wild-type C57BL/6 mice at the ages of 2 months, 6 months, 1 year, and 2 years. We observed that autofluorescent punctate aggregates begin to appear in the fundus at 1 year of age, and are very pronounced at 2 years of age (**Fig. 23, 24**). Then to evaluate the visual function of the aging mice, we performed electroretinogram (ERG) analysis. As mice age, the number and sensitivity of rods decreases[56]. Indeed, older mice displayed decreased scotopic response amplitude

by ERG (**Fig. 23, 25**). In addition, oscillatory potentials and flicker response decreased in older mice (**Fig. 26**).

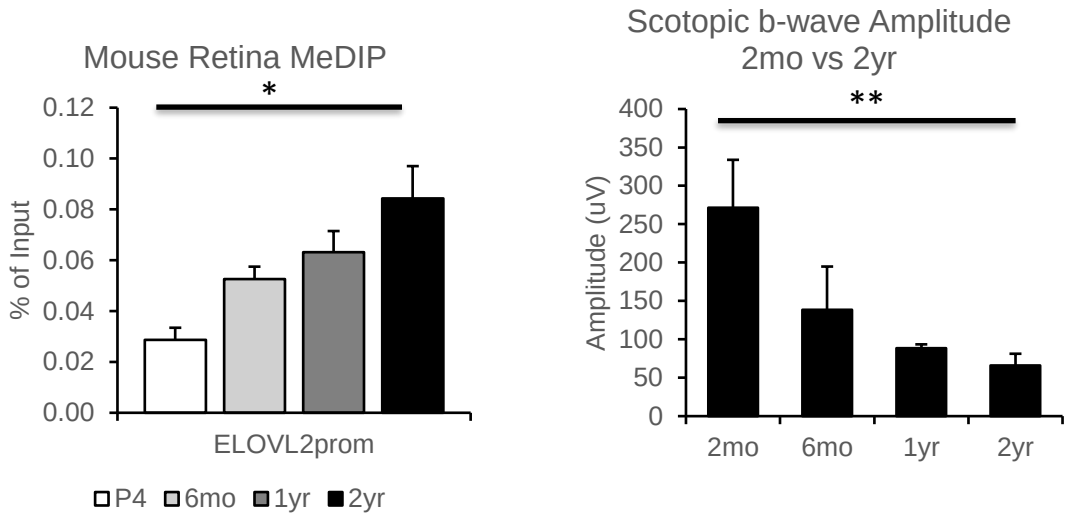

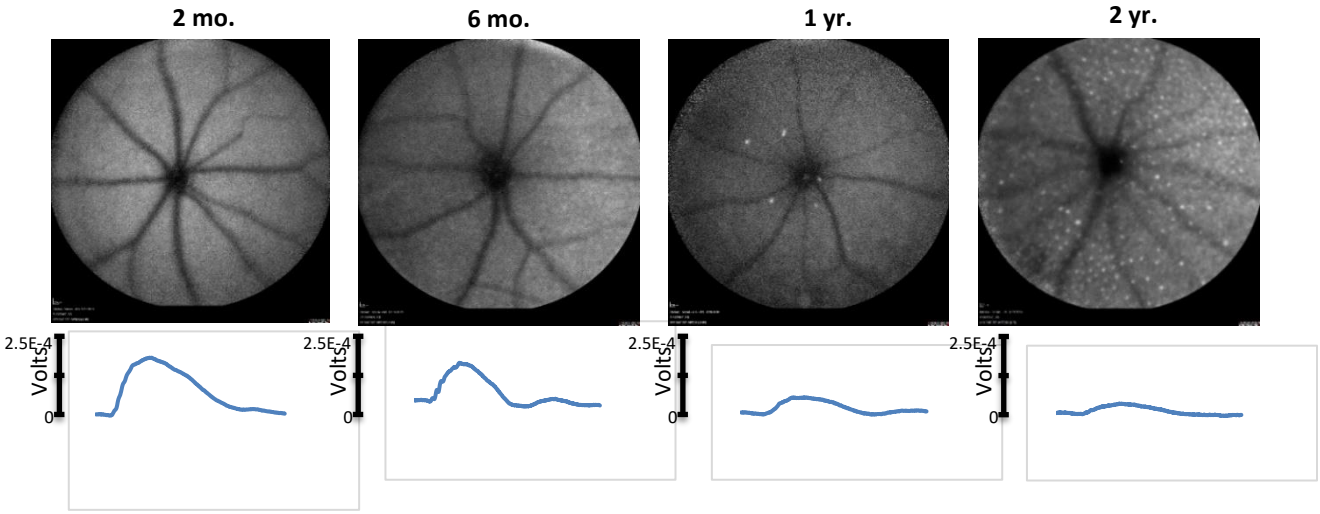

Figure 23. *ELOVL2* methylation, fundus autofluorescence images, and scotopic response in retinas of mice of varying age.

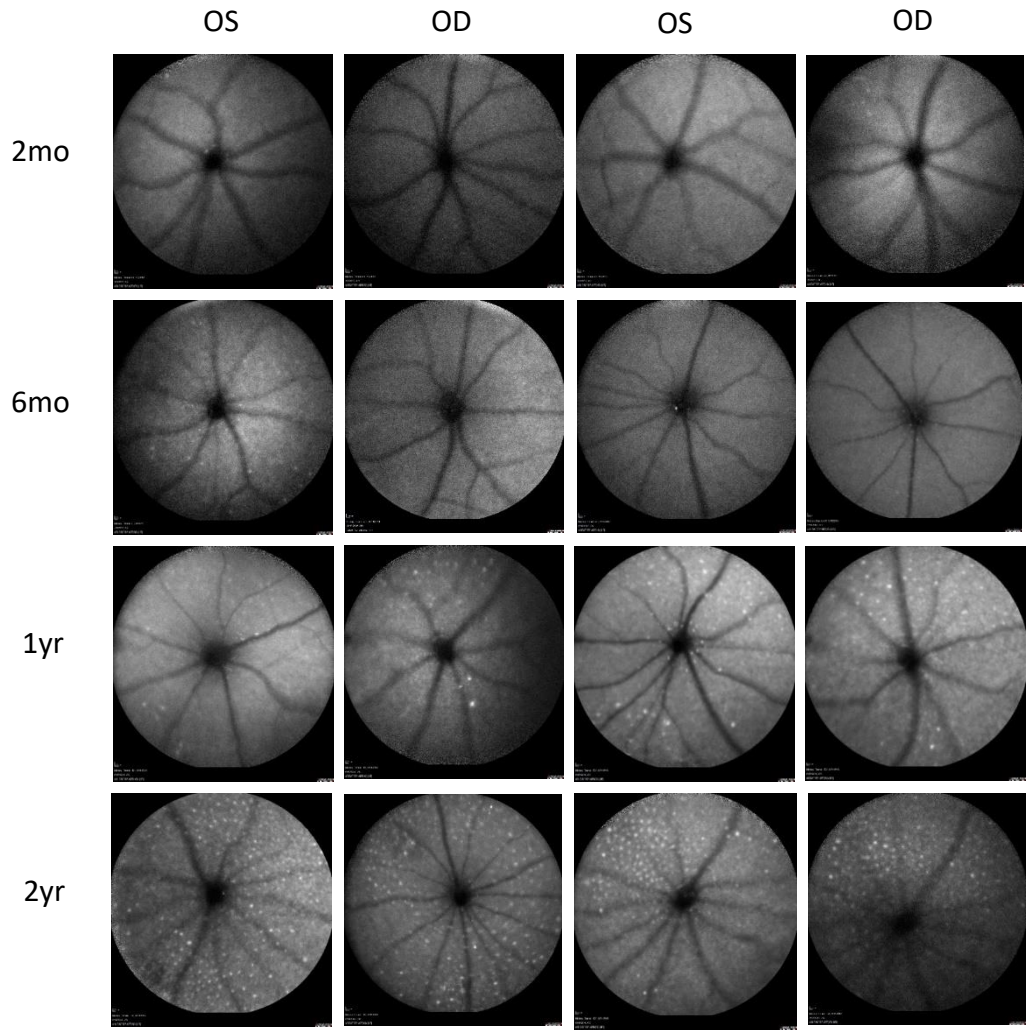

Figure 24. Additional fundus images of aging mice.

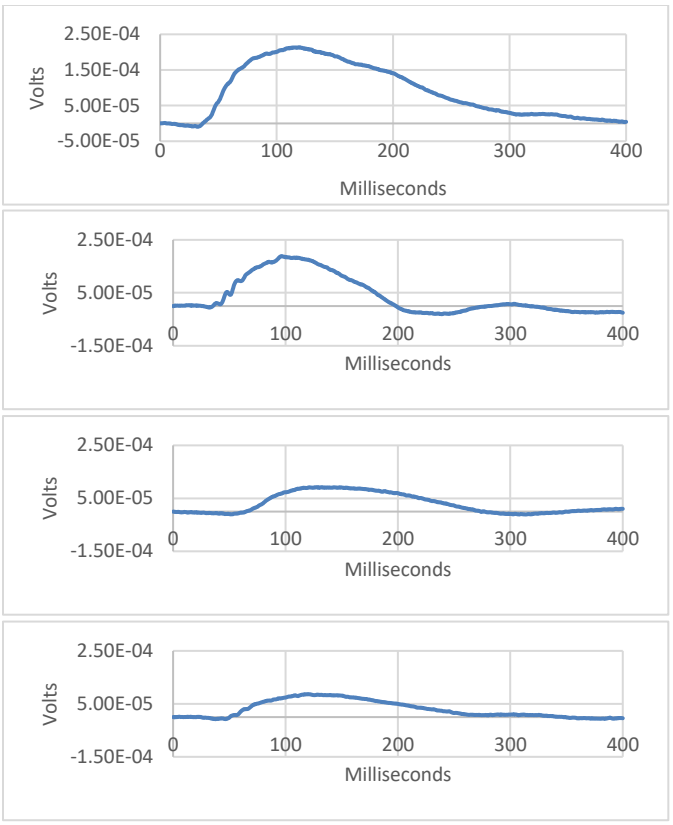

Figure 25. Additional scotopic response traces of aging mice.

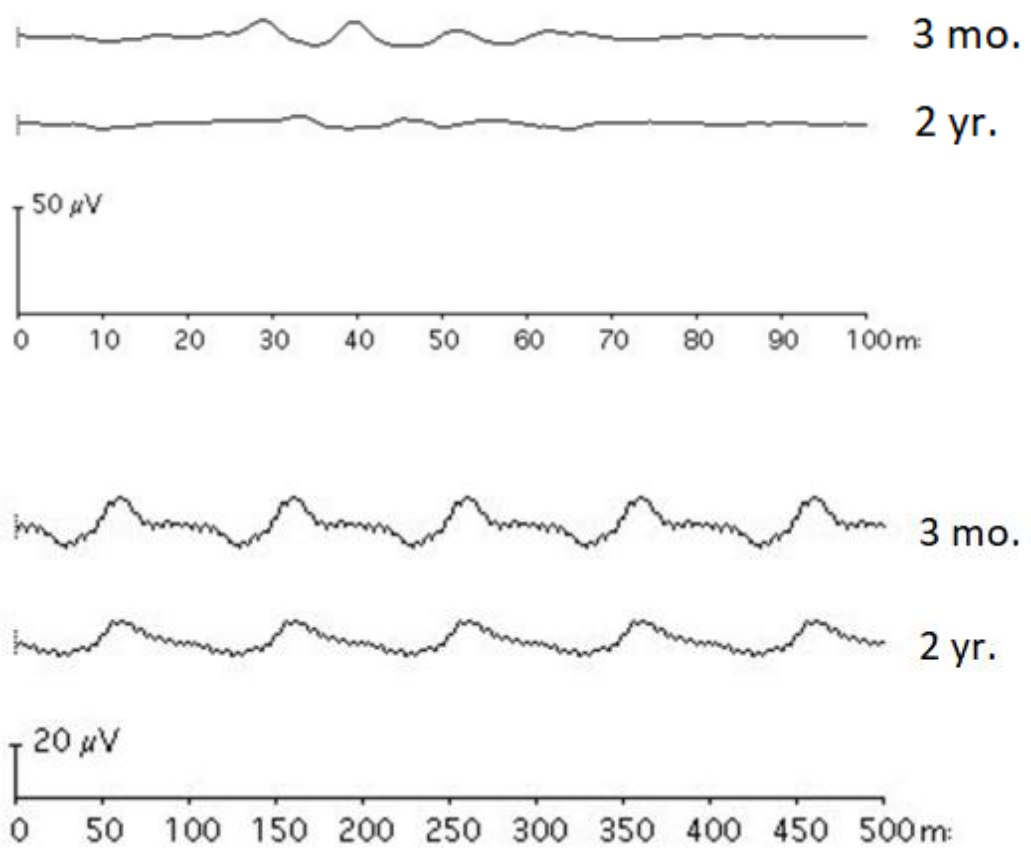

Figure 26. Additional ERG traces of aging mice. Top: oscillatory potentials from ERG in 3-month and 2-year old wild-type mice. Bottom: 10 Hz flicker response from ERG in 3-month and 2-year old wild-type mice.

In parallel, we investigated the Elovl2 promoter methylation and mRNA expression levels in the retinas dissected from Ames dwarf mice, which live significantly longer and exhibit many symptoms of delayed aging compared to wild-type mice[57]. We found that aged Ames mouse retinas display lower *Elovl2* promoter methylation and increased expression when compared to aged wild-type mice (**Fig. 27**). This suggests that ELOVL2 expression and methylation might be indicative of animal health.

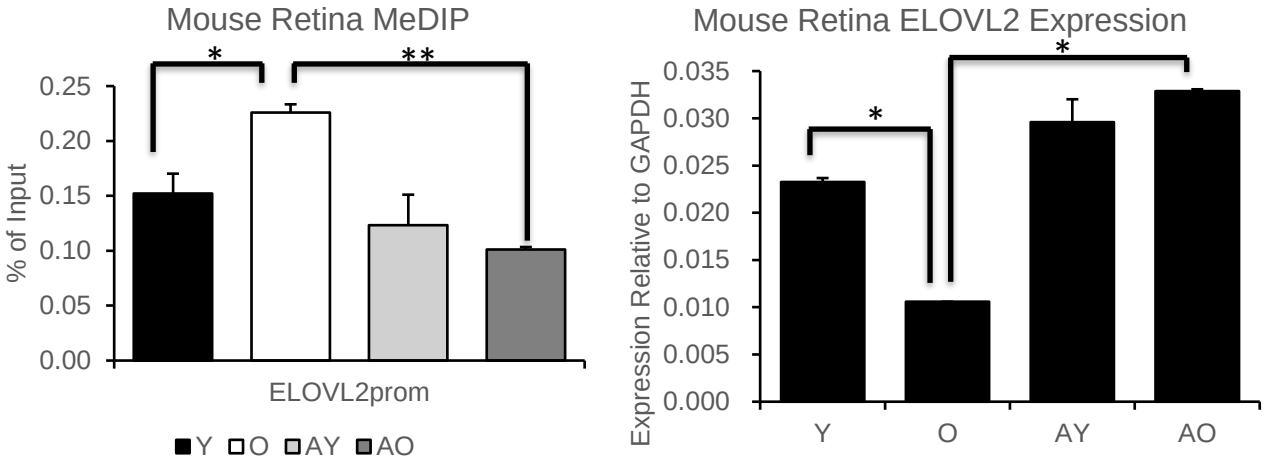

Figure 27. *ELOVL2* methylation and expression in young and old wild-type and Ames dwarf mice. Y=3 months, O= 2 years, A=Ames.

***Elovl2* knockout mice.**

To determine if *Elovl2* plays a role in aging on an organismal scale, we generated *Elovl2* knockout mice. Due to the importance of *Elovl2* to male fertility in mice[58], we were not able to establish a colony. However, we did find some aging phenotypes in the founding population. Heterozygous knockout mouse livers contained more senescent cells (**Fig. 28**). Mouse Het 4 had further increased liver senescence due to the presence of a tumor.

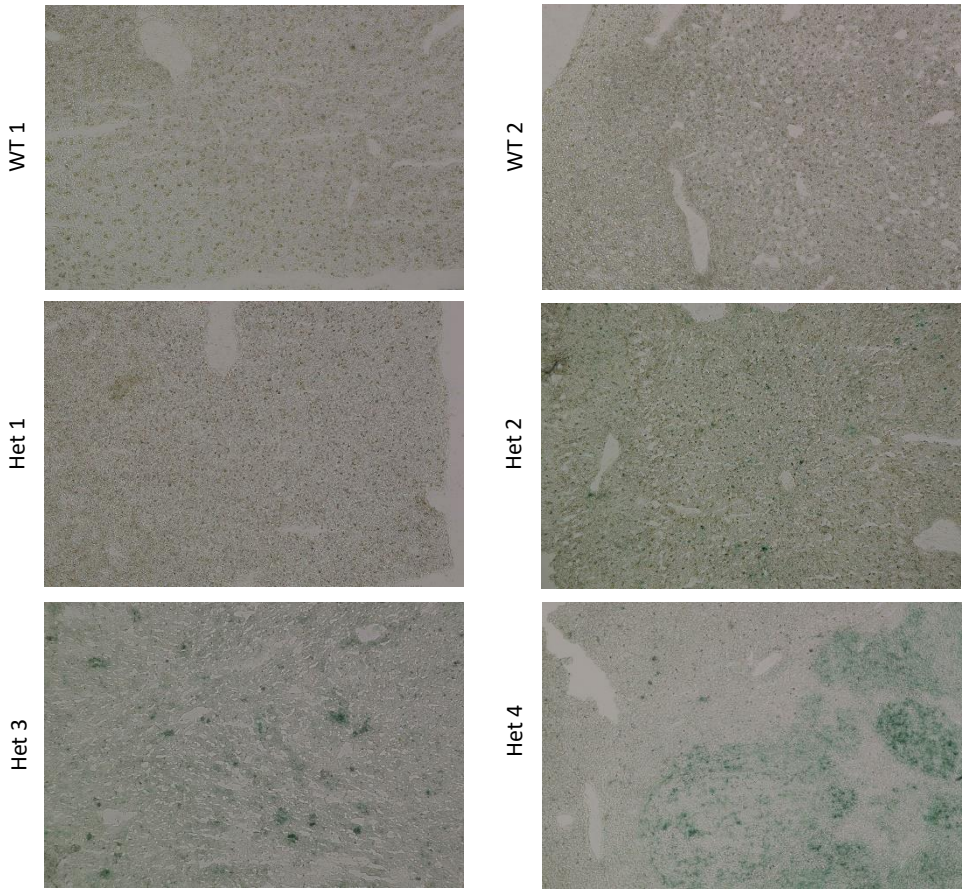

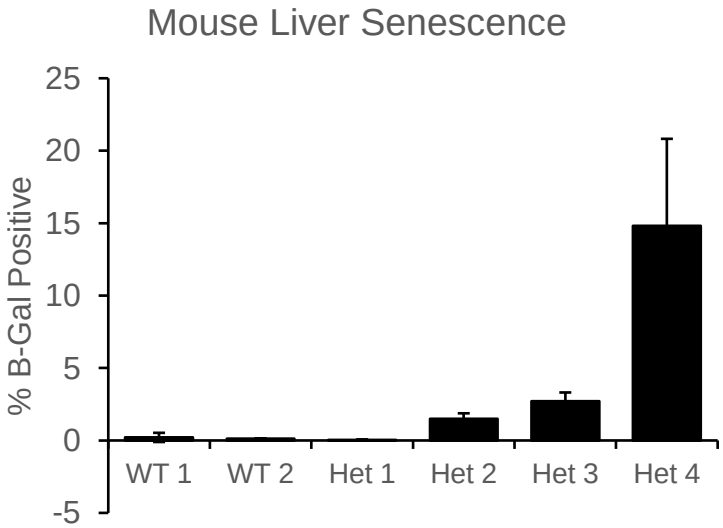

Figure 28. Liver senescence of ELOVL2 knockout mice. β-Galactosidase staining of liver sections of wild-type, heterozygous and homozygous *ELOVL2* knockout mice. Each image represents one mouse.

***Elovl2* mutant mice.**

Concurrently with *Elovl2* knockout mice, we generated *Elovl2* mutant C57BL/6 mice using CRISPR-Cas9 paired with homologous recombination. We generated a C217W mutation in the ELOVL2 protein that has been previously shown to change the substrate specificity of ELOVL2 to that of ELOVL5, effectively disrupting the unique ability of ELOVL2 to convert the C22 omega-3 PUFA docosapentaenoic acid (DPA) (22:5n-3) to 24:5n-3[43] (**Fig. 29**). We denote these mice as fate switch (FS) mice. A single gRNA was designed to target C217 on *Elovl2*. A repair oligo was designed with a single base pair mutation to generate the mutant C217W, along with four other silent mutations to disrupt the PAM sequences of the gRNAs, to prevent re-editing. The gRNA was injected into zygotes of C57BL/6 mice along with the repair oligo (**Fig. 30**). No off-target mutations were found (**Fig. 30**). Mice developed normally, not displaying any overt phenotypes.

Then we investigated whether eye structure and visual performance are changed in the fate switch (FS) mutant. Interestingly, in our *Elovl2* mutant mice, autofluorescent aggregates appear in the fundus at just 6 months of age, much earlier than in wild-type mice (**Fig. 31**), showing that ELOVL2 is crucial to maintaining a healthy retina. This phenotype was consistently observed in 4, 6, 8, and 12-month old mutant animals (**Fig. 33**). For comparison, a fundus image of human AMD is shown in **Figure 32**.

Then, we tested the photoreceptor function of these mutant mice using ERG. Compared to wild-type littermates, we observed a decrease in scotopic response amplitude in FS mutant mice (**Fig. 31**). This reduced response was consistently reproduced at other ages (**Fig. 34**). Although the most affected signal was scotopic

response, other types of ERG measurements- oscillatory potentials and flicker response, were also affected in *Elovl2* mutants (**Fig. 35**).

Figure 29. Protein alignment of human and mouse ELOVL5 and ELOVL2. Red arrows show position 217, the substrate specificity site. Changing the cysteine in ELOVL2 to tryptophan should switch the substrate specificity of ELOVL2 to that of ELOVL5.

Elovl2-subB Repair Oligo Sequence:

tgccttccagGTGCAGTTCGTACTCACCATCACGCACACGCTGAGTGCCGTGGTGAAGCCCTGTGGC
TTTCCCCTTCGGCTGGCTCATCTTCCAGTCTTCCTATATGATGACGTTAGTCATCCTGTTCTTAAA
CTTCTATATTCAGgtaagtaagatgtgagtgttcaggggcaggcaacatatcagacagccca

Protein sequence (top WT, bottom mutant):

```
 V   L   T   M   M   Y   S   S   Q   F   I   L   C   G   F   P   F
GAC-CAG-CGT-CAT-CAT-ATA-GGA-AGA-CTG-GAA-GAT-GAG-ACA-GCC-AAA-GGG-GAA

GAC-TAA-CGT-CAT-CAT-ATA-GGA-AGA-CTG-GAA-GAT-GAG-CCA-GCC-GAA-GGG-AAA
 V   L   T   M   M   Y   S   S   Q   F   I   L   W   G   F   P   F
```

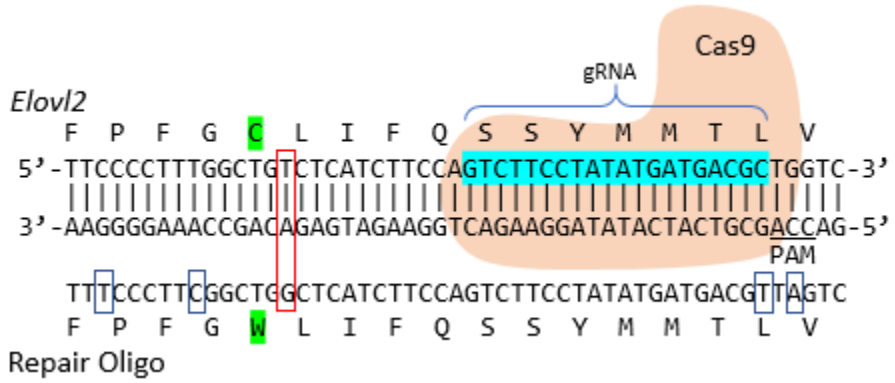

crRNA	DNA	Chromosome	Position	Direction	Mismatches	Bulge Size
GTCTTCCT--ATATGATGACGCNGG	GTCTcCCTTGATATGATGAaGCAGG	chr8	61376362	-	2	2
GTCTTCCTATATGATG-ACGCNGG	GTCTTCCTAaATGATGCAgGCAGG	chr10	77280542	-	2	1

Figure 30. CRISPR-Cas9 strategy for generating *ELOVL2* mutant mice. Table shows crRNA designed for off-target detection.

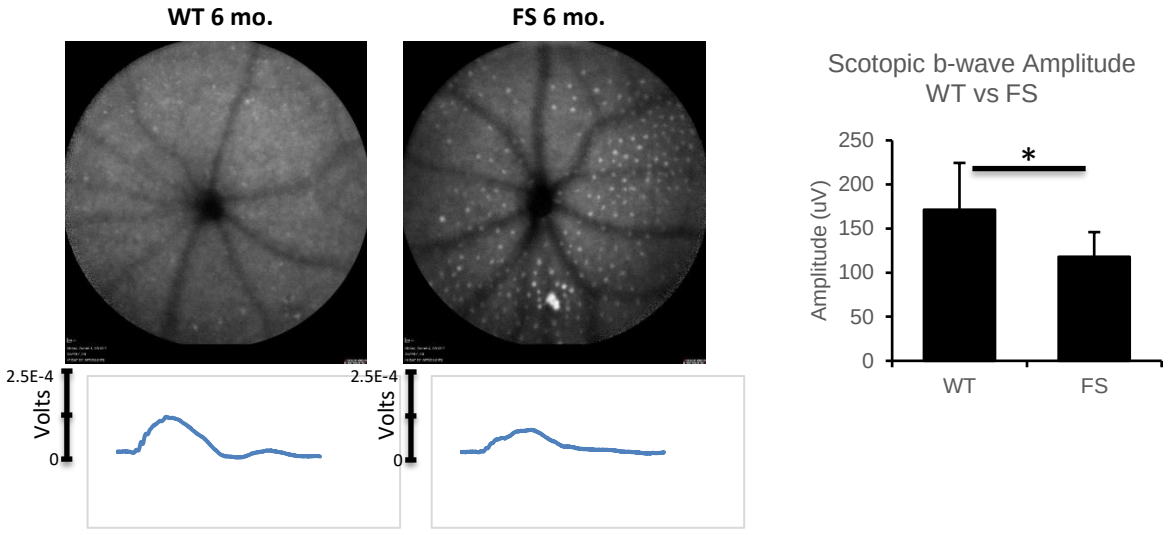

Figure 31. Retina autofluorescence imaging and scotopic response of *Elovl2* mutant mice. Left: wild-type, right: *Elovl2* mutant.

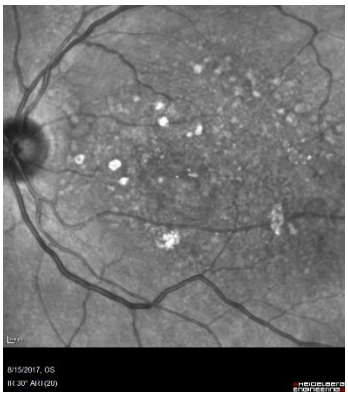

Figure 32. Human dry AMD. An example of fundus autofluorescence image of human dry AMD.

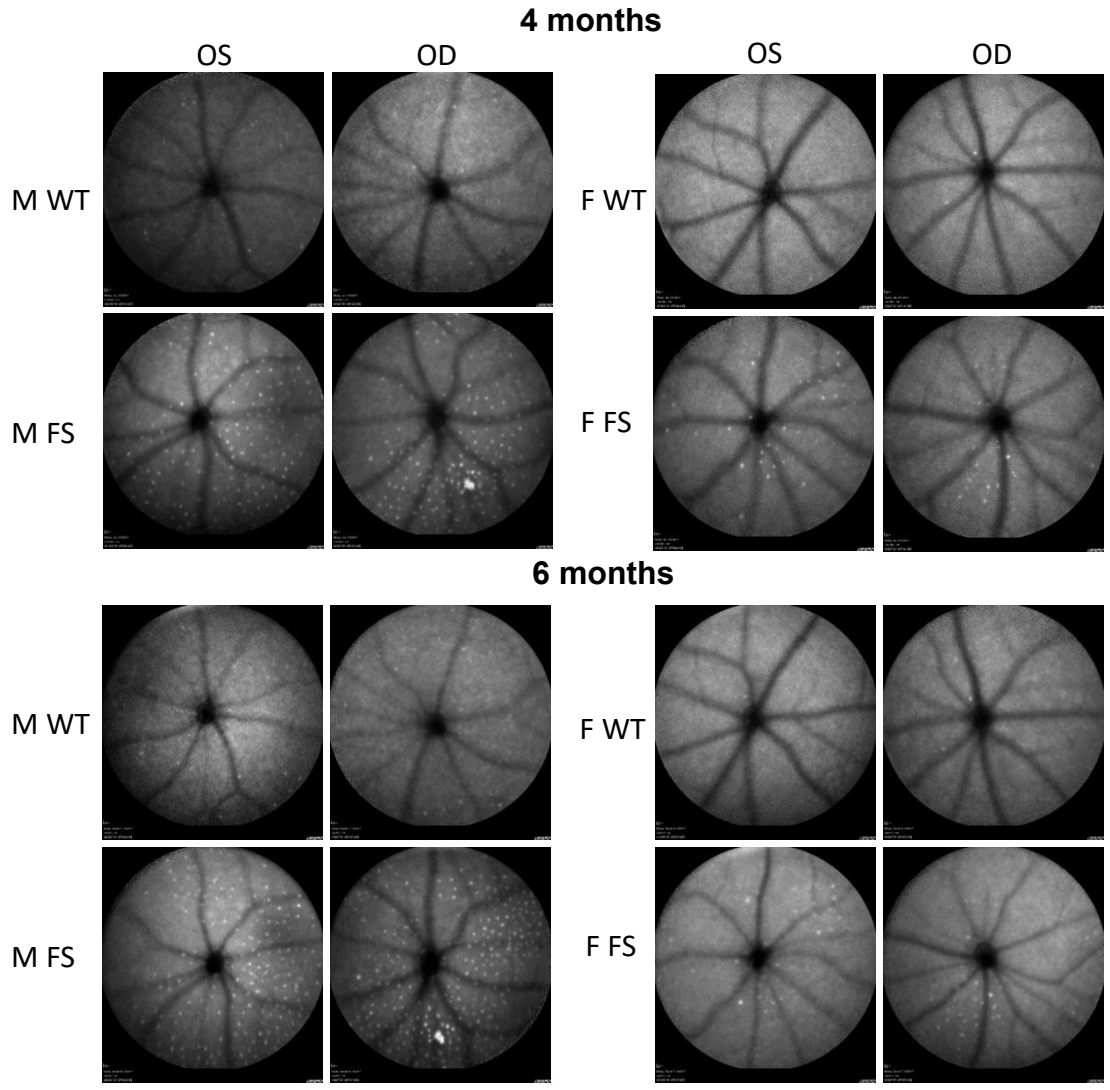

Figure 33. Fundus images of FS mouse retinas. Autofluorescence images of WT vs FS mouse retinas at 4 months, 6 months, 8 months, and 1 year of age.

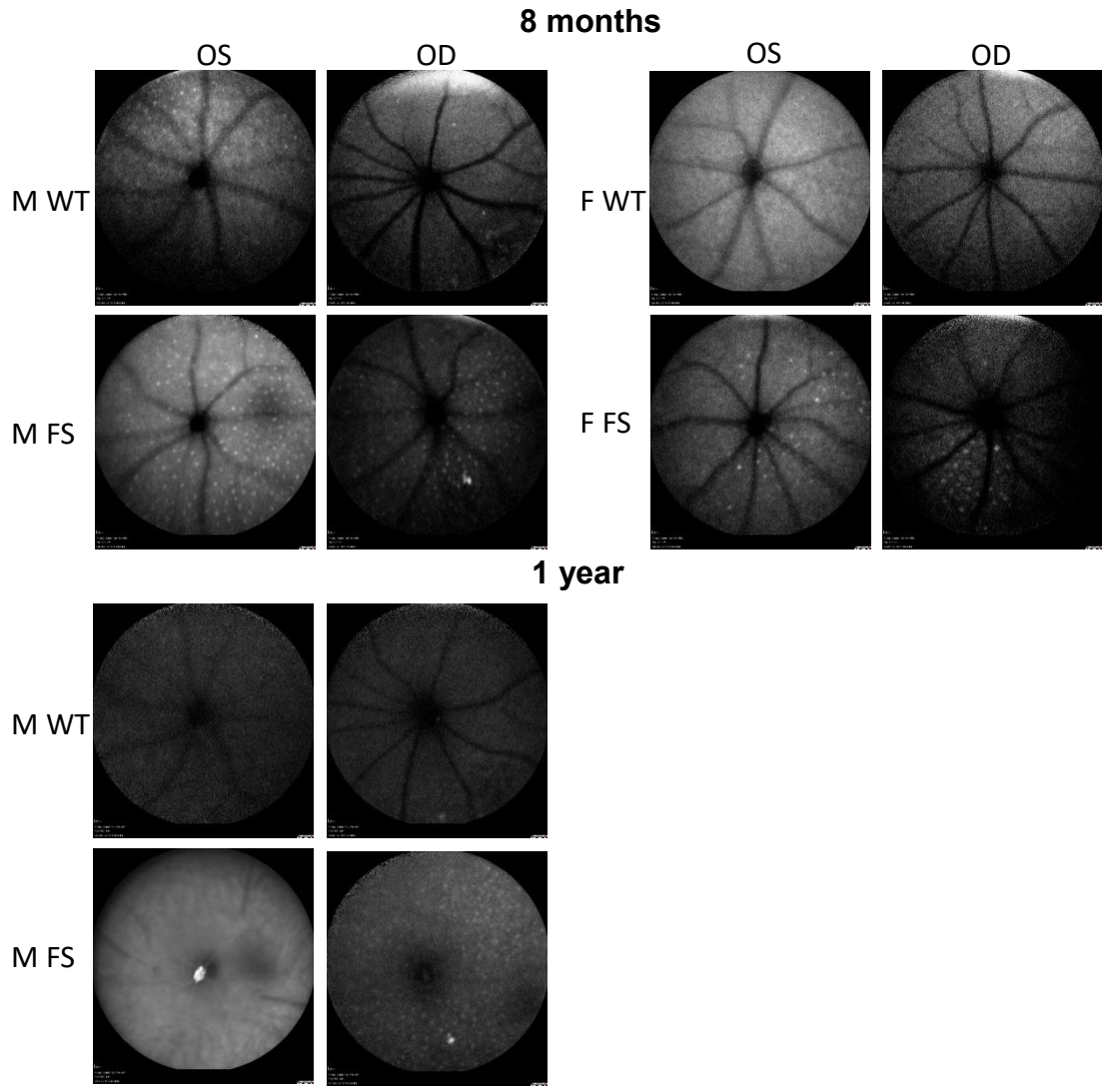

Figure 33 (continued). Fundus images of FS mouse retinas. Autofluorescence images of WT vs FS mouse retinas at 4 months, 6 months, 8 months, and 1 year of age.

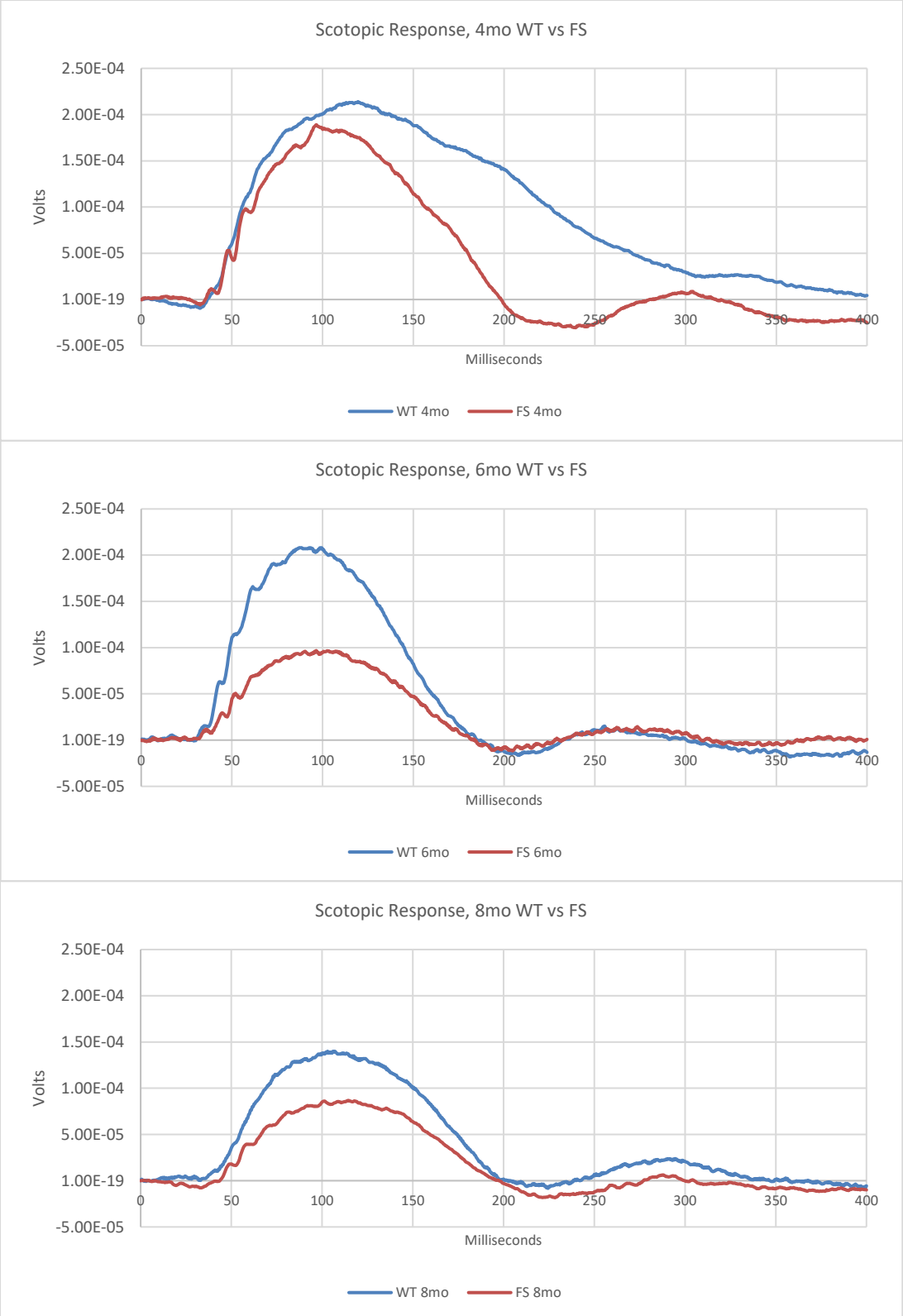

Figure 34. Scotopic response of FS mouse retinas. Scotopic response of ERG in WT vs. FS mice at 4 months, 6 months, and 8 months of age.

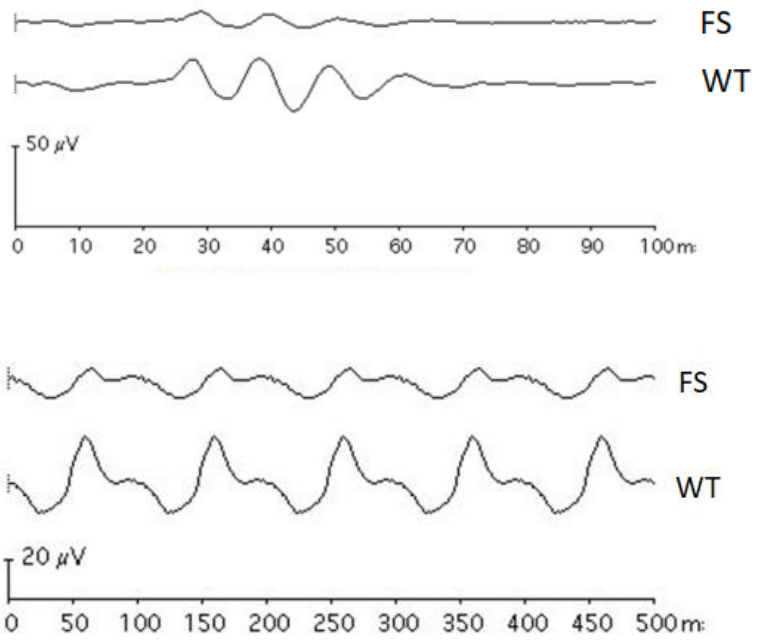

Figure 35. Other ERG measurements in FS mice. Top, oscillatory potentials from ERG in wild-type and frameshift mutation mice. Bottom, 10 Hz flicker response from ERG in wild-type and frameshift mutation mice.

Next, we immunostained the retinas of FS and WT mice for HTRA1, oxidized phosphocholine (with T-15 antibody), C3, C5b-9, and ApoE to investigate whether the aggregates observed as puncta in the autofluorescence fundus imaging were similar to drusen, that in humans are a risk factor for developing AMD[59]. Indeed, our immunostaining detected HTRA1, T-15, C3, C5b-9, and ApoE positive aggregates in the FS retinas only (**Fig. 36-39**). Given the prominence and early development of drusen-like aggregates in our mutant mice, they are likely showing signs of AMD.

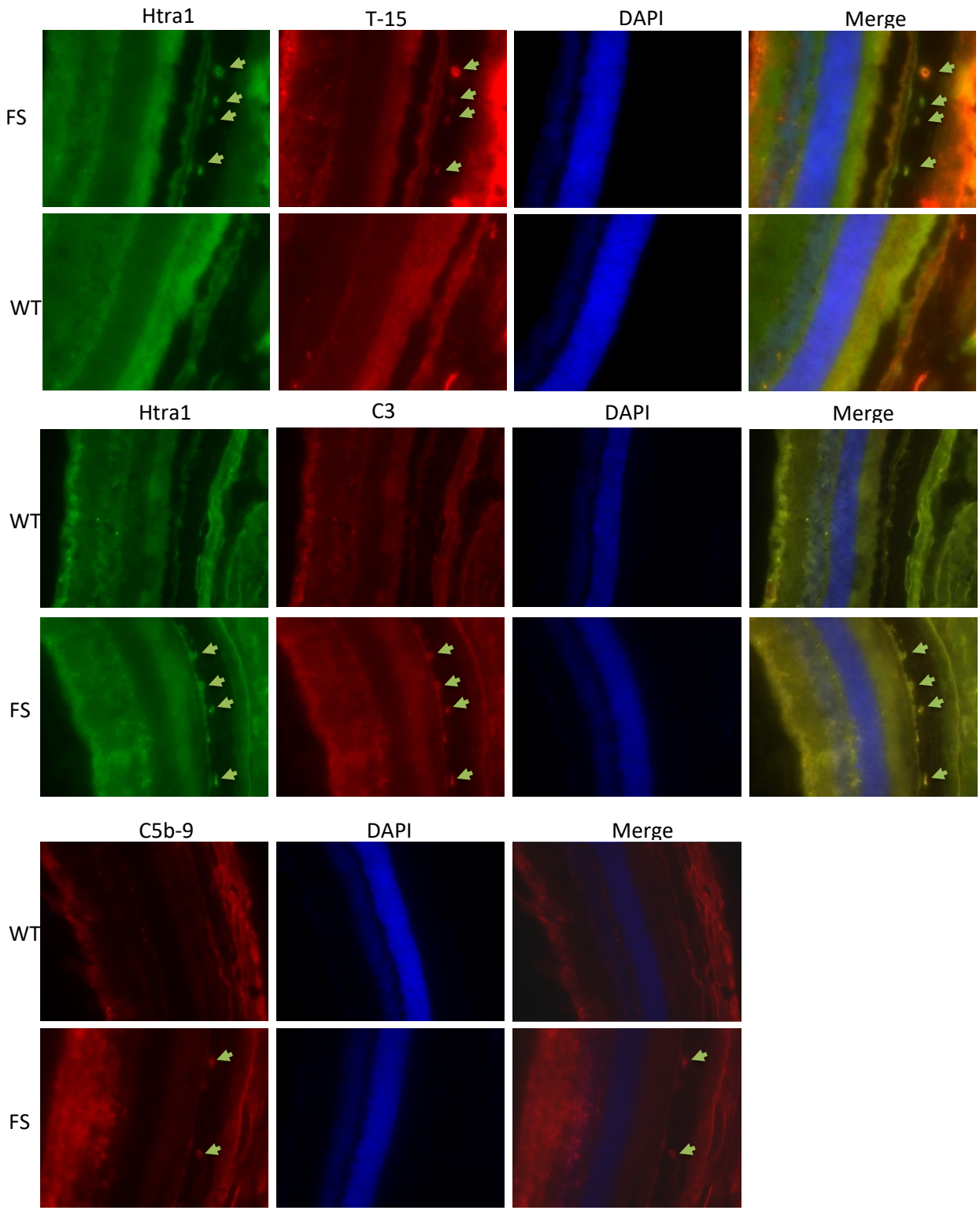

Figure 36. Htra1, T-15, C5b-9 immunostaining of *Elovl2* mutant mice.

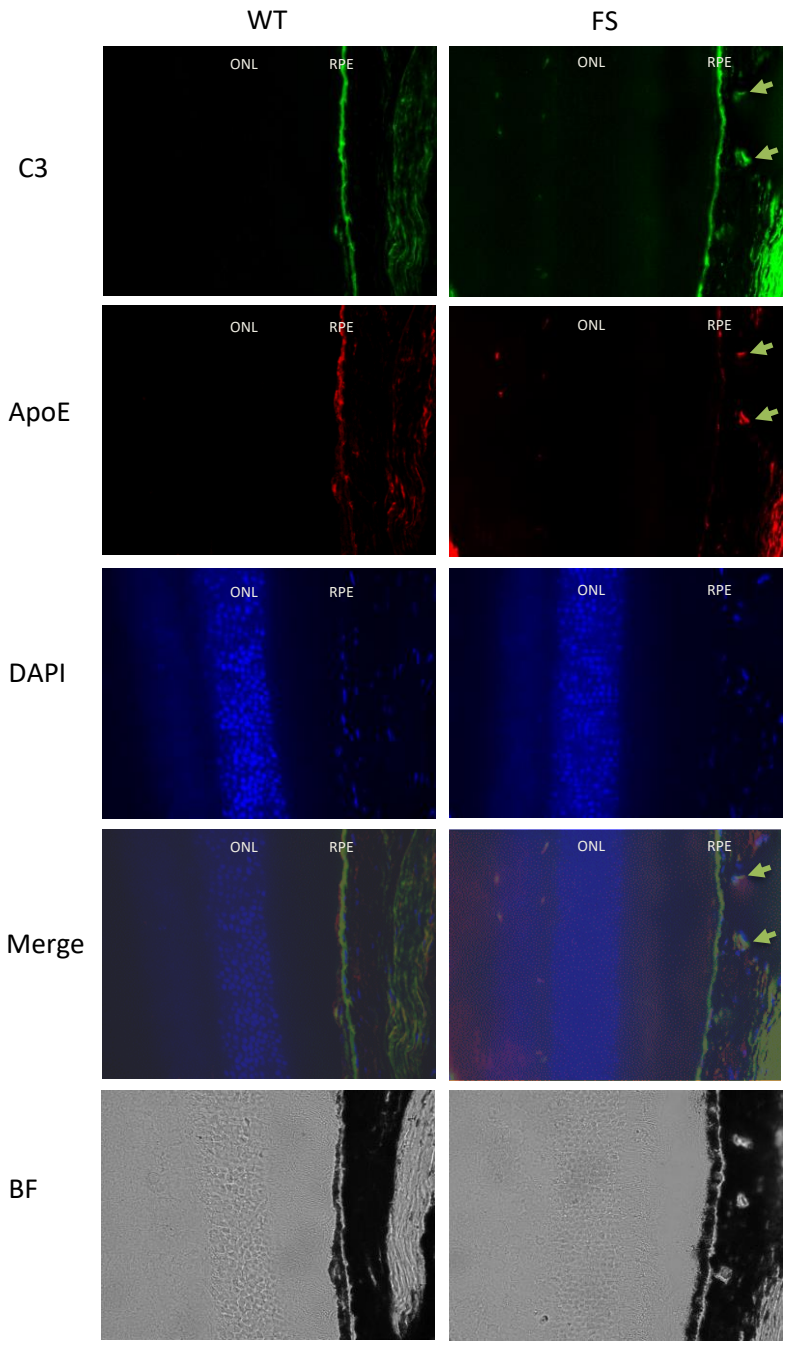

Figure 37. C3, ApoE immunostaining of *Elovl2* mutant mice.

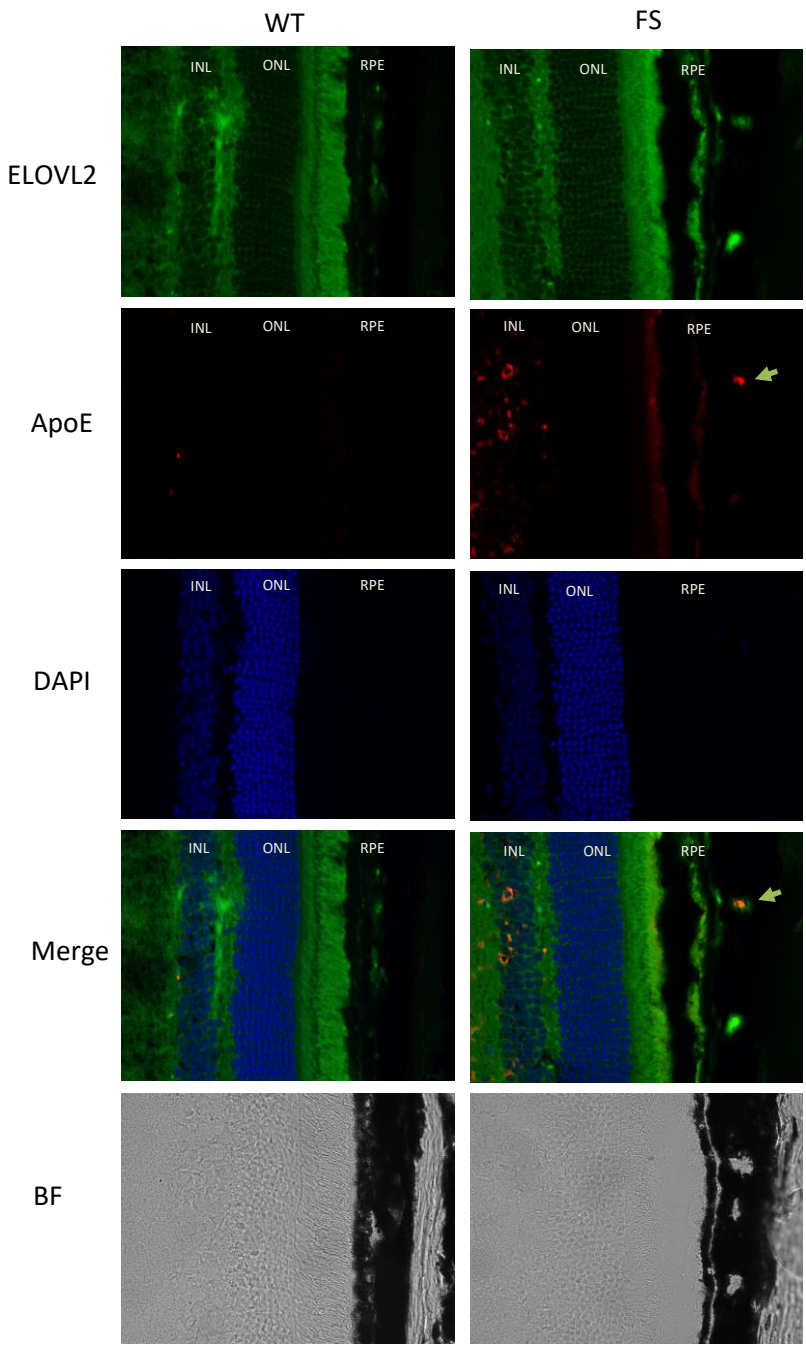

Figure 38. ELOVL2, ApoE immunostaining of *Elovl2* mutant mice.

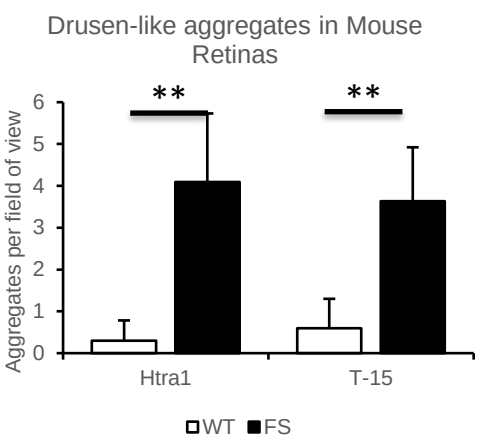

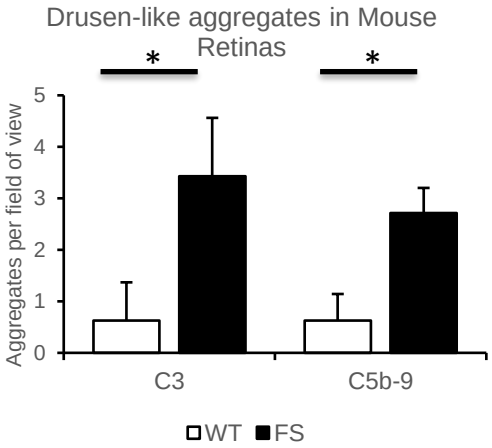

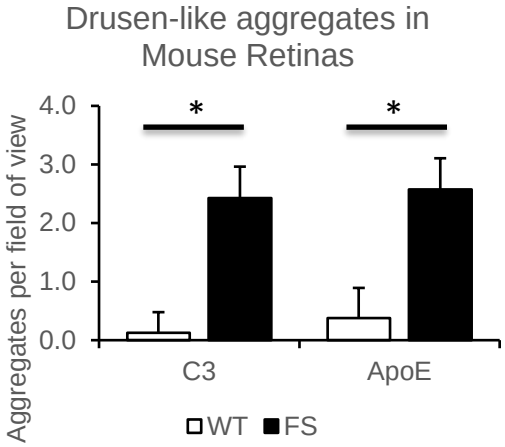

Figure 39. Retina immunostaining quantification.

Finally, we investigated whether the aging characteristics in mouse eyes could be reverted by demethylating the *Elovl2* promoter. To do that, we injected eyes with 1µL of PBS or 1µL of 2µM 5-Aza every other week over a period of 2 months starting at age of 10 months. We found, using the MeDIP method, that methylation of the *Elovl2* promoter decreased after treatment. We also found that *Elovl2* expression was upregulated in the treated eyes. Finally, we checked the photoreceptor function by ERG, and found that scotopic response was improved in the injected eyes (**Fig. 40,41**).

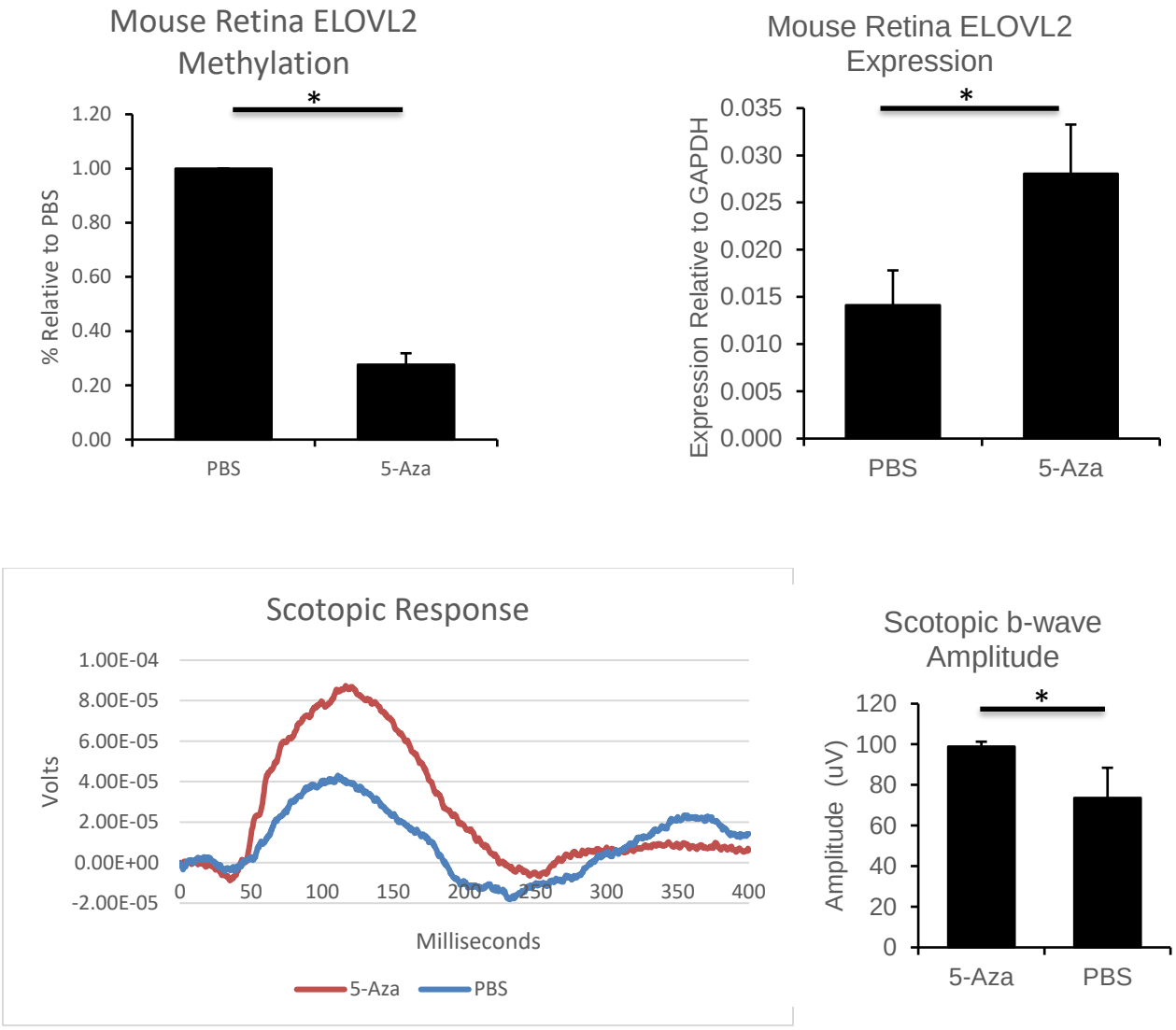

Figure 40. Retinal *Elovl2* methylation, expression, and scotopic response of mutant mice injected with 5-Aza, and PBS as control.

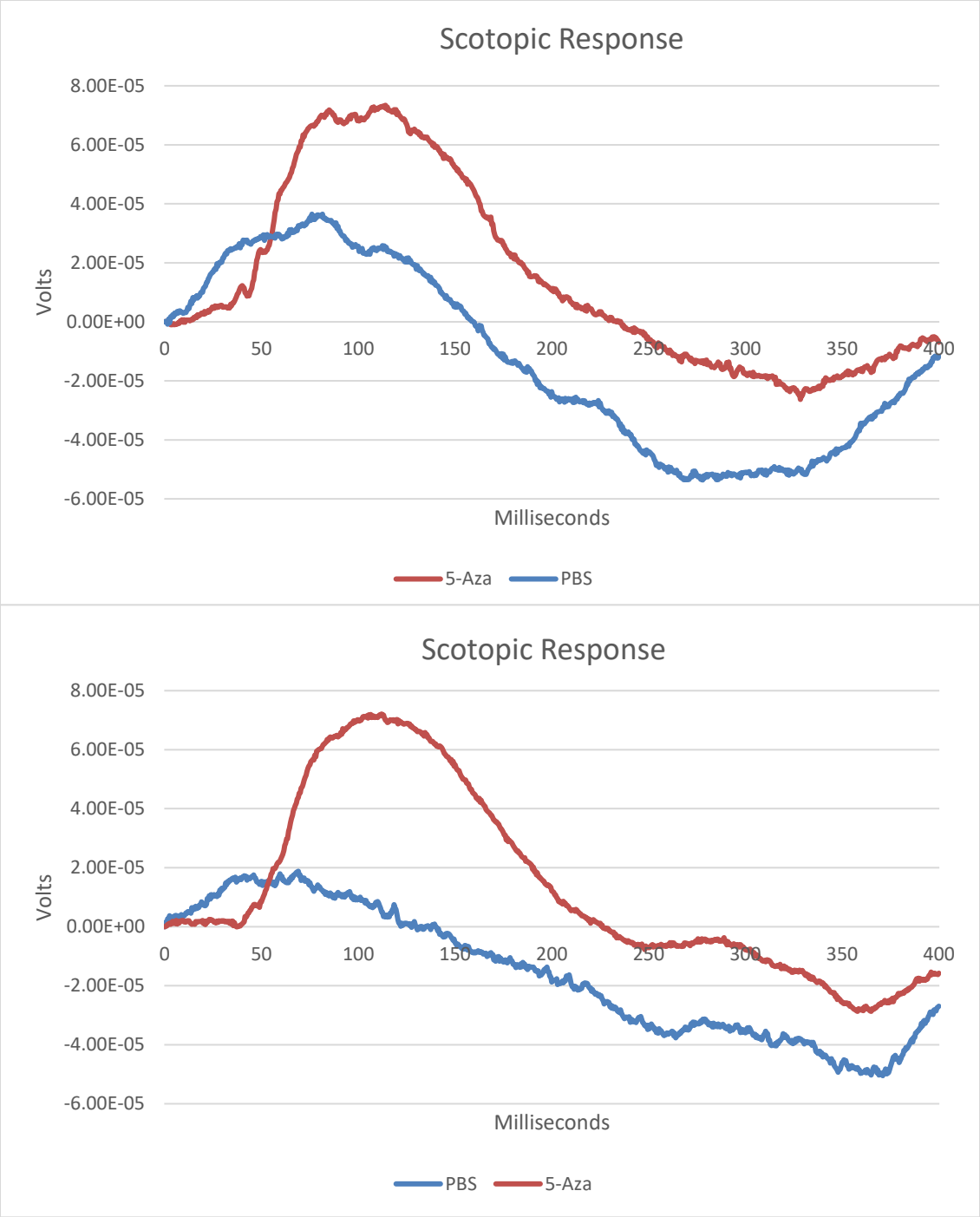

Figure 41. Additional scotopic responses of mutant mice injected with 5-Aza, and PBS as control.

To test for the potentially confounding rd8 mutation, a mutation in the *Crb1* gene which can produce ocular disease phenotypes when homozygous, we sequenced all mice in our study for rd8. FS mutant mice were heterozygous for rd8. Rd8 generally does not present eye disease phenotypes when heterozygous[60]. One of the ELOVL2 WT control littermates was homozygous for rd8, while another was heterozygous (**Fig. 42, 43**). ELOVL2 FS mice presented with eye aging phenotypes at a much earlier stage than both mice. Thus, the presence of rd8 does not affect our conclusion that ELOVL2 FS develop accelerated eye aging phenotypes.

Of the injected mice, two were WT for rd8, and two were heterozygous. The results were consistent regardless of rd8 genotype (**Fig. 43**). These data suggest that *Elovl2* methylation status can be altered to influence aging eye characteristics.

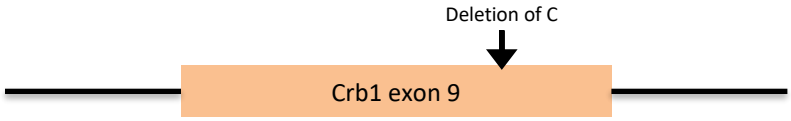

GTATCGCAAACGCTGTTTTCAGCGGATTAAGCAGAGAAATACTCTTCAGAAGC
AATGGGAACATTACCAGAGAACTCACCAATATCACATTTGCTTTCAGAACACA
TGATACAAATGTGATGATATTGCATGCAGAAAAAGAACCAGAGTTTCTTAATA
TTAGCATTCAAGATGCCAGATTATTCTTTCAATTGCGAAGTGGCAACAGCTTT
TATACGCTGCACCTGATGGGTTCCCAATTGGTGAATGATGGCACATGGCACCA
AGTGACTTTCTCCATGATAGACCCAGTGGCCCAGACCTCCCGGTGGCAAATGG
AGGTGAACGACCAGACACCCTTTGTGATAAGTGAAGTTGCTACTGGAAGCCTG
AACTTTTTGAAGGACAATACAGACATCTATGTGGGTGACCAATCTGTTGACAA
TCCGAAAGGCCTGCAGGGCTGTCTGAGCACAATAGAGATTGGAGGCATATATC
TTTCTTACTTTGAAAATCTACATGGTTTCCCTGGTAAGCCTCAGGAAGAGCAA
TTTCTCAAAGTTTCTACAAATATGGTACTTACTGGCTGTTTGCCATCAAATGC
CTGCCACTCCAGCCCCTGTTTGCATGGAGGAAACTGTGAAGACAGCTACAGTT
CTTATCGGTGTGCCTGTCTCTCGGGATGGTCAGGGACACACTGTGAAATCAAC
ATTGATGAGTGCTTTTCTAGCCCCTGTATCCATGGCAACTGCTCTGATGGAGT
TGCAGCCTACCACTGCAGGTGTGAGCCTGGATACACCGGTGTGAACTGTGAGG
TGGATGTAGACAATTGCAAGAGTCATCAGTGTGCAAATGGGGCCACCTGTGTT
CCTGAAGCTCATGGCTACTCTTGTCTCTGCTTTGGAAATTTTACCGGGAGATT
TTGCAG

Figure 42. Location of rd8 mutation. Deleted cytosine is highlighted in green.

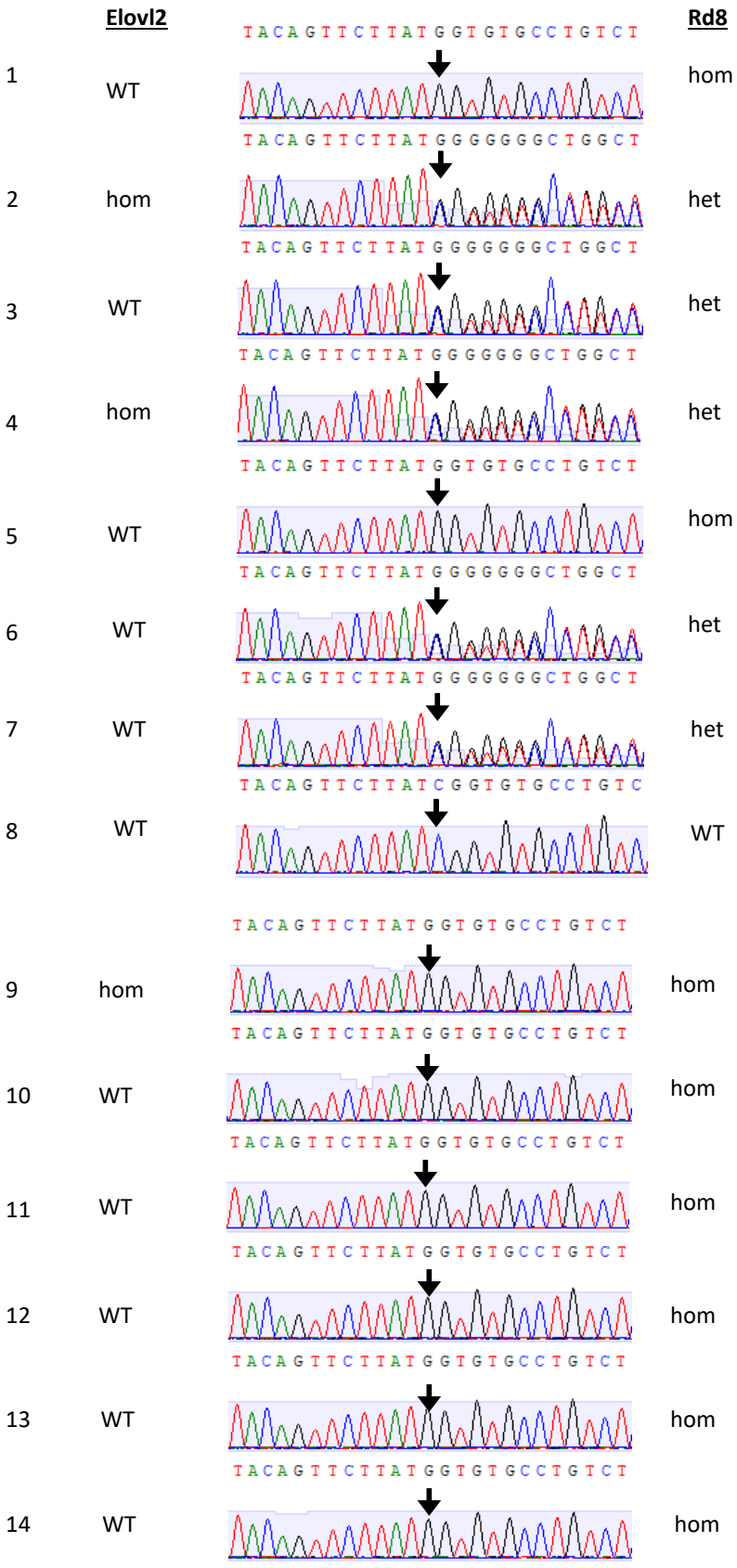

Figure 43. Rd8 genotyping of mice. Mice 1-4 were littermates used for ELOVL2 FS studies. Mice 9-16 were C57BL/6N founders. Mice 25-28 were used for 5-Aza ocular injection study. The rest of the mice were used as ELOVL2 WT controls.

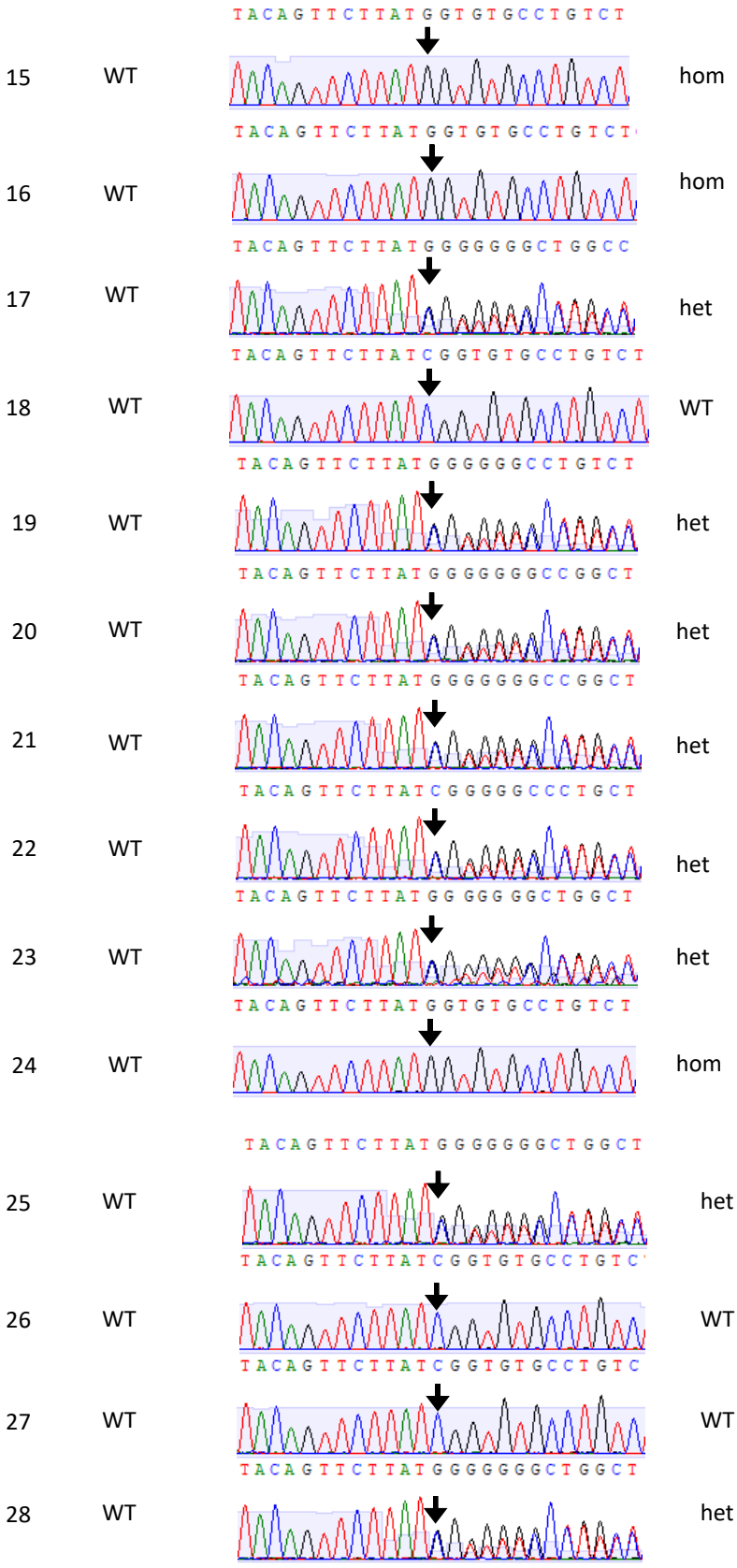

Figure 43 (continued). Rd8 genotyping of mice. Mice 1-4 were littermates used for ELOVL2 FS studies. Mice 9-16 were C57BL/6N founders. Mice 25-28 were used for 5-Aza ocular injection study. The rest of the mice were used as ELOVL2 WT controls.

SUMMARY

In our DNA methylation aging model, *ELOVL2* contains the single most significant age-correlated CpG mark, and 3 of the top 12 marks, in its promoter region. After identifying *ELOVL2* as a gene of interest in our aging model, we investigated the aging characteristics of WI-38 and IMR-90 fibroblasts in relation to this gene. We define young as population doubling (PD) 20-35, middle-age as PD 36-50, and old as PD 51 and on. WI-38 and IMR-90 cells are human fetal lung fibroblasts that show increased senescence and decreased proliferation rate upon each passage, and are commonly used in aging studies[61,62]. During normal passaging, they change from a shorter, more rounded morphology to a more elongated morphology in “old” age. In addition, they display alterations of the ‘methylomic age’ as determined by the analysis of CpG methylation with our predictive aging model. To assess apparent age, we quantified proliferation by confluency, senescence via β-galactosidase staining[47], and observed morphology change. We found that *ELOVL2* methylation increases, and expression decreases with increasing PD. Because of the increasing methylation in the *ELOVL2* promoter region with age in humans, and the fact that promoter methylation is generally inversely correlated with expression, we hypothesized that knocking down *ELOVL2* would give the fibroblasts increased aging phenotypes. Indeed, we found a negative influence on these phenotypes upon knockdown of *ELOVL2*. We then overexpressed *ELOVL2* in these cells. We did not find the expected amelioration of the aging characteristics of proliferation, senescence, or morphology, but after the cells reached population doubling 56, at which point they ceased to proliferate, *ELOVL2* overexpressing cells survived longer in culture than controls.

In a screen of molecules that modulate *ELOVL2* expression and aging phenotypes in fibroblasts, we identified vitamin C as a strong effector. Because of its well-known properties as an antioxidant, we examined 3 derivates of vitamin C—a phosphate-stabilized derivative which would only become active in redox upon coming into contact with cellular phosphatases (VcP), an oxidized derivative (DHAA), and regular ascorbic acid (Vc). We found that while DHAA did not have beneficial effects on cellular aging, Vc ameliorated cellular aging phenotypes at lower concentrations, and VcP did so at a large range of concentrations.

To test whether vitamin C was acting through its antioxidant function, we assessed ROS levels in fibroblasts with high and low concentrations of each vitamin C derivative. In cases where a derivative at a certain concentration benefited cellular aging phenotypes, it was found to decrease ROS levels, with the notable exception of vitamin C at high concentration. It was found to decrease ROS levels despite being detrimental to aging phenotypes. This suggests that the antioxidant function of vitamin C may not be the primary mechanism behind its effect on cellular aging.

To investigate if demethylation can influence cellular aging, we used 5-Aza at a low concentration to globally demethylate DNA in fibroblasts. We found that senescence was decreased, along with a decrease in *Elovl2* methylation and an increase in expression.

We then examined the function of *Elovl2* in mouse aging. We attempted to generate a colony of *Elovl2* knockout mice, but because male knockout mice display reduced fertility, we did not obtain enough mice to produce significant data. In the

heterozygotes that were generated, however, we observed an increase in liver senescence.

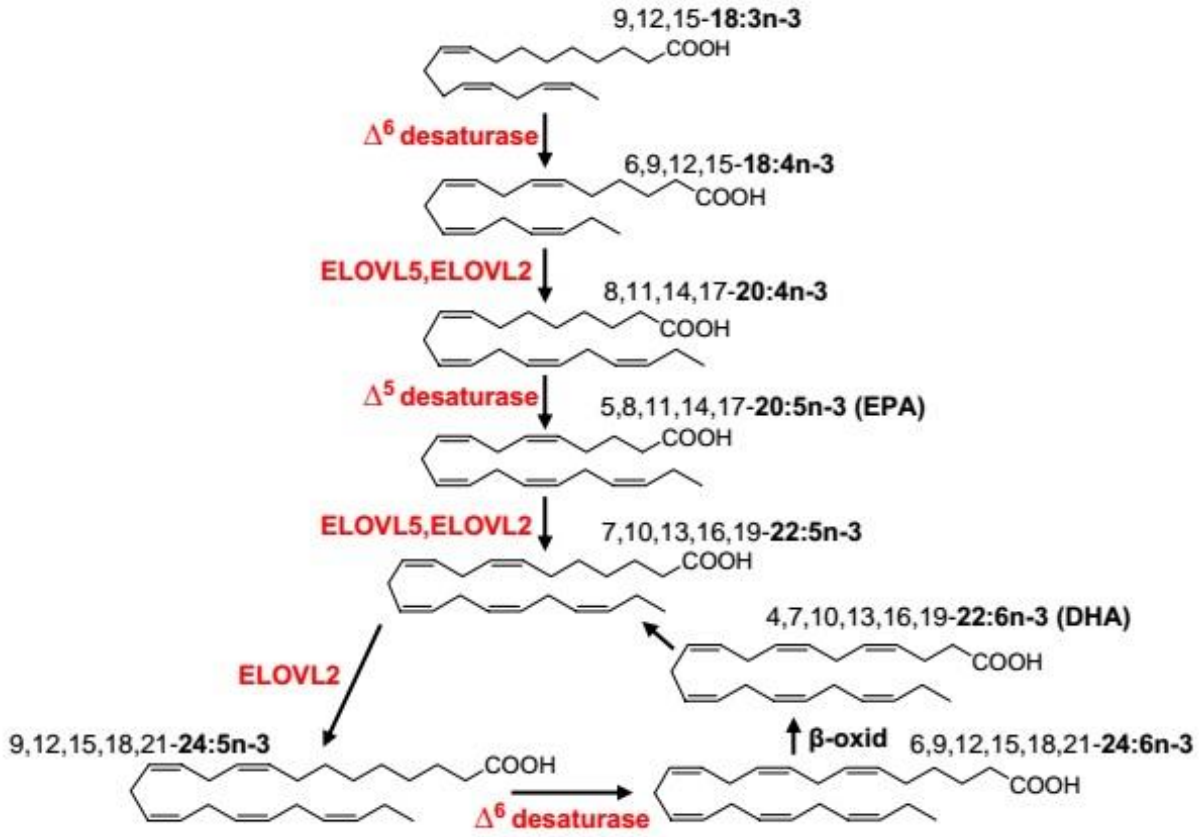

Figure 44. Function of ELOVL2 and ELOVL5.

We then generated C217W *Elovl2* mutant mice. Using CRISPR-Cas9 along with homology directed repair, we created a functional knockout by introducing a single base-pair mutation to change the function of *Elovl2* to that of *Elovl5*. Only ELOVL2 can convert docosapentaenoic acid (DPA) (22:5n-3) to 24:5n-3, which is the penultimate precursor of DHA. Meanwhile, ELOVL5 overlaps in function with ELOVL2 in elongating 18:4n-3 to 20:4n-3, and from EPA to DPA (**Fig. 44**)[43]. A mutation was targeted to position 217 of ELOVL2, converting a cytosine to a tryptophan, to switch the substrate specificity of

ELOVL2 to that of ELOVL5 (**Fig. 29**). Mutant mice did not exhibit outward signs of aging compared to their wild-type littermates, but they showed signs of aging-related retina dystrophy.

Finally, we injected 5-Aza into mouse eyes, and observed an increase in photoreceptor sensitivity as measured by ERG, showing that demethylation can potentially influence eye aging phenotypes.

DISCUSSION

Previous studies have revealed a highly significant correlation between *ELOVL2* promoter methylation and age in humans[1,70,71]. In the current study, we investigated whether *ELOVL2* methylation and expression plays a role in aging. First, we investigated *ELOVL2* in the aging human fibroblast model.

WI-38 fibroblasts were isolated by Hayflick and Moorhead in the 1960s, and were observed to gradually experience signs of senescence as they divided, first slowing then stopping their division at 50+/-10 population doublings, a phenomenon which would later become known as the Hayflick limit[62]. In addition, cells were found to senesce *in* vivo with increasing age[72], and primary cells from different species were found to have a maximum *in* vitro lifespan correlated with the maximum lifespan of the species[73].

We found that *ELOVL2* expression decreases with passage number in human fibroblasts. Because promoter methylation is generally inversely correlated with expression, we expected that promoter methylation would increase with cellular aging, and found this to be true. Because of the decreasing expression in cells and increasing promoter methylation in both cells and humans with age, we hypothesized that knocking down *ELOVL2* would result in advanced aging phenotypes. Indeed, this was shown by a decreased proliferative capacity, increased senescence, and a corresponding change in morphology.

To further investigate aging phenotypes, we created *Elovl2* mutant mice. Using CRISPR-Cas9, we generated a C217W mutation, shown previously to switch the substrate specificity of the *Elovl2* catalytic site to the equivalent of *Elovl5*, effectively disrupting the unique ability of ELOVL2 to convert the C22 omega-3 PUFA

docosapentaenoic acid (DPA) (22:5n-3) to 24:5n-3[43]. Both *Elovl2* and *Elovl5* have been found to elongate eicosapentaenoic acid (EPA; 20:5n-3) to docosapentaenoic acid (DPA; 22:5n-3), but only Elovl2 is known to further elongate DPA to 24:5n-3, the penultimate precursor of DHA[43]. Altered levels of DHA have been linked to cardiovascular and eye disease[63]. We therefore investigated the health of the eyes of the *Elovl2* mutant mice.

By switching the substrate specificity of Elovl2 to that of Elovl5 in mice, we expected a similar effect on aging as a simple *Elovl2* knockout, but there may be some interesting phenotypes to observe by increasing the amount of effective Elovl5 in mice. Both Elovl2 and Elovl5 have been found to elongate eicosapentaenoic acid (EPA; 20:5n-3) to docosapentaenoic acid (DPA; 22:5n-3), but only Elovl2 is known to further elongate DPA to 24:5n-3, the penultimate precursor of DHA[43]. Thus, we expect to observe a pooling of DPA, and a lack of DHA in these mice.

We observed the presence of protein aggregates on the retina at 6 months of age, compared to 1 year in wild-type mice by autofluorescence imaging. We then stained retina sections for oxidized phosphocholine and HTRA1, two proteins found in drusen, which are commonly found in patients with age-related macular degeneration (AMD). AMD is a degenerative disease of the macula, is the leading cause of blindness among the elderly in developed countries. It is a multifactorial disease involving genetic, environmental, and metabolic factors, and there is currently no cure or effective prevention for it. A number of genes have been identified as risk factors, but many are still unknown. As AMD progresses, the center of vision becomes blurred, and eventually blind spots can develop. AMD occurs in two forms, wet AMD and dry AMD. In dry AMD, which affects about 90% of AMD patients, the focal deposition of acellular, polymorphous debris occurs between

the retinal pigment epithelium and Bruch's membrane. These focal deposits, called drusen, are usually the first observed clinical hallmarks of AMD. ELOVL4, another fatty acid elongase involved in the synthesis of VLC-PUFAs, is implicated in Stargardt macular dystrophy, a juvenile form of macular degeneration causing vision loss[55,74].

AMD has been associated with oxidative stress in the retina[75]. Oxidative stress can result in inflammation and contribute to the development of macrophage activation[76]. Oxidized phospholipids have been shown to be reliable markers of oxidative stress, and they initiate inflammation by binding to the retinal pigment epithelium (RPE) and macrophages, activating downstream inflammatory cascades[77]. Oxidation-modified proteins and lipids have also been found in drusen and Bruch's membrane[59]. Phosphatidylcholine, a phospholipid highly enriched in the retina, contains the head group phosphocholine. The oxidation epitope of phosphocholine can be recognized by a natural antibody to phosphocholine, TEPC-15[78], and has been shown to colocalize with drusen in the human AMD eye[79]. HTRA1, one of the main proteins associated with AMD, is also found to colocalize with drusen in the AMD eye[80]. In addition, several components of the complement cascade, including C3 complement fragments, C5 and the membrane attack complex C5b-9 have been found within drusen[81].

To assess photoreceptor function, we used ERG. ERG measures the electrical signals produced by the retina in response to light stimulus, and so can detect functional abnormalities of photoreceptors. Because the mouse retina contains mostly rod photoreceptors, the functional differences in their electrical signals (scotopic response) are most relevant in assessing visual performance. Besides scotopic response, we also investigated cone response and 10Hz flicker. All of these signals, but most notably

scotopic response, decreased in amplitude both with age and in mutant mice. Together with the presence of drusen-like aggregates, these indicators of decreased photoreceptor function are signs of AMD. Therefore, we conclude that ELOVL2 function is crucial for preventing early onset of drusen-like aggregates and maintaining healthy photoreceptor function in mice. Combined with the accelerated appearance of drusen-like aggregates, the loss of photoreceptor function in *Elovl2* mutant mice shows that ELOVL2 is an important part of maintaining a healthy retina through old age in mice. In addition, we have found that ELOVL2 plays an important role in influencing aging phenotypes in human cells, and could potentially be influencing the process of aging on a broader level.

The rd8 mutation of the *Crb1* gene is found in certain lines of C57BL/6 mice. C57BL/6J are generally WT for *Crb1*, while C57BL/6N are homozygous for rd8. This mutation can produce ocular disease phenotypes when homozygous, but generally do not present with these phenotypes when heterozygous[60]. Our founder mice were of the C57BL/6N substrain, and they were bred with C57BL/6J mice. The mice used for examination of ocular phenotypes in our study are progeny of C57BL/6N and C57BL/6J, and thus are a mixture of homozygous, heterozygous, and WT for rd8. The ELOVL2 FS mice examined in this study were all heterozygous for rd8. Of the control littermates, one was heterozygous for rd8, and the other was WT. We found that the ELOVL2 FS mice presented with drusen-like aggregates and decreased photoreceptor sensitivity at a significantly earlier stage than either of the control littermates. We conclude that the ELOVL2 FS mutation is responsible for the accelerated eye aging phenotype, although we cannot exclude the possibility that rd8 heterozygosity may also play a role.Taken together, our study shows evidence that ELOVL2 plays a role in aging characteristics,

and in particular, eye function. Further, the level of methylation at the promoter region of *ELOVL2* is correlated with its expression, and can be altered to potentially influence aging characteristics. Further studies are needed to discover the mechanisms by which ELOVL2 plays a role in aging and eye disease.

FUTURE DIRECTIONS

5hmC is known to serve as an intermediate in the process of active demethylation, but it also has been shown to be a stable epigenetic mark. While 5mC at promoter and enhancer sites typically marks for gene repression, 5hmC can positively correlate with gene activation[48,64,65]. Since the traditional bisulfite sequencing method that the lab previously employed to map 5mC in the aging model measures the sum of 5mC+5hmC (it cannot differentiate these two modifications), we plan to conclusively establish the identity of the epigenetic marks on *ELOVL2*. We will observe the correlation of DNA methylation, hydroxymethylation, and demethylation with expression of these two genes and aging rate. The dynamic equilibrium most likely affects expression regulation of these genes, and precisely mapping the demethylation sites will allow us to investigate their relationships with gene expression and aging.

5hmC can be present as a stable mark with high abundance at specific sites in the genome, so it is possible that some of the 5mC which we previously found are actually 5hmC. We will utilize TET-Assisted Bisulfite Sequencing (TAB-Seq) to investigate 5hmC content in *ELOVL2* in human blood samples of varying age, human lung fibroblasts of varying passage number, and mice of varying age. Combined with traditional bisulfite sequencing data, this will reveal which marks are 5mC and which are 5hmC. Further, we will investigate the corresponding gene expression of *ELOVL2* in each sample by qPCR. A second group of methods that we will use is methylated and hydroxymethylated DNA immunoprecipitation (MeDIP and hMeDIP). This method will assess the relative levels of methylation and hydroxymethylation in a region of DNA. Briefly, antibodies specific to

methylated and hydroxymethylated cytosines will be used to pull down fragments of DNA, and quantified by qPCR.

A fraction of the 5mC marks in *ELOVL2* may be revealed as 5hmC. Given that high levels of 5hmC and reciprocally low levels of 5mC can be found near binding sites of transcription factors, and that 5hmC may be an activating mark[26,48], we anticipate that any 5hmCs we discover will give further insight into the dynamic regulation of epigenetic markers and expression of *ELOVL2*.

Knowing the identities of the epigenetic marks on *ELOVL2*, we will next observe the effects of modifying them. Because *ELOVL2* was identified the top genes in our aging model due to its differential methylation with age, directly modifying its methylation may reveal further insight into the relationship between DNA methylation and aging. It is possible that altering specific CpG methylation marks will modify aging phenotypes. In potential therapeutic applications, epigenetic modification would be an attractive alternative to direct modification of the gene due to its intrinsic reversibility and thus decreased potential toxicity. Targeted epigenetic modifications have been successful in the past. Hui Chen et. al. have achieved successful targeted demethylation of promoters by fusing TET proteins to DNA binding zinc fingers[66]. Maeder et al. have successfully achieved demethylation and activation of genes with TALE-TET fusions[67].

We plan to fuse demethylating and methylating proteins to dCas9, then guide them by various sgRNAs to selectively demethylate and methylate CpG sites on *ELOVL2* in WI-38 and IMR-90 cells of varying passage number. For demethylation, we will use TET1, TET2, and TET3, and for methylation, we will use DNMT1, DNMT3A, and DNMT3B. We will target methylation marks that are best correlated with age, i.e. the highest bars in

meth.pVal in **Figure 45**. We will transfect dCas9 fusion proteins in transient expression vectors, along with gRNAs. As a second strategy, we will deliver dCas9 and gRNA both as DNA, in transient vectors. As controls, we will target dCas9 fusion proteins to loci that contain CpG sites that are not correlated with age. We will verify changes in DNA methylation with Droplet Digital PCR (Bio-Rad). To ensure that no off-target modifications occur, we will assess the methylation marks of candidate off-target sites by bisulfite sequencing, as well as the 470,000 CpG markers originally observed in our aging model by the Illumina Infinium BeadChip assay.

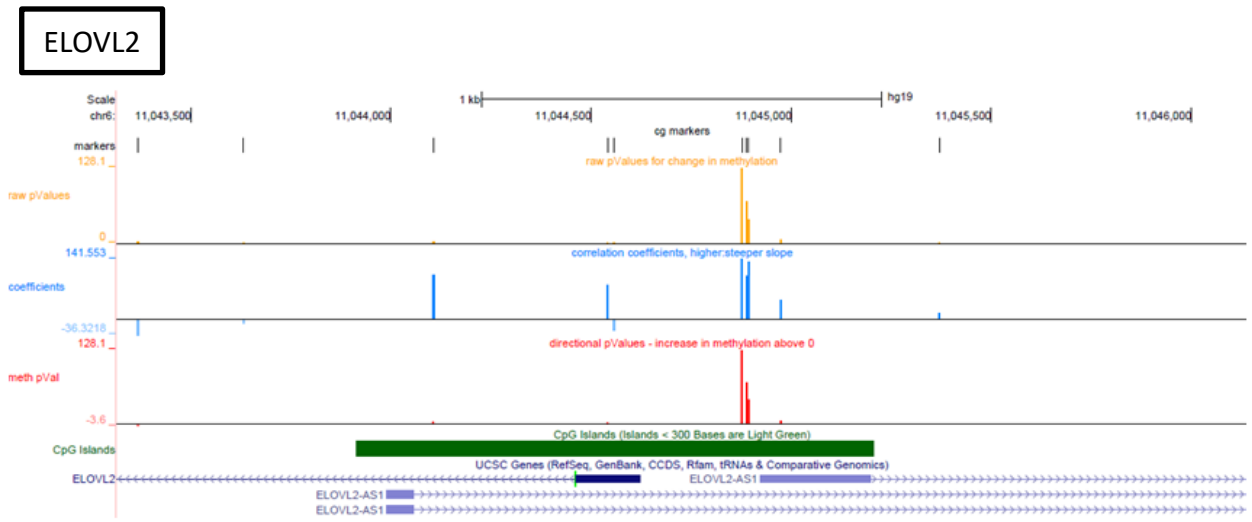

Figure 45. Methylation markers on *ELOVL2*. Raw p values refer to correlation to age. Higher bar = higher correlation. Coefficients refer to the slope of methylation fraction versus age. Methylation p values = raw p values multiplied by coefficients.

Upon dCas9-mediated methylation of *ELOVL2*, we expect to observe changes in aging phenotypes. We will quantify proliferation by cell count, and senescence via β-galactosidase staining[47]. Senescent cells have been shown to accumulate lysosomal β-galactosidase[68]. We will measure metabolic activity by MTT assay, which surveys the activity of NAD(P)H-dependent cellular oxidoreductase enzymes. We will also observe any changes in the morphology of the cells. In addition, we will assess the methylation status of the top genes in our aging model using the Illumina Infinium BeadChip assay.

We expect that, as is usually the case with promoter methylation, upon demethylation of the associated CpG island of *ELOVL2*, the genes will be upregulated, and that upon methylation, they will be downregulated. We expect TET2 to demethylate DNA more effectively than TET1, as shown previously[66]. DNMT3A and DNMT3B, having

higher de novo methyltransferase activity than DNMT1, are expected to more successfully methylate the targeted regions. Furthermore, it is possible that a TET protein will change 5mC to stable 5hmC, and not continue down the active demethylation pathway. Given that 5hmC could be an activating mark, this could result in upregulation of *ELOVL2*.

It is important to optimize the length of time to which the cells are exposed to dCas9. The cells should be exposed just long enough for targeted methylation or demethylation to occur, since when dCas9 is bound to DNA, it can sterically hinder transcription[69]. We expect RNA delivery of our CRISPR parts to be the least toxic to the cells, as there is no risk of genomic integration. Since the above proteins have not been used with CRISPR systems, we anticipate that troubleshooting will be required to achieve successful demethylation/methylation. Successful demethylation/methylation will likely depend on the distance between the protein and the DNA. We will vary the linker length between the protein to achieve the best results.

Further studies on the effects of *ELOVL2* overexpression are needed. We expect the apparent age and the methylation age of the cells to decrease upon upregulating *ELOVL2*. Observable phenotypes would include increased proliferation, decreased senescence, and a shorter, rounder morphology. If we only observe the correct shift in the apparent age of the cells but not the methylation state, it would suggest that *ELOVL2* influences aging phenotypes in the cells, but not through methylation state. Conversely, if we observe a shift in the methylation age but not in apparent age, then it may be the case that methylation age is not causative of apparent age in cells, or that other assays for apparent age should be used. We can also assess other properties of cells that could

indicate age, such as metabolic activity and telomere length. If we see that proliferation, senescence, and methylation state all trend in the expected direction, then we can be reasonably confident that *ELOVL2* influences the apparent age of cells, and that the apparent age of cells is correlated with methylation age.

We recently identified VcP as a modulator of aging phenotypes in human fibroblasts. VcP increased proliferation, decreased senescence, and increased *ELOVL2* expression in WI-38 and IMR-90 cells. VcP was effective at a wide range of concentrations, in contrast to regular ascorbic acid, which had detrimental effects at higher dosages. Because of the ability of vitamin C to induce Tet-dependent DNA demethylation[6], we hypothesize that it could demethylate CpG sites in *ELOVL2*, resulting in increased expression. We plan to investigate how the role of vitamin C in DNA demethylation could contribute to changes in aging phenotypes.

Previously, we found that methylation age as calculated by our aging model increases with increasing PD in WI-38 cells, while *ELOVL2* expression decreases (see Preliminary Data). First we will check that methylation of *ELOVL2* specifically increases with PD. With Droplet Digital PCR (ddPCR, Bio-Rad), we can reveal the percentage of specific CpG sites that are methylated in *ELOVL2.* The drawback of this technology is that it cannot distinguish methylated cytosines from hydroxymethylated ones. Using methylated DNA immunoprecipitation (MeDIP) and hydroxymethylated DNA immunoprecipitation (hMeDIP), we can distinguish between methylated and hydroxymethylated regions. The drawback of these methods is that they are not specific to individual cytosines. We can only determine relative amounts of each mark.

Given that VcP increases *ELOVL2* expression, we plan to interrogate CpG methylation in *ELOVL2* as well as genome-wide upon VcP treatment in fibroblasts and mice. WI-38 and IMR-90 cells will be treated at low and high concentrations of VcP at varying PDs. They will be monitored for proliferation rate, senescence, and morphology. At varying ages, we will assess their methylation states genome-wide with the Illumina Infinium BeadChip assay, with particular focus on *ELOVL2* methylation. Hydroxymethylation of cytosines will be assessed in comparison to methylation with TAB-seq and hMeDIP, as mentioned previously.

In addition, we will treat 2-year-old wild-type and *ELOVL2* mutant mice with 10 g/L VcP dissolved in drinking water. If results are not seen, intravenous injection is a more direct route of delivery. We will monitor their health, behavior, and methylation status of blood at 2 month intervals until their natural death. Behaviorial tests will be those commonly used in aging studies: the Barnes maze, eyeblink classical conditioning, fear conditioning, Morris water maze, grip strength, and rotarod tests. We will isolate cells from the mice every two months, and assess proliferation, senescence, and methylation status. Methylation and expression of *ELOVL2* will be assessed in a variety of organs upon natural death, with the same methods proposed for assessing methylation in fibroblasts.

Given that VcP plays a role in TET-mediated DNA demethylation, we predict that it will demethylate DNA at regions that influence the proliferative and senescence related phenotypes we have previously observed in fibroblasts. Extending these aging phenotypes to our mouse model, we predict that VcP can extend the lifespan of mice, as well as improve performance in aging-related behavioral tests. Because *ELOVL2* is clearly the top gene in our DNA methylation aging model, we expect that VcP will

influence its methylation state significantly. If it does not, our genome-wide methylation assay may reveal some other interesting sites of demethylating activity, which we could then pursue in our aging studies.

METHODS

Cell culture and treatment.

WI38 and IMR90 human fibroblasts were cultured in EMEM (ATCC) supplemented with 10% fetal bovine serum (Omega) and 1% penicillin/streptomycin (Gibco), and kept in a humidfied incubator at 5% CO_2 and 37°C. Confluence was calculated via ImageJ imaging software, including 3 fields of view per sample (10x). The cell lines were obtained from ATCC at a PD of 20 to 30, and maintained in culture until old age (PD 60+), with aliquots frozen at varying PDs. Knockdown lentivirus was generated using MISSION shRNA (Sigma) according to the manufacturer's instructions. Cumate-inducible vectors were purchased from Applied Biological Materials Inc, and lentivirus was generated and transduced into cells. Cells were then treated with cumate per manufacturer's instructions. Materials used in chemical screen were purchased from Sigma. 5-Aza-2'-deoxycitidine was purchased from TSZ Chem (CAS#2353-33-5), and dissolved in cell culture medium at a concentration of 2μM. Cells were treated for a period of 48 hours. The medium was then replaced with regular cell culture medium, and the cells were cultured for 5 more days.

Senescence-associated β-galactosidase (SA-β-gal) activity.

The SA-β-gal activity in cultured cells was determined using the Senescence β-Galactosidase Staining Kit (Cell Signaling Technology), according to the manufacturer's instructions. Cells were stained with DAPI afterwards, and percentages of cells that stained positive were calculated with imaging software (Keyence), including 3 fields of view (10x).

Nucleic acid analysis.

DNA and RNA were isolated from human fibroblasts and mouse tissues with TRIzol (Ambion) according to manufacturer's instructions. RNA was converted to cDNA with iScript cDNA Synthesis Kit (Bio-Rad). qPCR was performed using SsoAdvanced Universal SYBR Green Supermix (Bio-Rad).

Methylated DNA Immunoprecipitation (MeDIP) was performed by shearing DNA by Bioruptor (Diagenode) for 8 cycles on the high setting, each cycle consisting of 30 seconds on and 30 seconds off. Sheared DNA was denatured, incubated with 5mC antibody MABE146 (Millipore) for 2 hours, then with SureBeads protein G beads (Bio-Rad) for 1 hour. After washing, DNA was purified with QIAquick PCR Purification Kit (Qiagen). qPCR was then performed as above.

Fluorescent ROS Assay

Fibroblasts were split into a 96-well plate and treated under the specified conditions for 3 days. The reactive oxidative species were analyzed using the OxiSelect Intracellular ROS Assay Kit (Cell Biolabs, San Diego, CA). After PBS wash, Dichloro-dehydro-fluorescein diacetate (DCFH-DA) diluted to 100µM in media was added to the wells. The fibroblasts were incubated at 37°C for an hour and washed again twice with PBS. Regular media was added to the fibroblasts and the wells were imaged using a Keyence BZ-9000 fluorescent microscope for both fluorescent and brightfield microscopy.

Western Blotting.

10µg of total protein isolated with TRIzol (Ambion) from retinas of WT mice of varying stages of development was subject to SDS-PAGE. Western blotting was performed using 1.5 µg/ml anti-human ELOVL2 polyclonal antibody using a well-accepted protocol. ELOVL2 protein expression level was normalized to H3.

CRISPR-Cas9 design.

The CRISPR-Cas9 constructs were generated as previously described[82]. T7 promoter was added to Cas9 coding region by PCR amplification. The T7-Cas9 product was then gel purified and used as the template for in vitro transcription (IVT) using mMESSAGE mMACHINE T7 ULTRA kit (Life Technologies). T7 promoter was added to sgRNAs template by PCR amplification. The T7-sgRNA PCR product was gel purified and used as the template for IVT using the MEGAshortscript T7 kit (Life Technologies).

Animal injection and analysis.

All animal procedures were conducted with the approval of the Institutional Animal Care Committee at the University of California, San Diego. C57BL/6J mouse zygotes were injected with CRISPR-Cas9 constructs. Oligos were injected into the cytoplasm of the zygotes at the pronuclei stage. Mice were housed on static racks in a conventional animal facility, and were fed *ad libitum* with Teklad Global 2020X diet. For the 5-Aza injection study, Mice were anesthetized an intraperitoneal injection of ketamine/xylazine (100 mg/kg and 10 mg/kg, respectively), and given an analgesic eye drop of Proparacaine (0.5%, Bausch & Lomb). Animals were intraocularly injected with 1µL of PBS in one eye, and 1 µL of 2µM 5-Aza dissolved in PBS in the contralateral eye, every other week over a period of 2 months.

Electroretinograms (ERGs) were performed following a previously reported protocol[83]. Briefly, mice were dark-adapted for 12 h, anesthetized with a weight-based intraperitoneal injection of ketamine/xylazine, and given a dilating drop of Tropicamide (1.5%, Alcon) as well as a drop of Proparacaine (0.5%, Bausch & Lomb) as analgesic. Mice were examined with a full-field Ganzfeld bowl setup (Diagnosys LLC), with

electrodes were placed on each cornea, with a subcutaneous ground needle electrode placed in the tail, and a reference electrode in the mouth (Grass Telefactor, F-E2). Lubricant (Goniovisc 2.5%, HUB Pharmaceuticals) was used to provide contact of the electrodes with the eyes. Amplification (at 1–1,000 Hz bandpass, without notch filtering), stimuli presentation, and data acquisition are programmed and performed using the UTAS-E 3000 system (LKC Technologies). For scotopic ERG, the retina was stimulated with a xenon lamp at -2 and -0.5 log cd·s/m2. For photopic ERG, mice were adapted to a background light of 1 log cd·s/m2, and light stimulation was set at 1.5 log cd·s/m2. Recordings were collected and averaged in manufacturer's software (Veris, EDI) and processed in Excel.

Mouse retina analysis.

Retinas were collected immediately after sacrificing mice, fixed in 4% paraformaldehyde for 1 hour, and stored in PBS at 4°C. For immunostainings, retinas were sectioned, mounted on slides, then incubated with 5%BSA 0.1% Triton-X PBS blocking solution for 1 hour. Primary antibodies (Sigma M1421, Santa Cruz Biotechnology sc-377050, sc-58926, sc-66190) were added 1:50 in 5%BSA PBS, and incubated at 4°C for 16 hours. Following 3x PBS wash, secondary antibodies were added 1:1000 in 5%BSA PBS for 30 minutes at room temperature. Samples were then washed 3x with PBS, stained with DAPI for 5 minutes at room temperature, mounted, and imaged (Keyence).

Table 1. List of primers used in the study.

Off-target checking	**Sequence (5' -> 3')**
chr8 off-targ F	GTAATTCCGTGATCACCGTC
chr8 off-targ R	CCAATAAATAACAGCAGAAG
chr10 off-targ F	CAATATGCTCATCATTGTCT
chr10 off-targ R	CCACACATGTCTACCTTCCT
MeDIP primers	
hELOVL2 prom. F	CGATTTGCAGGTCCAGCCG
hELOVL2 prom. R	CAGCGGGTGGGTATTCCTG
hACTB prom. F	CTAGGTGTGGACATCTCTTG
hACTB prom. R	TGCAGGAGCGTACAGAA
mELOVL2 prom. F	AGCTCCTCCGCTACTC
mELOVL2 prom. R	CCAGCCCTTGGTCATC
mACTB prom. F	TAGGCCCAGATGTACAGGAA
mACTB prom. R	CCAGAATGCAGGCCTAGTAA
qPCR primers	
hELOVL2 F	GCGGATCATGGAACATCTAA
hELOVL2 R	CCAGCCATATTGAGAGCAGA
hACTB F	CACCATTGGCAATGAGCGGTTC
hACTB R	AGGTCTTTGCGGATGTCCACGT
Rd8 primers	
Rd8 F	GGTGACCAATCTGTTGACAATCC
Rd8 R	GCCCCATTTGCACACTGATGAC

Table 2. List of antibodies used in the study.

Immunostaining	**Company, Cat#**	**RRID**
TEPC 15	Sigma M1421	AB_1163630
HtrA	Santa Cruz sc-377050	
C3	Santa Cruz sc-58926	AB_1119819
C5-b9	Santa Cruz sc-66190	AB_1119840
ApoE	Santa Cruz sc-13521	AB_626691
MeDIP		
5-methylcytosine	Millipore MABE146	AB_10863148
Western blot		
ELOVL2	Santa Cruz sc-54874	AB_2262364
Histone H3	Cell Signaling 9715	AB_331563

REFERENCES

1. Hannum, G., Guinney, J., Zhao, L., Zhang, L., Hughes, G., Sadda, S., Klotzle, B., Bibikova, M., Fan, J.-B., Gao, Y., Deconde, R., Chen, M., Rajapakse, I., Friend, S., Ideker, T. & Zhang, K. Genome-wide Methylation Profiles Reveal Quantitative Views of Human Aging Rates. *Mol. Cell* **49,** 359–367 (2013).

2. Matsumoto, M., Tatsumi, H. & Murai, A. [Lipid metabolism and aging]. *Rinsho Byori* **38,** 530–533 (1990).

3. Guarente, L. Sir2 links chromatin silencing, metabolism, and aging. *Genes Dev.* **14,** 1021–1026 (2000).

4. Barzilai, N., Huffman, D. M., Muzumdar, R. H. & Bartke, A. The critical role of metabolic pathways in aging. *Diabetes* **61,** 1315–1322 (2012).

5. Ulrey, C. L., Liu, L., Andrews, L. G. & Tollefsbol, T. O. The impact of metabolism on DNA methylation. *Hum. Mol. Genet.* **14,** R139–R147 (2005).

6. Vitamin C induces Tet-dependent DNA demethylation and a blastocyst-like state in ES cells - Vitamin C Induces Tet-dependent DNA.pdf. at <http://santoslab.ucsf.edu/sites/santoslab.ucsf.edu/files/wysiwyg/Vitamin%20C%20Induces%20Tet-dependent%20DNA.pdf>

7. Health, C. O. on S. and. Smoking and Tobacco Use; Surgeon General's Reports; 2004. *Smok. Tob. Use* at <http://www.cdc.gov/tobacco/data_statistics/sgr/2004/>

8. Law, J. A. & Jacobsen, S. E. Establishing, maintaining and modifying DNA methylation patterns in plants and animals. *Nat. Rev. Genet.* **11,** 204–220 (2010).

9. Ehrlich, M. & Wang, R. Y. 5-Methylcytosine in eukaryotic DNA. *Science* **212,** 1350–1357 (1981).

10. Wu, H. & Zhang, Y. Reversing DNA Methylation: Mechanisms, Genomics, and Biological Functions. *Cell* **156,** 45–68 (2014).

11. Lopatina, N., Haskell, J. F., Andrews, L. G., Poole, J. C., Saldanha, S. & Tollefsbol, T. Differential maintenance and de novo methylating activity by three DNA methyltransferases in aging and immortalized fibroblasts. *J. Cell. Biochem.* **84,** 324–334 (2002).

12. Robertson, K. D. DNA methylation and human disease. *Nat. Rev. Genet.* **6,** 597–610 (2005).

13. Jackson-Grusby, L., Beard, C., Possemato, R., Tudor, M., Fambrough, D., Csankovszki, G., Dausman, J., Lee, P., Wilson, C., Lander, E. & Jaenisch, R. Loss of genomic methylation causes p53-dependent apoptosis and epigenetic deregulation. *Nat. Genet.* **27,** 31–39 (2001).

14. Fraga, M. F., Ballestar, E., Paz, M. F., Ropero, S., Setien, F., Ballestar, M. L., Heine-Suñer, D., Cigudosa, J. C., Urioste, M., Benitez, J., Boix-Chornet, M., Sanchez-Aguilera, A., Ling, C., Carlsson, E., Poulsen, P., Vaag, A., Stephan, Z., Spector, T. D., Wu, Y.-Z., Plass, C. & Esteller, M. Epigenetic differences arise during the lifetime of monozygotic twins. *Proc. Natl. Acad. Sci. U. S. A.* **102,** 10604–10609 (2005).

15. Casillas, M. A., Lopatina, N., Andrews, L. G. & Tollefsbol, T. O. Transcriptional control of the DNA methyltransferases is altered in aging and neoplastically-transformed human fibroblasts. *Mol. Cell. Biochem.* **252,** 33–43 (2003).

16. Fraga, M. F. & Esteller, M. Epigenetics and aging: the targets and the marks. *Trends Genet.* **23,** 413–418 (2007).

17. Horvath, S. DNA methylation age of human tissues and cell types. *Genome Biol.* **14,** R115 (2013).

18. Ahuja, N. & Issa, J. P. Aging, methylation and cancer. *Histol. Histopathol.* **15,** 835–842 (2000).

19. Bell, C. G., Teschendorff, A. E., Rakyan, V. K., Maxwell, A. P., Beck, S. & Savage, D. A. Genome-wide DNA methylation analysis for diabetic nephropathy in type 1 diabetes mellitus. *BMC Med. Genomics* **3,** 33 (2010).

20. Lu, H., Liu, X., Deng, Y. & Qing, H. DNA methylation, a hand behind neurodegenerative diseases. *Front. Aging Neurosci.* **5,** 85 (2013).

21. Heyn, H., Moran, S. & Esteller, M. Aberrant DNA methylation profiles in the premature aging disorders Hutchinson-Gilford Progeria and Werner syndrome. *Epigenetics Off. J. DNA Methylation Soc.* **8,** 28–33 (2013).

22. He, Y.-F., Li, B.-Z., Li, Z., Liu, P., Wang, Y., Tang, Q., Ding, J., Jia, Y., Chen, Z., Li, L., Sun, Y., Li, X., Dai, Q., Song, C.-X., Zhang, K., He, C. & Xu, G.-L. Tet-Mediated Formation of 5-Carboxylcytosine and Its Excision by TDG in Mammalian DNA. *Science* **333,** 1303–1307 (2011).

23. Ito, S., Shen, L., Dai, Q., Wu, S. C., Collins, L. B., Swenberg, J. A., He, C. & Zhang, Y. Tet Proteins Can Convert 5-Methylcytosine to 5-Formylcytosine and 5-Carboxylcytosine. *Science* **333,** 1300–1303 (2011).

24. Song, C.-X., Yi, C. & He, C. Mapping recently identified nucleotide variants in the genome and transcriptome. *Nat. Biotechnol.* **30,** 1107–1116 (2012).

25. Pfaffeneder, T., Hackner, B., Truß, M., Münzel, M., Müller, M., Deiml, C. A., Hagemeier, C. & Carell, T. The Discovery of 5-Formylcytosine in Embryonic Stem Cell DNA. *Angew. Chem. Int. Ed.* **50,** 7008–7012 (2011).

26. Yu, M., Hon, G. C., Szulwach, K. E., Song, C.-X., Zhang, L., Kim, A., Li, X., Dai, Q., Shen, Y., Park, B., Min, J.-H., Jin, P., Ren, B. & He, C. Base-Resolution Analysis of 5-Hydroxymethylcytosine in the Mammalian Genome. *Cell* **149,** 1368–1380 (2012).

27. Shen, L. & Zhang, Y. 5-Hydroxymethylcytosine: generation, fate, and genomic distribution. *Curr. Opin. Cell Biol.* **25,** 289–296 (2013).

28. Stadler, M. B., Murr, R., Burger, L., Ivanek, R., Lienert, F., Schöler, A., van Nimwegen, E., Wirbelauer, C., Oakeley, E. J., Gaidatzis, D., Tiwari, V. K. & Schübeler, D. DNA-binding factors shape the mouse methylome at distal regulatory regions. *Nature* **480,** 490–495 (2011).

29. Fu, Y. & He, C. Nucleic Acid Modifications with Epigenetic Significance. *Curr. Opin. Chem. Biol.* **16,** 516–524 (2012).

30. Ferrarelli, L. K. Epigenetic Regulation by Vitamin C. *Sci Signal* **6,** ec113–ec113 (2013).

31. Boyera, N., Galey, I. & Bernard, B. A. Effect of vitamin C and its derivatives on collagen synthesis and cross-linking by normal human fibroblasts. *Int. J. Cosmet. Sci.* **20,** 151–158 (1998).

32. Montecinos, V., Guzmán, P., Barra, V., Villagrán, M., Muñoz-Montesino, C., Sotomayor, K., Escobar, E., Godoy, A., Mardones, L., Sotomayor, P., Guzmán, C., Vásquez, O., Gallardo, V., Zundert, B. van, Bono, M. R., Oñate, S. A., Bustamante, M., Cárcamo, J. G., Rivas, C. I. & Vera, J. C. Vitamin C Is an Essential Antioxidant That Enhances Survival of Oxidatively Stressed Human Vascular Endothelial Cells in the Presence of a Vast Molar Excess of Glutathione. *J. Biol. Chem.* **282,** 15506–15515 (2007).

33. Valko, M., Rhodes, C. J., Moncol, J., Izakovic, M. & Mazur, M. Free radicals, metals and antioxidants in oxidative stress-induced cancer. *Chem. Biol. Interact.* **160,** 1–40 (2006).

34. Hata, R.-I. & Senoo, H. L-ascorbic acid 2-phosphate stimulates collagen accumulation, cell proliferation, and formation of a three-dimensional tissuelike substance by skin fibroblasts. *J. Cell. Physiol.* **138,** 8–16 (1989).

35. He, X.-B., Kim, M., Kim, S.-Y., Yi, S.-H., Rhee, Y.-H., Kim, T., Lee, E.-H., Park, C.-H., Dixit, S., Harrison, F. E. & Lee, S.-H. Vitamin C facilitates dopamine neuron differentiation in fetal midbrain through TET1- and JMJD3-dependent epigenetic control manner. *Stem Cells Dayt. Ohio* **33,** 1320–1332 (2015).

36. Pasonen-Seppänen, S., Suhonen, T. M., Kirjavainen, M., Suihko, E., Urtti, A., Miettinen, M., Hyttinen, M., Tammi, M. & Tammi, R. Vitamin C enhances differentiation of a continuous keratinocyte cell line (REK) into epidermis with normal stratum corneum ultrastructure and functional permeability barrier. *Histochem. Cell Biol.* **116,** 287–297 (2001).

37. Cameron, E. & Pauling, L. Supplemental ascorbate in the supportive treatment of cancer: Prolongation of survival times in terminal human cancer. *Proc. Natl. Acad. Sci. U. S. A.* **73,** 3685–3689 (1976).

38. Takamizawa, S., Maehata, Y., Imai, K., Senoo, H., Sato, S. & Hata, R.-I. Effects of ascorbic acid and ascorbic acid 2-phosphate, a long-acting vitamin C derivative, on the proliferation and differentiation of human osteoblast-like cells. *Cell Biol. Int.* **28,** 255–265 (2004).

39. Yun, J., Mullarky, E., Lu, C., Bosch, K. N., Kavalier, A., Rivera, K., Roper, J., Chio, I. I. C., Giannopoulou, E. G., Rago, C., Muley, A., Asara, J. M., Paik, J., Elemento, O., Chen, Z., Pappin, D. J., Dow, L. E., Papadopoulos, N., Gross, S. S. & Cantley, L. C. Vitamin C selectively kills KRAS and BRAF mutant colorectal cancer cells by targeting GAPDH. *Science* aaa5004 (2015). doi:10.1126/science.aaa5004

40. Sapers, G. M., Douglas, F. W., Ziolkowski, M. A., Miller, R. L. & Hicks, K. B. Determination of ascorbic acid, dehydroascorbic acid and ascorbic acid-2-phosphate in infiltrated apple and potato tissue by high-performance liquid chromatography. *J. Chromatogr. A* **503,** 431–436 (1990).

41. Tsutsumi, K., Fujikawa, H., Kajikawa, T., Takedachi, M., Yamamoto, T. & Murakami, S. Effects of L-ascorbic acid 2-phosphate magnesium salt on the properties of human gingival fibroblasts. *J. Periodontal Res.* **47,** 263–271 (2012).

42. Leonard, A. E., Kelder, B., Bobik, E. G., Chuang, L.-T., Lewis, C. J., Kopchick, J. J., Mukerji, P. & Huang, Y.-S. Identification and expression of mammalian long-chain PUFA elongation enzymes. *Lipids* **37,** 733–740 (2002).

43. Gregory, M. K., Cleland, L. G. & James, M. J. Molecular basis for differential elongation of omega-3 docosapentaenoic acid by the rat Elovl5 and Elovl2. *J. Lipid Res.* **54,** 2851–2857 (2013).

44. Zou, H. & Hastie, T. Regularization and variable selection via the elastic net. *J. R. Stat. Soc. Ser. B Stat. Methodol.* **67,** 301–320 (2005).

45. Bibikova, M., Barnes, B., Tsan, C., Ho, V., Klotzle, B., Le, J. M., Delano, D., Zhang, L., Schroth, G. P., Gunderson, K. L., Fan, J.-B. & Shen, R. High density DNA methylation array with single CpG site resolution. *Genomics* **98,** 288–295 (2011).

46. Pignolo, R. J., Rotenberg, M. O. & Cristofalo, V. J. Alterations in contact and density-dependent arrest state in senescent WI-38 cells. *In Vitro Cell. Dev. Biol. Anim.* **30A,** 471–476 (1994).

47. Schäuble, S., Klement, K., Marthandan, S., Münch, S., Heiland, I., Schuster, S., Hemmerich, P. & Diekmann, S. Quantitative Model of Cell Cycle Arrest and Cellular Senescence in Primary Human Fibroblasts. *PLoS ONE* **7,** e42150 (2012).

48. Jin, S.-G., Wu, X., Li, A. X. & Pfeifer, G. P. Genomic mapping of 5-hydroxymethylcytosine in the human brain. *Nucleic Acids Res.* **39,** 5015–5024 (2011).

49. Jones, P. L., Jan Veenstra, G. C., Wade, P. A., Vermaak, D., Kass, S. U., Landsberger, N., Strouboulis, J. & Wolffe, A. P. Methylated DNA and MeCP2 recruit histone deacetylase to repress transcription. *Nat. Genet.* **19,** 187–191 (1998).

50. Lee, C., Zeng, J., Drew, B. G., Sallam, T., Martin-Montalvo, A., Wan, J., Kim, S.-J., Mehta, H., Hevener, A. L., de Cabo, R. & Cohen, P. The Mitochondrial-Derived Peptide MOTS-c Promotes Metabolic Homeostasis and Reduces Obesity and Insulin Resistance. *Cell Metab.* **21,** 443–454 (2015).

51. Castillo-Quan, J. I. & Blackwell, T. K. Metformin: Restraining Nucleocytoplasmic Shuttling to Fight Cancer and Aging. *Cell* **167,** 1670–1671 (2016).

52. Momparler, R. L. Pharmacology of 5-Aza-2'-deoxycytidine (decitabine). *Semin. Hematol.* **42,** S9–16 (2005).

53. Swindell, W. R., Ensrud, K. E., Cawthon, P. M., Cauley, J. A., Cummings, S. R. & Miller, R. A. Indicators of 'Healthy Aging' in older women (65-69 years of age). A data-mining approach based on prediction of long-term survival. *BMC Geriatr.* **10,** 55 (2010).

54. Xue, X., Feng, C. Y., Hixson, S. M., Johnstone, K., Anderson, D. M., Parrish, C. C. & Rise, M. L. Characterization of the fatty acyl elongase (elovl) gene family, and hepatic elovl and delta-6 fatty acyl desaturase transcript expression and fatty acid responses to diets containing camelina oil in Atlantic cod (Gadus morhua). *Comp. Biochem. Physiol. B Biochem. Mol. Biol.* **175,** 9–22 (2014).

55. Agbaga, M.-P., Brush, R. S., Mandal, M. N. A., Henry, K., Elliott, M. H. & Anderson, R. E. Role of Stargardt-3 macular dystrophy protein (ELOVL4) in the biosynthesis of very long chain fatty acids. *Proc. Natl. Acad. Sci.* **105,** 12843–12848 (2008).

56. Kolesnikov, A. V., Fan, J., Crouch, R. K. & Kefalov, V. J. Age-Related Deterioration of Rod Vision in Mice. *J. Neurosci. Off. J. Soc. Neurosci.* **30,** 11222–11231 (2010).

57. Bartke, A. & Brown-Borg, H. Life extension in the dwarf mouse. *Curr. Top. Dev. Biol.* **63,** 189–225 (2004).

58. Zadravec, D., Tvrdik, P., Guillou, H., Haslam, R., Kobayashi, T., Napier, J. A., Capecchi, M. R. & Jacobsson, A. ELOVL2 controls the level of n-6 28:5 and 30:5 fatty acids in testis, a prerequisite for male fertility and sperm maturation in mice. *J. Lipid Res.* **52,** 245–255 (2011).

59. Crabb, J. W., Miyagi, M., Gu, X., Shadrach, K., West, K. A., Sakaguchi, H., Kamei, M., Hasan, A., Yan, L., Rayborn, M. E., Salomon, R. G. & Hollyfield, J. G. Drusen proteome analysis: An approach to the etiology of age-related macular degeneration. *Proc. Natl. Acad. Sci.* **99,** 14682–14687 (2002).

60. Mattapallil, M. J., Wawrousek, E. F., Chan, C.-C., Zhao, H., Roychoudhury, J., Ferguson, T. A. & Caspi, R. R. The Rd8 Mutation of the Crb1 Gene Is Present in Vendor Lines of C57BL/6N Mice and Embryonic Stem Cells, and Confounds Ocular Induced Mutant Phenotypes. *Invest. Ophthalmol. Vis. Sci.* **53,** 2921–2927 (2012).

61. Forsyth, N. R., Evans, A. P., Shay, J. W. & Wright, W. E. Developmental differences in the immortalization of lung fibroblasts by telomerase. *Aging Cell* **2,** 235–243 (2003).

62. Hayflick, L. The limited in vitro lifetime of human diploid cell strains. *Exp. Cell Res.* **37,** 614–636 (1965).

63. Bucher, H. C., Hengstler, P., Schindler, C. & Meier, G. N-3 polyunsaturated fatty acids in coronary heart disease: a meta-analysis of randomized controlled trials. *Am. J. Med.* **112,** 298–304 (2002).

64. Liutkeviciute, Z., Lukinavicius, G., Masevicius, V., Daujotyte, D. & Klimasauskas, S. Cytosine-5-methyltransferases add aldehydes to DNA. *Nat. Chem. Biol.* **5,** 400–402 (2009).

65. Wu, S. C. & Zhang, Y. Active DNA demethylation: many roads lead to Rome. *Nat. Rev. Mol. Cell Biol.* **11,** 607–620 (2010).

66. Chen, H., Kazemier, H. G., de Groote, M. L., Ruiters, M. H. J., Xu, G.-L. & Rots, M. G. Induced DNA demethylation by targeting Ten-Eleven Translocation 2 to the human ICAM-1 promoter. *Nucleic Acids Res.* **42,** 1563–1574 (2014).

67. Maeder, M. L., Angstman, J. F., Richardson, M. E., Linder, S. J., Cascio, V. M., Tsai, S. Q., Ho, Q. H., Sander, J. D., Reyon, D., Bernstein, B. E., Costello, J. F., Wilkinson, M. F. & Joung, J. K. Targeted DNA demethylation and activation of endogenous genes using programmable TALE-TET1 fusion proteins. *Nat. Biotechnol.* **31,** 1137–1142 (2013).

68. Lee, B. Y., Han, J. A., Im, J. S., Morrone, A., Johung, K., Goodwin, E. C., Kleijer, W. J., DiMaio, D. & Hwang, E. S. Senescence-associated β-galactosidase is lysosomal β-galactosidase. *Aging Cell* **5,** 187–195 (2006).

69. Gilbert, L. A., Larson, M. H., Morsut, L., Liu, Z., Brar, G. A., Torres, S. E., Stern-Ginossar, N., Brandman, O., Whitehead, E. H., Doudna, J. A., Lim, W. A., Weissman, J. S. & Qi, L. S. CRISPR-Mediated Modular RNA-Guided Regulation of Transcription in Eukaryotes. *Cell* **154,** 442–451 (2013).

70. Garagnani, P., Bacalini, M. G., Pirazzini, C., Gori, D., Giuliani, C., Mari, D., Di Blasio, A. M., Gentilini, D., Vitale, G., Collino, S., Rezzi, S., Castellani, G., Capri, M., Salvioli, S. & Franceschi, C. Methylation of ELOVL2 gene as a new epigenetic marker of age. *Aging Cell* **11,** 1132–1134 (2012).

71. Bacalini, M. G., Boattini, A., Gentilini, D., Giampieri, E., Pirazzini, C., Giuliani, C., Fontanesi, E., Remondini, D., Capri, M., Del Rio, A., Luiselli, D., Vitale, G., Mari, D., Castellani, G., Di Blasio, A. M., Salvioli, S., Franceschi, C. & Garagnani, P. A meta-analysis on age-associated changes in blood DNA methylation: results from an original analysis pipeline for Infinium 450k data. *Aging* **7,** 97–109 (2015).

72. Herbig, U., Ferreira, M., Condel, L., Carey, D. & Sedivy, J. M. Cellular senescence in aging primates. *Science* **311,** 1257 (2006).

73. Röhme, D. Evidence for a relationship between longevity of mammalian species and life spans of normal fibroblasts in vitro and erythrocytes in vivo. *Proc. Natl. Acad. Sci. U. S. A.* **78,** 5009–5013 (1981).

74. Harkewicz, R., Du, H., Tong, Z., Alkuraya, H., Bedell, M., Sun, W., Wang, X., Hsu, Y.-H., Esteve-Rudd, J., Hughes, G., Su, Z., Zhang, M., Lopes, V. S., Molday, R. S., Williams, D. S., Dennis, E. A. & Zhang, K. Essential Role of ELOVL4 Protein in Very Long Chain Fatty Acid Synthesis and Retinal Function. *J. Biol. Chem.* **287,** 11469–11480 (2012).

75. Beatty, S., Koh, H., Phil, M., Henson, D. & Boulton, M. The role of oxidative stress in the pathogenesis of age-related macular degeneration. *Surv. Ophthalmol.* **45,** 115–134 (2000).

76. Hollyfield, J. G., Bonilha, V. L., Rayborn, M. E., Yang, X., Shadrach, K. G., Lu, L., Ufret, R. L., Salomon, R. G. & Perez, V. L. Oxidative damage-induced inflammation initiates age-related macular degeneration. *Nat. Med.* **14,** 194–198 (2008).

77. Curcio, C. A., Johnson, M., Huang, J.-D. & Rudolf, M. Apolipoprotein B-containing lipoproteins in retinal aging and age-related macular degeneration. *J. Lipid Res.* **51,** 451–467 (2010).

78. Shaw, P. X., Hörkkö, S., Chang, M. K., Curtiss, L. K., Palinski, W., Silverman, G. J. & Witztum, J. L. Natural antibodies with the T15 idiotype may act in atherosclerosis, apoptotic clearance, and protective immunity. *J. Clin. Invest.* **105,** 1731–1740 (2000).

79. Shaw, P. X., Zhang, L., Zhang, M., Du, H., Zhao, L., Lee, C., Grob, S., Lim, S. L., Hughes, G., Lee, J., Bedell, M., Nelson, M. H., Lu, F., Krupa, M., Luo, J., Ouyang, H., Tu, Z., Su, Z., Zhu, J., Wei, X., Feng, Z., Duan, Y., Yang, Z., Ferreyra, H., Bartsch, D.-U., Kozak, I., Zhang, L., Lin, F., Sun, H., Feng, H. & Zhang, K. Complement factor H genotypes impact risk of age-related macular degeneration by interaction with oxidized phospholipids. *Proc. Natl. Acad. Sci. U. S. A.* **109,** 13757–13762 (2012).

80. Cameron, D. J., Yang, Z., Gibbs, D., Chen, H., Kaminoh, Y., Jorgensen, A., Zeng, J., Luo, L., Brinton, E., Brinton, G., Brand, J. M., Bernstein, P. S., Zabriskie, N. A., Tang, S., Constantine, R., Tong, Z. & Zhang, K. HTRA1 variant confers similar risks to geographic atrophy and neovascular age-related macular degeneration. *Cell Cycle Georget. Tex* **6,** 1122–1125 (2007).

81. Sivaprasad, S. & Chong, N. V. The complement system and age-related macular degeneration. *Eye* **20,** 867 (2006).

82. Wang, H., Yang, H., Shivalila, C. S., Dawlaty, M. M., Cheng, A. W., Zhang, F. & Jaenisch, R. One-Step Generation of Mice Carrying Mutations in Multiple Genes by CRISPR/Cas-Mediated Genome Engineering. *Cell* **153,** 910–918 (2013).

83. Luo, J., Baranov, P., Patel, S., Ouyang, H., Quach, J., Wu, F., Qiu, A., Luo, H., Hicks, C., Zeng, J., Zhu, J., Lu, J., Sfeir, N., Wen, C., Zhang, M., Reade, V., Patel, S., Sinden,

J., Sun, X., Shaw, P., Young, M. & Zhang, K. Human retinal progenitor cell transplantation preserves vision. *J. Biol. Chem.* **289,** 6362–6371 (2014).